ROYAUME DU MAROC
Université Mohammed V - RABAT -
جامعة محمد الخامس – الرباط –
Faculté des sciences
كلية العلوم

CENTRE D'ETUDES DOCTORALES - SCIENCES ET TECHNOLOGIES

N° d'ordre 3620

THESE

En vue de l'obtention du : ***DOCTORAT***

Structure de Recherche : Laboratoire de la Matière Condensée et Sciences Interdisciplinaires
Discipline : Physique
Spécialité : Sciences des Matériaux

Présentée et soutenue le 09/04/2022 par :

Soufiane BAHOU

Magnesium Vacancies and Hydrogen Doping in Magnesium Hydride MgH_2 and Lithium Hydride LiH for Improving Hydrogen Storage Properties: Ab initio Calculations

JURY

Mohammed BENAISSA	PES, Faculté des Sciences, Université Mohammed V-Rabat	Président/rapporteur
Driss ZEJLI	PES, Ecole Nationale des Sciences Appliquées-Kénitra	Rapporteur/examinateur
Rachid BENCHRIFA	PES, Faculté des Sciences, Université Mohammed V-Rabat	Rapporteur/examinateur
Rachid El BOUAYADI	PES, Ecole Nationale des Sciences Appliquées-Kénitra	Rapporteur/examinateur
Hicham LABRIM	PA, Ecole Nationale des Sciences Appliquées-Kénitra	Codirecteur
Hamid EZ-ZAHRAOUY	PES, Faculté des Sciences, Université Mohammed V-Rabat	Directeur

Année Universitaire : **2021/2022**

✉ Faculté des Sciences, Avenue Ibn Battouta, BP. 1014 RP, Rabat–Maroc
☎ 00212(05) 37 77 18 76 🖷 00212(05) 37 77 42 61; http://www. fsr.um5.ac.ma

ROYAUME DU MAROC
Université Mohammed V - RABAT -
جامعة محمد الخامس – الرباط –
Faculté des sciences
كلية العلوم

DOCTORAL THESIS

By

Soufiane Bahou[1]

Magnesium Vacancies and Hydrogen Doping in Magnesium Hydride MgH_2 and Lithium Hydride LiH for Improving Hydrogen Storage Properties: Ab initio Calculations

President:

Mohammed BENAISSA	PES	Faculté des Sciences, Université Mohammed V-Rabat

Examiners:

Driss ZEJLI	PES	Ecole Nationale des Sciences Appliquées-Kénitra
Rachid BENCHRIFA	PES	Faculté des Sciences, Université Mohammed V-Rabat
Rachid El BOUAYADI	PES	Ecole Nationale des Sciences Appliquées-Kénitra
Hicham LABRIM	PA	Ecole Nationale des Sciences Appliquées-Kénitra
Hamid EZ-ZAHRAOUY	PES	Faculté des Sciences, Université Mohammed V-Rabat

[1] e-mail: soufiane_bahou@um5.ac.ma

To my family

Acknowledgments

This thesis was carried out at the Laboratory of Condensed Matter and Interdisciplinary Sciences (LaMCScI) of Mohammed V University, Faculty of Sciences, Morocco under the direction of Prof. **Hamid EZ-ZAHRAOUY** and Prof. **Hicham LABRIM**.

First and foremost, all praises and thanks to Almighty Allah for his unlimited blessings.

I would like to express my sincere gratitude and warmest thanks to my supervisor **Hamid EZ-ZAHRAOUY**, who accepted me to his laboratory for these three years and provided me a scientific atmosphere of independence and creativity. I thank him very much for his faith in me, and his advice and support during my research. I would like also to thank Prof. **Hamid EZ-ZAHRAOUY** for reviewing this PhD thesis.

Words are not enough to thank my co-supervisor **Hicham LABRIM** for his advice, his availability and above all his personal qualities, which were an inspiration, steady and strong for me. The person without whom this work would not have been possible. He has been my "guide" in the true sense of the term. His encouragement and motivation made me feel confident about my capabilities and lead me to become more accomplished and self-reliant. I would like also to thank Prof. **Hicham LABRIM** for reviewing this PhD thesis.

Special thanks go to the thesis committee members for carefully reviewing my work and for their useful and insightful comments to improve this thesis. It is an honor for me that they accept to review and report this work.

I also warmly thank to offer my thanks to Prof. **Mohammed BENAISSA** from Faculty of Sciences, Mohammed V University in Rabat, for being the president of the jury and reporting this PhD thesis.

I would like also to offer my thanks to Prof. **Rachid BENCHRIFA** from Faculty of Sciences, Mohammed V University in Rabat, for reviewing and reporting this PhD thesis.

I would like also to thank Prof. **Driss ZEJLI** from National School of Applied Sciences, Ibn Tofail University in Kenitra, for reviewing and reporting this PhD thesis.

I would also like to extend my thanks to Prof. **Rachid El BOUAYADI** from National School of Applied Sciences, Ibn Tofail University in Kenitra, for reviewing and reporting this PhD thesis.

My sincere gratitude goes to Prof. **Marwan LAKHAL** for his ideas, creativity, kindness and advice that helped me a lot to achieve this work.

I would like to thank all the members of the Laboratory of Condensed Matter and Interdisciplinary Sciences (LaMCScI) as well as my colleagues, in particular, Dr. **Mohamed BHIHI.**

Abstract

Hydrogen is currently regarded as an attractive and promising energy carrier in order to be a substitute for fossil fuels due to its zero carbon emissions, high energy value and natural abundance. However, hydrogen suffers from several problems concerning its storage. To address this problem, there are at least four big methods of hydrogen storage system including compressed hydrogen, liquefied hydrogen, adsorbed hydrogen on materials with a high specific surface area and absorbed hydrogen through metal hydrides (e.g. Magnesium hydrides). The latter is our interest in this thesis due to its high hydrogen storage capacities including the volumetric and gravimetric density.

To study the fundamental mechanism of the magnesium hydride (MgH_2) and the lithium hydride (LiH) and provide approaches that allow improving their hydrogen storage properties, an ab initio study is performed to inspect the thermodynamic and electronic properties using the Korringa – Kohn – Rostoker method and the coherent potential approximation.

Based on our calculations, the pure MgH_2 and LiH show a high formation energy and a high desorption temperature, which are consistent with the theoretical and experimental values obtained in other studies. The simulation results show that the magnesium vacancies and the hydrogen doping improve the thermodynamic properties of MgH_2 considerably. Moreover, the desorption temperature and formation energy of LiH have also improved by creating vacancies inside the material.

Key words: Ab initio calculations; Hydrogen storage; Magnesium hydride; Vacancies; Hydrogen dopant atoms; Thermodynamic properties; Gravimetric hydrogen capacity.

Résumé

L’hydrogène est actuellement considéré comme un vecteur énergétique prometteur et attrayant afin d’être un substitut aux combustibles fossiles en raison de ses émissions de carbone nulles, de sa valeur énergétique élevée et de son abondance naturelle. Cependant, l’hydrogène souffre de plusieurs problèmes concernant son stockage. Pour traiter ce problème, il existe au moins quatre grandes méthodes de stockage de l’hydrogène comprenant l’hydrogène comprimé, l’hydrogène liquéfié, l'hydrogène adsorbé par des matériaux ayant une surface spécifique élevée, l’hydrogène absorbé par des hydrides métalliques (p. ex. les hydrures de magnésium et de lithium).

Afin d’étudier le mécanisme fondamental de l’hydrure de magnésium (MgH_2) et l'hydrure de lithium (LiH) et de fournir des approches qui permettent d’améliorer ses propriétés de stockage de l’hydrogène, une étude ab initio (DFT) est effectuée pour inspecter les propriétés thermodynamiques et électroniques en utilisant la méthode de Korringa – Kohn – Rostoker et l'approximation du potentiel cohérent.

En se basant sur notre calcul, les résultats obtenus montrent que le MgH_2 et LiH pur présentent une température de désorption élevée et une énergie de formation élevée, qui sont en accord avec les valeurs théoriques et expérimentales obtenues dans d'autres études. Les résultats de la simulation montrent que les lacunes de magnésium et le dopage par l'hydrogène améliorent considérablement les propriétés thermodynamiques de l’hydrure MgH_2. De plus, la température de désorption et l'énergie de formation du LiH ont également été améliorées par la création de lacunes à l'intérieur du matériau.

Mots clés : Calculs ab initio; Stockage d’hydrogène; Hydrure de magnésium; Lacunes; Dopage par l'hydrogène; Propriétés thermodynamiques; Capacité gravimétrique d'hydrogène.

Résumé détaillé

Compte tenu de la croissance remarquable de la population humaine, de l'épuisement des combustibles fossiles, de la consommation d'énergie et des défis du changement climatique, le développement de sources d'énergie alternatives et nouvelles est devenu l'un des principaux sujets dans le monde. Récemment, l'hydrogène (H_2) a été considéré comme un candidat retenu pour obtenir une énergie durable et propre. Cependant, l'hydrogène souffre de plusieurs problèmes concernant son stockage. En fait, il existe au moins quatre grandes méthodes de stockage de l'hydrogène comprenant l'hydrogène comprimé, l'hydrogène liquéfié, l'hydrogène adsorbé par des matériaux ayant une surface spécifique élevée, l'hydrogène absorbé par des hydrides métalliques (p. ex. les hydrures de magnésium et de lithium).

Aujourd'hui, l'hydrure de magnésium (MgH_2) est l'un des matériaux les plus attrayants pour le stockage de l'hydrogène en raison de ses capacités gravimétrique et volumétrique de stockage élevées (7.6wt.% et 110gH_2/L, respectivement) ainsi que son forte densité énergétique (9MJ/kg Mg). Mais il souffre d'une énergie de formation élevée (-75KJ/mol), d'une température de désorption élevée (300-400°C) et d'une cinétique lente. Ce qui freine son intégration aux systèmes de stockage pour les applications mobiles. Donc l'hydrure de magnésium peut être un matériau optimal pour les applications de stockage de l'hydrogène, à condition que la cinétique et les propriétés thermodynamiques de MgH_2 soient améliorées. D'autre part, l'hydrure LiH figure parmi les hydrures métalliques réversibles les plus légers avec une densité gravimétrique élevée allant jusqu'à 12,6 % et une densité énergétique de 4970 Wh/Kg et 3870 Wh/L. Cependant, l'hydrure de lithium présente également certains défis, notamment son énergie de formation élevée (-90,5 KJ/mol) et sa température de désorption élevée (400- 750°C).

L'objectif de ce travail est de proposer une nouvelle approche théorique pour réduire l'énergie de formation et la température de désorption des hydrures de magnésium et de lithium afin de satisfaire les différentes applications sans sacrifier sa capacité gravimétrique élevée. Pour cela, une étude ab initio (DFT) est effectuée pour étudier les propriétés thermodynamiques en utilisant la méthode de Korringa – Kohn – Rostoker et l'approximation du potentiel cohérent (KKR-CPA). La recherche vise à étudier l'effet des lacunes et le dopage par l'hydrogène sur les propriétés de stockage de les hydrures de magnésium et de lithium et de donner une explication plausible à la diminution observée en utilisant la densité d'état (DOS).

Premièrement, nous avons étudié les propriétés structurales de MgH_2 et Mg en utilisant la méthode de relaxation pour optimiser les paramètres de maille. Nous avons d'abord fixé les paramètres de maille de MgH_2 et Mg à leurs valeurs expérimentales. Puis, nous avons optimisé les paramètres en fixant les positions atomiques et en variant le volume de la maille élémentaire et ensuite en calculant l'énergie totale de MgH_2 et Mg en fonction du volume.

Deuxièmement, nous avons examiné les propriétés thermodynamiques de MgH_2 pur par les calculs ab initio basés sur la méthode KKR-CPA. Les résultats obtenus montrent que le MgH_2 pur a une haute stabilité et par conséquent une température de désorption élevée et une énergie de formation élevée, ce qui est en accord avec les valeurs théoriques et expérimentales obtenues dans d'autres études.

Troisièmement, nous avons étudié la structure électronique de MgH_2 afin de comprendre et d'expliquer le mécanisme responsable de la haute stabilité du système. Nous avons montré que la forte hybridation entre les atomes de magnésium et d'hydrogène est la principale raison d'avoir une haute stabilité dans l'hydrure de magnésium et que la création des lacunes de magnésium avec ou sans le dopage par l'hydrogène réduit considérablement cette hybridation, ce qui conduit d'améliorer les propriétés thermodynamiques, qui incluent l'énergie de formation et la température de désorption, dans l'hydrure de magnésium.

Quatrièmement, nous avons utilisé la même approche pour calculer les propriétés thermodynamiques et électroniques de l'hydrure de lithium. En particulier, nous avons varié la concentration des lacunes de lithium dans l'hydrure, et nous avons trouvé que les propriétés thermodynamiques ont été améliorées en augmentant l'énergie de formation et la capacité gravimétrique et en diminuant la température de désorption et la stabilité dans l'hydrure LiH.

Contents

List of Figures

List of Tables

List of abbreviations

$\mathbf{MgH_2}$	Magnesium hydride
SMR	Steam methane reforming
POX	Partial oxidation
ATR	Autothermal reforming
HTS	High-temperature-shift
LTS	Low-temperature-shift
PSA	Pressure swing adsorption process
CCS	Carbon capture and storage
UCG	Underground coal gasification
HTSE	High temperature steam electrolysis
TWSCs	Thermochemical water splitting cycles
SIC	Sulfur-iodine cycle
SOFC	Solid oxide fuel cell
PV	Photovoltaic
CFRP	Carbon fiber reinforced polymer
GFRP	Glass fiber reinforced polymer
MOFs	Metal organic frameworks
PEMFC	Polymer electrolyte membrane fuel cell
LOHC	Liquid organic hydrogen carrier
NEC	N-ethyl-carbazole
MOF	Metal organic framework
PEMFC	Proton exchange membrane fuel cell
HCP	Hexagonal close-packed
C_g	Gravimetric capacity
C_v	Volumetric capacity
wt.	Weight
T_{des}	Desorption Temperature
CB	Conduction band
SCW	Supercritical water
PCT	Pressure Concentration Temperature
KKR	Korringa-Kohn-Rostoker
CPA	Coherent Potential Approximation
ab initio	First principal calculation
ψ	Many-body wave function of electrons
m_e	Mass of the electron
M_I	Mass of the nucleus
E	Charge of the electron
Z_I	Charge of the nucleus
r_i	Position of electron
R_I	Position of the nuclei
H	Hamiltonian operator
T_e	Kinetic energies of the electrons
T_n	kinetic energies of the the nuclei
V_{int}	Internal potential
V_{ext}	External potential
V_{nn}	nucleus-nucleus potential
V_{KS}	Effective potential
$\hbar$	Planck's constant devised by 2π
LDA	Local density approximation
GGA	Generalized gradient approximation
DFT	Density functional theory
P	Equilibrium pressure
T	Temperature
R	The universal gas constant
G	Free energy
ΔH	Heat of formation
ΔS	Entropy
E_{tot}	Energy total
DOS	Density of states
VB	Valence band
FHK	Hohenberg-Kohn universal functional
V_{KS}	Effective Kohn-Sham potential
XC	Exchange-correlation

Introduction

The non-renewable fossil fuel resources, which involve petroleum and natural gas as well as coal, supply the vast majority of global energy demand. However, the depletion of fossil fuels driven by the growing demand for energy around the world is unsustainable. In addition, the use of fossil fuel as a main resource to meet our energy needs is responsible for greenhouse gas emissions and global warming on our planet. Thus, due to environmental and sustainable concerns, the transition from the non-renewable to renewable energy resources is the required solution to address these problems. Obviously, hydrogen is regarded as the most effective and cleanest fuel compared to other fuels by generating the highest amount of energy per unit weight without emitting harmful gases such as carbon dioxide. Hence, hydrogen is currently considered as an attractive and promising energy carrier that allows storing and delivering clean energy on demand. Another remarkable point for the high interest generated by hydrogen is that hydrogen can be a key player in establishing a sustainable and environmentally-friendly energy system in the future.

As the simplest, lightest and most abundant chemical element in the Earth's crust, hydrogen exists as a compound with other elements (such as carbon, oxygen in water, oxygen in organic compounds) to form chemical materials. However, hydrogen suffers from several problems concerning its storage. Such a storage requires a high gravimetric and volumetric capacity as well as a fast absorption and desorption rate at low temperatures. Nowadays, there are at least four big methods of hydrogen storage system including compressed hydrogen, liquefied hydrogen, adsorbed hydrogen on materials with a high specific surface area and absorbed hydrogen through metal hydrides (e.g. magnesium hydride) [1, 2, 3, 4, 5, 6, 7]. The latter is our interest in this thesis due to its high hydrogen storage capacities including the volumetric and gravimetric density.

Up to day, the magnesium hydride (MgH_2) is considered as one of the most promising materials for hydrogen storage applications with the advantages of high gravimetric capacity (7.6wt.%) and high volumetric capacity ($110gH_2/l$) as well as high energy density (9MJ/kg Mg) [8, 9, 10, 11, 12, 13, 14, 15, 16, 17]. However, the MgH_2 has some challenges including a high formation energy (ΔH = -75KJ/mol) and a high desorption temperature (above 573K) as well as the slow kinetics of absorption and desorption of hydrogen [13,14, 15, 16, 17, 18]. These

disadvantages have to be overcome in order to be the optimal material for using it in applications concerning the hydrogen storage [19, 20, 21, 22, 23].

Therefore, many efforts and attempts have been made and are currently being made to address and improve the hydrogen storage characteristics of magnesium hydride. In this context, using the density functional theory, the thesis aims to improve the thermodynamic properties of MgH_2 by creating magnesium vacancy defects and introducing hydrogen dopant atoms into the hydride.

On the other hand, the LiH figures among the lightest reversible metal hydrides with a high gravimetric density up to 12.6 wt.% and an energy density of 4970 $Wh.Kg^{-1}$ and 3870 $Wh.L^{-1}$ [24, 25, 26, 27, 28, 29, 30, 31]. However, the lithium hydride also has some challenges including its high formation energy (-90.5 KJ/mol) and high desorption temperature (700-1000 K) [30, 31, 32, 33, 34]. In addition, the lithium hydride reacts easily with humidity to irreversibly generate surface corrosion layers such as lithium oxide and lithium hydroxide. However, the controlled hydrolysis of LiH under low relative humidity is considered as an efficient hydrogen generator for mobility applications [35, 36, 37]. There are some attempts to overcome the thermodynamic problems of LiH. For example, the carbon is one of the additives which can be improved the absorption/desorption of H_2 by decreasing the temperature below 200°C [38].

Our thesis is divided into the following five chapters:

- In chapter 1 of the thesis, different kinds of storage are discussed to highlight their current situations in cost, eco-friendly and scalable-up. Besides this, an overview of magnesium and its hydride in terms of their structures and thermodynamic properties is provided in this chapter.
- Chapter 2 is devoted to giving an overview of the first principles calculations based on the density functional theory and other methods to solve the Kohn-Sham equations.
- In chapter 3, we study the electronic structure and the thermodynamic properties of the magnesium hydride containing magnesium vacancy defects and hydrogen dopant atoms.
- Chapter 4 is devoted to comparing the effect of the vacancy defects and the doping with metal transitions on the thermodynamic properties of the magnesium hydride.
- Chapter 5 studies the effect of the lithium vacancy defects on the thermodynamic properties of the lithium hydride.

- Finally, a general conclusion is given to summarize the main results obtained.

1 Hydrogen Storage and Metal hydrides

Contents

1.1 Hydrogen storage

The purpose of this chapter is to provide an overview of the most used and reliable technologies for hydrogen storage. As shown in Figure 1.1, two routes composed of seven methods are taken into consideration for hydrogen storage in this chapter. These routes are based on the kind of storage: hydrogen storage in pure form or material-based storage. The details of these methods are explained and discussed below.

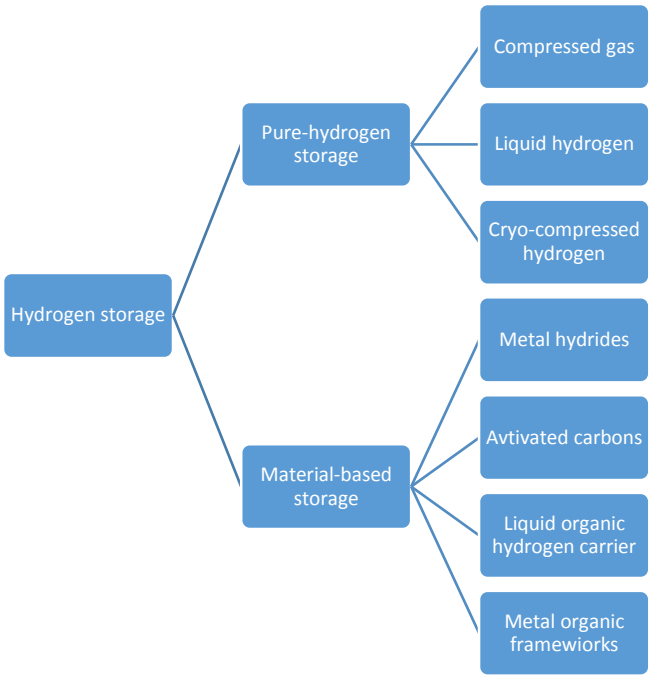

Figure 1.1: Hydrogen storage methods.

1.1.1 Hydrogen storage in pure form

Hydrogen storage in pure form refers to hydrogen that is stored using physical and/or chemical method without any reaction between hydrogen and other substances. This option is usually simple, but it has some technical difficulties in terms of the hydrogen pretreatment as well as the tank design. There are three types of storage options for pure hydrogen: compressed hydrogen storage, cryogenic hydrogen storage, and cryo-compressed storage. The details of these options are discussed in the next sections.

1.1.1.1 Compressed hydrogen

The compressed hydrogen storage in different sizes of vessels is the most widespread technology in the world, and the storage of hydrogen in high-pressure tanks represents a key enabling technology for all automotive applications that are commercially available or being

developed with pressures up to 700bar. Thus, the tank design takes a major place in this kind of storage for hydrogen vehicles.

Generally, the high-pressure storage technique for hydrogen is similar to other gases. Additionally, the primary components, which are currently used on the market or under development, are the same in all high-pressure hydrogen storage tanks. They consist of a valve, and a tank shell, which allows withstanding the high compression, and enough space to contain hydrogen. There are two kinds of shapes for compressed tank system, namely cylinder or sphere. The use of these specific shapes has the ability to handle the high stresses involved inside the storage tank in a more effective way.

One feature for this storage system is that the thermal management of the tank is not complex to handle. In addition, this kind of tanks also provides a low weight for mobile applications. Besides this, the amount of hydrogen storage keeps constant during long parking times, because the tank system operates at ordinary temperatures. The only main disadvantages of this storage system are that the tank has to provide a high pressure to operate and a strong material to withstand the high pressure. Such a high-pressure method represents a challenge in terms of security and safety. Thus, there are currently many efforts to protect the high-pressure vessels against any kind of incidents and explosions.

Carbon fiber reinforced polymer (CFRP) is considered as a successful candidate to be widely used in the hydrogen storage tanks with pressures up to 700bar. In such tanks, a gas tight liner is placed into the CFRP-tank to prevent diffusion of hydrogen out of the system over time. The high-pressure tank systems can be typically categorized into four main classifications:

- Classification I: the storage tank is manufactured from steel with a pressure ranging from about 200 to 300bar.
- Classification II: the tank shell is manufactured from steel mixed with carbon fiber reinforced plastic that is fully wrapped around the cylinder. This tank offers lighter-weight structure compared with tank I. Besides, the pressure and the energy density of the tank are higher, and this leads to storing more hydrogen.
- Classification III: the tank is manufactured from GFRP (glass fiber reinforced polymer) or CFRP (carbon fiber reinforced polymer) wrapped around the cylinder. This design strengthened with advanced composite material can withstand high pressures inside the tank. Additionally, the gas-tight liner placed in the CFRP shell is made out of aluminum and/or steel. These tank systems can operate at a pressure level of 350bar.

- Classification IV (see Figure 1.2): this type has a similar concept to the last one; the only difference is that the liner is made from polymer, which allows increasing the pressure to around 700bar. Therefore, this type is considered as an alternative option for mobile applications [39]. In addition, the CFRP classification IV tanks are still under development stage by many laboratories and companies throughout the world for more improvement. However, great strides have currently been made in this stage. Since this type is a promising technological tank, the main components of such a tank are explained in more detail below.

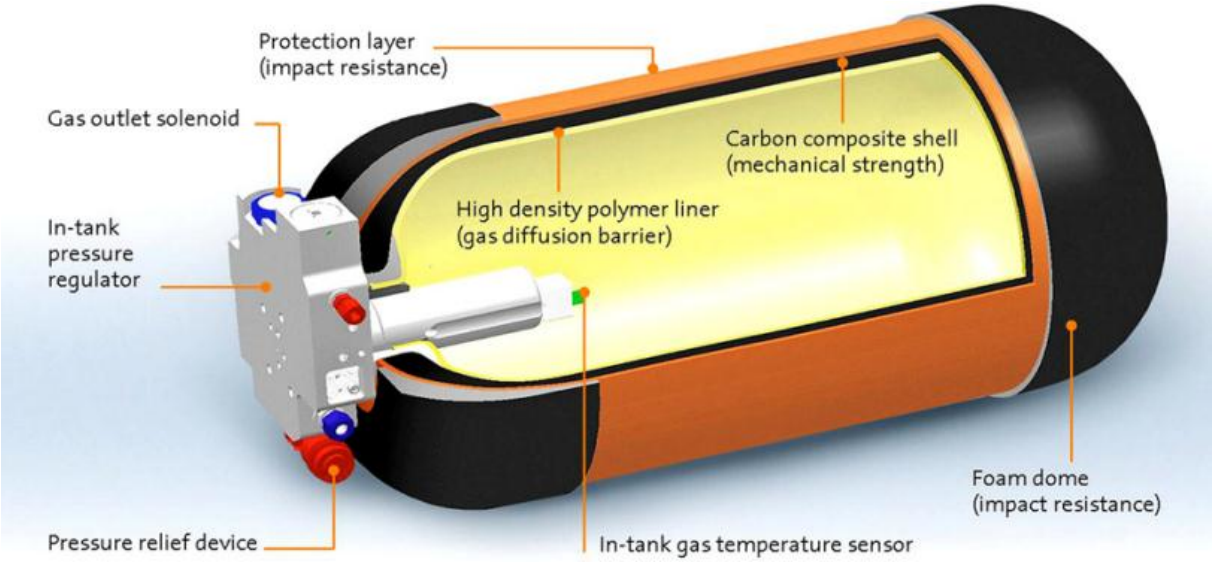

Figure 1.2: Carbon fiber reinforced polymer tank type IV for hydrogen vehicles [40].

In addition, the safety and security surrounding the use of hydrogen gas are a major issue for high-pressure tank systems. Thus, several standards (such as ISO/TC 197) are used to organize and define the specific components of hydrogen storage.

In the case of high-pressure storage tanks, hydrogen offers a safety pathway for mobile applications compared to classical liquid transportation fuels due to its physical properties. For example, hydrogen has a much lighter weight than atmospheric air. As a result, hydrogen can disperse and disappear immediately into air if there is a leak in the storage tank. This helps to prevent any toxic atmosphere surrounding the car. Additionally, hydrogen has been proven safer than many other fuels (such as diesel and gasoline fuel) in case of fire.

The materials used and the applied pressure in the tank are based on the particular application involved. For mobile applications, the CFRP tanks with a pressure level of 350 and 700bar represent the most ambitious technologies for the tank shell. The storage of hydrogen

with a pressure up to 700bar can consume about 18MJ/kgH_2. Therefore, the cost of this storage tank is usually high due to the compression as well as the losses during hydrogen storage.

The costs of storage are also based on the applied pressure inside the tank. Typically, such a tank of 700bar, it costs approximately 20US$/kWh. Compared to a tank of 350 bar, it costs cheaper by about 13.4US$/kWh. The tank fill rate for both pressures outlined above is 1.5–2kgH_2/min at the hydrogen-refueling stations [41].

Currently, the storage tank with a pressure level of 700 bar are commonly used for cars (Figure 1.3) because the energy density of hydrogen in the tanks of 700 bar is considerably higher than pressure tanks with a lower pressure. Therefore, the high energy density is a very important feature, especially in cars, because it allows minimizing the tank volume inside cars. In contrast, busses have more space to store hydrogen. Thus, it is recommended to install the tanks of 350 bar inside such vehicles. Additionally, these tanks provide others features such as easy and quick to load, high efficiency and low cost compared to the tanks of 700 bar. The experience gained and the management of compressed gases within industry are also considered as clear advantages for the high-pressure hydrogen storage tanks. Therefore, it is most likely that the two pressure levels outlined above will grow on the hydrogen storage market in the coming years.

In this context, this kind of storage is considered one of the optimal choices for our country, Morocco, to be used for hydrogen storage. Morocco has ambitious plans in the future to produce large quantities of hydrogen gas using renewable energy. In 2020, Morocco installed a capacity of around 40% renewable energy (such as wind, solar and hydropower), and it is expected to grow this production to 52% by 2030. These achievements can make Morocco one of the world market leaders in this sector by producing and exporting green hydrogen to the world.

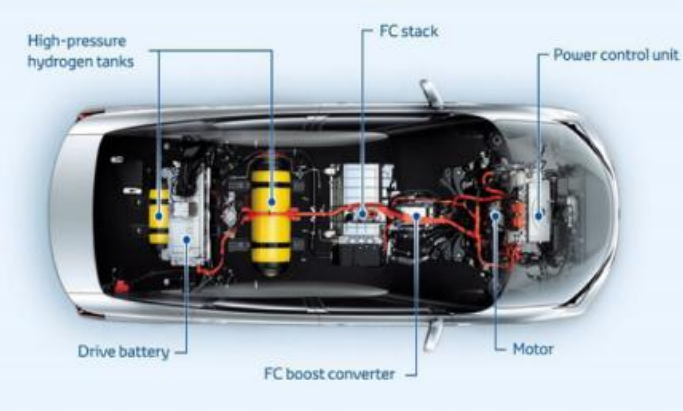

Figure 1.3: High-pressure hydrogen storage tanks in car [42].

1.1.1.2 Cryogenic hydrogen

The storage of hydrogen in the liquid phase is an alternative way to store hydrogen with high energy density. In terms of technical aspect, there are many benefits in using liquid rather than compressed gases. However, the difficulty with liquid hydrogen is that it needs to be condensed at low temperatures. Therefore, such a storage tank requires a considerable expenditure of energy for guaranteeing the liquefaction and regasification processes of liquid hydrogen. The state of technology of such a tank (Figure 1.4) is explained and discussed in more detail below.

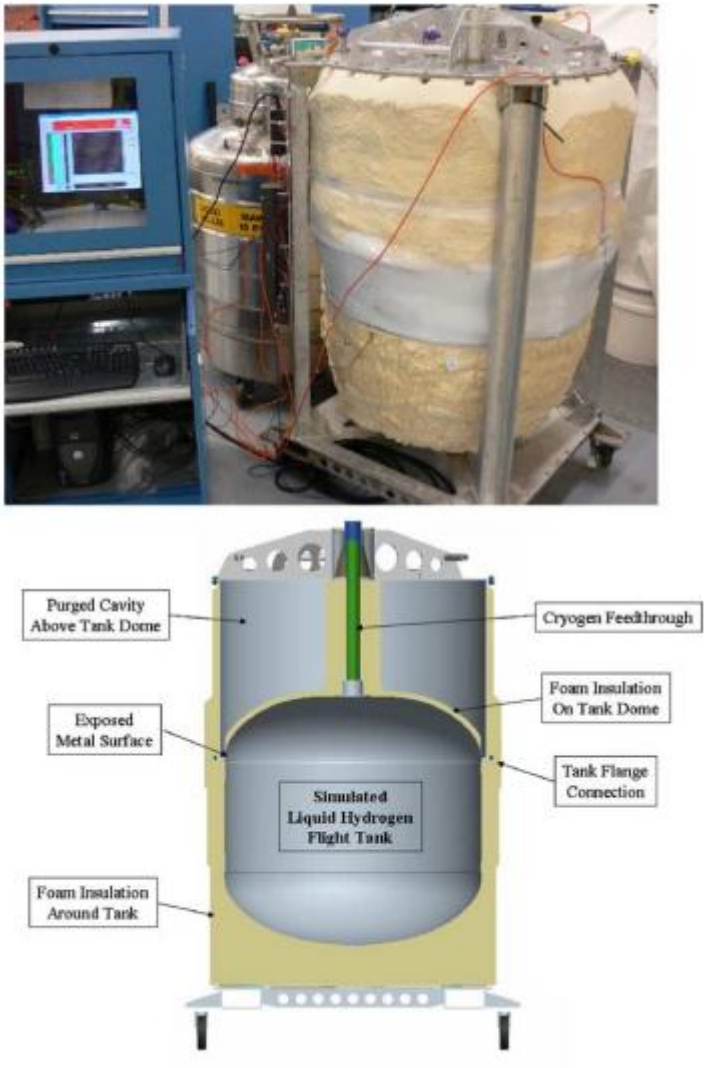

Figure 1.4: Liquid hydrogen tank [43].

As a liquid, hydrogen has to be stored under cryogenic conditions at 20K due to its physical properties. Therefore, the insulation takes a major place in such liquid hydrogen tanks

due to the temperature difference between the inside and outside of the tank. Thus, in terms of efficiency, the tank concept is designed to minimize the thermodynamic losses that depend on the surface area to the ambient environment. In addition, some smaller tanks, which are typically used for vehicles, have a design mixed between a cylinder and sphere because this mixture is more suitable for the design of a vehicle. Such a design typically aims to minimize the radiation and convection losses. Additionally, the boil-off losses also pose techno-economic constraints to spread such a storage tank for vehicles. These losses are attributed to hydrogen gases released to the air without its utilization. Therefore, there are some technological options, which are under development, to make use of these boil-off losses. To date, these technological options are expensive and still under development.

Liquid hydrogen storage is capable of achieving a higher density of storage as compared to high-pressure storage within a tank. Therefore, liquid hydrogen is currently regarded as an alternative pathway for mobile applications, especially for some airplanes. However, all this is realized by a consumption of one-third of the stored hydrogen energy in order to cool hydrogen gas at a low temperature level. Besides, so far, there is no storage system to have the possibility of storing the liquefied hydrogen for more than two days without technically creating any significant losses. This is due to the tank temperature from the inside is lower than the outside by a difference up to 275K or more in the summer. Consequently, amounts of liquid hydrogen are vaporized, which results in increasing pressure within the tank to maximum levels. Therefore, it is necessary to blow off the hydrogen gas from the tank to prevent any explosion in this high-pressure environment. However, most times these blow-off gases are released into the ambient atmosphere. Thus, it is absolutely forbidden to park vehicles equipped with liquid storage tanks within a parking garage because the blow-off gases can react with air to cause explosion. Another disadvantage of the blow-off gases is that liquid hydrogen vaporizes within the storage tank without stopping, making the tank empty after a while. Therefore, such vehicles have to be refilled consistently and continuously even if not used. For this reason, such a liquid storage tank is recommended to be used for commercial vehicles (such as trains, trucks, planes and ships), which are characterized by a predictable demand and a constant use of energy.

The liquid hydrogen has a higher density energy of 70.8kg/m^3 as compared to uncompressed hydrogen gas of 0.09kg/m^3. Thus, this difference is considered as a significant advantage and a strength for liquid hydrogen. However, this benefit requires specific conditions to fulfill a regulated liquefaction for hydrogen. As a liquid, hydrogen must be liquefied to a temperature level between 20 and 30K. Additionally, the pressure level of such a storage tank

is between ambient pressure and 6bar [44, 45]. Hydrogen liquefaction requires around 35% of the stored hydrogen energy with a storage efficiency of about 22.3%. The fill rate of a suitable tank sums up to 1.5-2kgH_2/min. Such a storage system, it is expected to have higher costs than a high-pressure storage [41, 45, 46, 47, 48].

The use of liquefied hydrogen as a fuel have been tested and proven in several applications, especially in space applications (such as space shuttle). Moreover, for cars, liquid storage tank does not exist in the current mass market. Besides, it is not expected that such a storage tank will have a major place for cars in the coming years. So far, there is no existing infrastructure for the refueling stations as opposed to the high-pressure hydrogen stations. Additionally, liquid hydrogen storage tank requires many expensive tests for demonstration because such a technology is still immature for cars. Generally, hydrogen as a liquid phase has a limited scope for storage.

1.1.1.3 Cryo-compressed hydrogen

When hydrogen is stored at cryogenic temperatures in a vessel with under pressure, the technology is called cryo-compressed storage. This option offers a high volumetric energy density without changing the chemical nature of matter.

This technology is a mix between the characterizations of liquefied hydrogen and compressed hydrogen storage systems with a temperature of up to 20K and a pressure level of about 350 or 700 bar. Under these conditions, the system storage capacity is realized at the expense of a large amount of energy and a range of technologies for cooling and compressing hydrogen. In addition, such a technology, the design vessel requires specific materials properties to store hydrogen at low temperatures and high pressures for a long time.

It is expected that the cost of the overall tank system is around 12 to 30 US$/kWh due to few commercial applications and technical uncertainties on the market. Additionally, a cryo-compressed hydrogen storage system shows an overall efficiency of 41%; it is a storage efficiency between the liquid hydrogen and high-pressure hydrogen storage systems [41, 48].

There are already various attempts to use such a tank system for automotive applications. This kind of storage offers a high storage capacity that is useful especially for cars. As an example, Toyota has a model called Prius that is designed with a cryo-compressed hydrogen storage system. This car recorded a high long-distance average by about 1050km [49]. The cryo-compressed hydrogen tank system offers clear advantages (such as high energy density)

and different possibilities to fill the storage tank compared to other technologies. However, the existing refueling stations are only designed for the distribution of high-pressure hydrogen.

1.1.2 Material-based storage

In addition to the three technologies explained above for the storage of hydrogen in pure form, there is also another revolutionary category of hydrogen storage based on promising materials (Figure 1.1). To describe this category in a simple way, hydrogen can accumulate on or react with materials under reversible chemical reactions or physical effects. This catalogue includes several storage methods that are based on materials for hydrogen storage, these methods are explained in detail below. To keep in mind, the material-based storage options are still under development and not ready to be widely used. Some of them are still in small pilot applications, while others exist already in the lab phase.

1.1.2.1 Liquid Organic Hydrogen Carrier (LOHC)

A liquid organic hydrogen carrier is another storage technology that can handle easily with hydrogen. This technology allows storing hydrogen for a long time at ambient pressure as well as without losses.

In such a LOHC, hydrogen is absorbed and desorbed in a liquid state by using organic fluids such as N-ethyl-carbazole (NEC). These fluids are similar to metal hydrides in terms of the storage principle, with the primary difference is that LOHC is stored hydrogen in the liquid phase and hydrides in the solid phase. Therefore, LOHCs offer great features for the storage system as well as for the design of a vehicle.

As an example, N-ethyl-carbazole (NEC) is one of the LOHC fluids that is currently under development. During the storage phase, first fluid reacts with hydrogen gas within a reactor at 150-200°C under 20–50bar (depending on the storage fluid). This chemical reaction takes place using a catalyst such as ruthenium. During the reverse phase, hydrogen gas is released from the fluid. Here a dehydrogenation reaction takes place using a catalyst at temperatures ranging from 270°C to 310°C under low pressures [50, 51]. Such storage fluids can store between 5.8 and 7.2wt.% of hydrogen. Therefore, the efficiency of this method can reach about 44%. Additionally, the fill rate of a suitable tank sums up to 4kgH_2/min.

LOHCs can be integrated in different automotive applications (such as car and truck) with several concepts [51]. During the loading or unloading hydrogen cycle, LOHCs allow storing

and transporting hydrogen with a typical tank used for fossil fuels. However, this operation has to be realized by using two separated tanks or by placing a membrane inside a single tank to subdivide the tank into two different regions.

The management of liquid storage tanks is common within the chemical industry, and the experience, which has already been gained with liquid fluids, offers a clear advantage for LOHCs. Besides, the dehydrogenation reaction requires a catalytic to release hydrogen from the organic fluid. In addition, hydrogen gas released during desorption is not completely pure. Thus, an additional cleaning step is necessary for fuel cell vehicles because they need a high purity of hydrogen for avoiding the destruction of the electrodes.

LOHCs are always in the liquid state. Thus, such LOHCs can be used easily with the existing technology of liquid fuels based on fossil energy. Therefore, LOHCs are compatible with the known and existing infrastructure for the refueling stations.

One of the major advantages of LOHC is the possibility to merge the existing fueling stations with this type of storage technology to a certain extent. Therefore, it is possible to use the same trucks of conventional liquid fuels to transport LOHCs in large quantities. There are already some applications of LOHCs, especially for large-scale applications such as fuel cell ships. So, this shows that this kind of energy storage is successful with the large amounts of hydrogen. For other applications, there is no expectation that this technology will have a significant part of the consumer market in the coming years.

1.1.2.2 Metal Organic Framework (MOF)

A metal organic framework is a coordination network that consists of organic linkers and metal ions/clusters to form dimensional structures with the ability to absorb hydrogen.

Hydrogen is stored inside the porous medium using physical adsorption and fixed at the surface, particularly at the inorganic part of MOF. The porous structure of MOF is characterized by a high surface area per gram (about 1000m2/g). However, this method of storage operates only at low temperatures (below 100K) and allows storing between 5 and 7.5wt.% of hydrogen. One example of MOFs is shown in Figure 1.5 under the name “MOF-5”. It is composed of Zn_4O unit (inorganic part), which is combined with 1,4 benzene-dicarboxylate in a cubic structure.

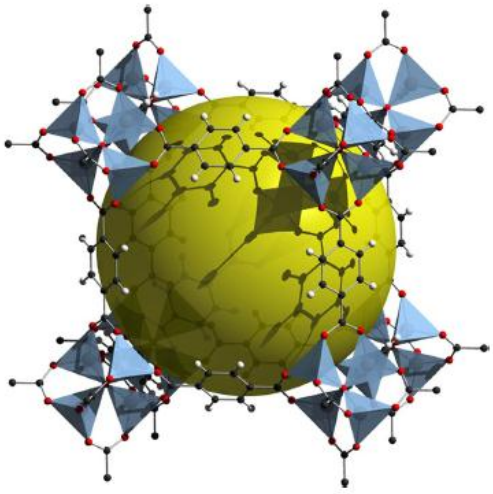

Figure 1.5: MOF-5 Structure.

There are already some tests and experiments of MOFs with small tanks. However, it is not expected that this technology will have a significant part of the consumer market in the coming years. One feature of this storage technology is the ability to integrate this technology with other methods. As an example, MOF tanks can maximize the storage density in cryo-compressed hydrogen tanks. Another advantage is that the possibility to use the MOFs for methane storage.

1.1.2.3 Activated Carbon

Activated carbon is an adsorptive medium that is used in a range of applications thanks to its high porosity and high surface area. This material is used as a storage medium by adsorbing hydrogen onto the free surface of the pores.

Depending on van der Waals forces, hydrogen is adsorbed in the molecular state and fixed at the carbon surface. These forces are unstable enough to hold hydrogen at ambient temperature. Thus, hydrogen has to be cooled to about 70K before storage. Therefore, activated carbon is usually combined with cryo-compressed hydrogen tanks to maximize the storage capacity of the vessel [52]. In addition, carbon is inexpensive and easy to handle. Therefore, this promising material is under research in many institutions and universities in the world [53, 54, 55].

Other options exist to store hydrogen in carbon including activated carbon fibers, carbon nanotubes and graphite. These options use the same participle of activated carbon by using the surface area to accumulate hydrogen, with the main difference being that the appearance of porous carbon is the indicator of each material.

Currently, the activated carbon can store at room temperature about 1wt.% for 100bar and about 2wt.% at pressure levels up to 400bar. But, at cryogenic temperature (77K), it can store a capacity between 5.5 and 6 wt.% at 20bar [53], and 8wt% of hydrogen at 400bar [54]. There are already prototype tanks for storing hydrogen in activated carbon. Most of these tanks operate at low temperatures of around 70K with an adsorptive-cryogenic storage [46, 56, 57].

There is no market ready for this method at this moment. However, this method is already available and offers the advantages of easy to handle and low cost. If this storage can take place with other options, it is expected that this storage will be combined with a cryo-compressed storage tank. However, it is not foreseeable that this material will have a significant part of the consumer market in the coming years because it is still under development by different research groups.

1.1.2.4 Metal hydride

Metal hydrides have been used as hydrogen storage media since the 1980s. There was a car fleet equipped with hydrogen storage tanks that were based on a metal hydride. The weight of the storage system was too high with 140 kg. Titanium-iron (TiFe) was used as an active material for these tests. This material has a low gravimetric capacity with 1.8wt.%. Since then, there has been much progress in this field to access to reliable materials. At present, a number of modern metal hydrides have the ability to overcome the difficulties related to hydrogen storage. For example, magnesium hydride (MgH_2) represents a promising material candidate for hydrogen carrier with a high theoretical gravimetric density of up to 7.6wt.% [58, 59].

Hydrogen is stored in metal hydrides using chemical absorption process; hydrogen gas diffuses into the metal structure where hydrogen reacts with the metal to form metal hydride. This process is similar to a sponge by absorbing hydrogen gas. To understand the mechanism of hydrogen storage by using metal hydrides, it is essential to take a view on the general reaction related to this process. The chemical reaction related to the storage of hydrogen into the metals is shown in equation 1.1

$$H_2 + Metal \rightarrow Metal\ Hydride \tag{1.1}$$

The general reaction of hydrogen storage is characterized by an exothermic nature. Therefore, the reverse reaction of hydrogen is endothermic. Figure 1.6 displays the four steps of the chemical absorption reaction of hydrogen.

First, the hydrogen gas molecules reach the metal surface. Second, the molecules are dissociated into atoms of hydrogen. Third, the atoms of hydrogen are dissolved into the crystal structure of the metal. In the final step, the atoms of hydrogen react with the metal to form a hydride. In this step, a heat flux is released during the hydrogenation of metal due to the exothermic nature of reaction (equation 1.1). The same procedure is taken place in the backward reaction by providing enough endothermic heat for the backward reaction to proceed.

The lattice of the metal is influenced during the interaction between hydrogen molecules and metal by changing its volume. Consequently, there is an expansion during hydrogen absorption and a contraction during hydrogen desorption. This leads to an increase in volume by about 30 to 40% (depending on the amount of stored hydrogen and the metals used) [53].

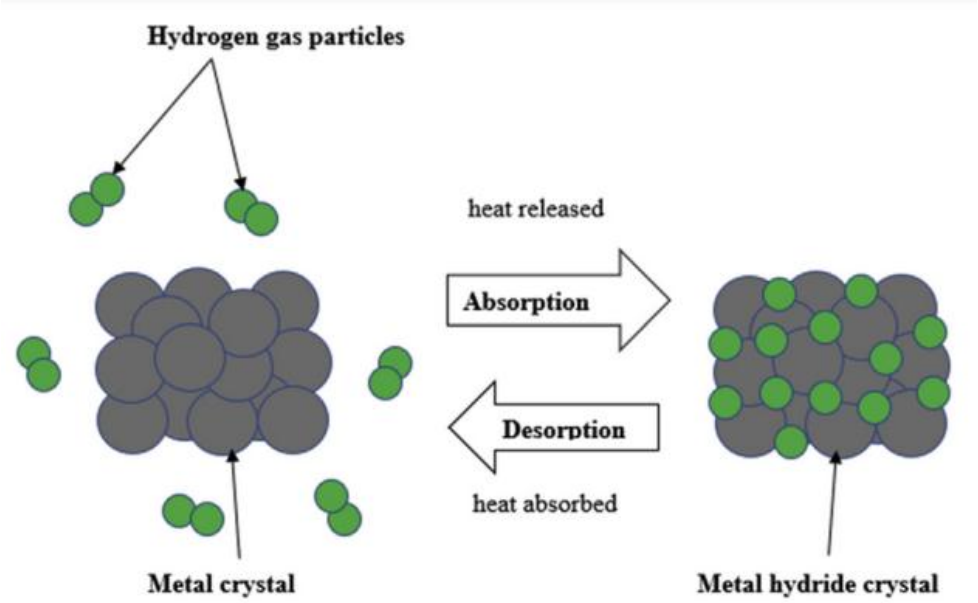

Figure 1.6: A simplified model of a metal hydride hydrogen storage [4].

Nearly all elements listed in the Mendeleev's periodic table can be used as media for hydrogen storage. Accordingly, these elements can primarily be classified into three main categories according to the chemical bond of the element with hydrogen:

- Ionic hydrides: this category includes all chemical elements of alkaline earth metals and alkali metals in the Mendeleev's table. These hydrides have the same physical properties of the original metals including the crystal structure, brittleness, hardness and other properties. Hydrogen behaves as an anion within this kind of hydrides. The most common hydrides of this category are calcium hydride (CaH_2), lithium hydride (LiH) and sodium hydride (NaH) [45, 53].

- Covalent hydrides: all elements of nonmetal are included in this category. The chemical bond of the element with hydrogen is van der Waals interactions. Thus, the majority of covalent hydrides are either gases or liquids at room temperature. Some examples of these covalent hydrides are methane (CH_4), hydrogen sulfide (H_2S), ammonia (NH_3) and water (H_2O). The formation of this kind of hydrides is not easy, because a significant effort is needed for synthesizing most of such hydrides by using complex reactions between hydrogen and the element. For this reason, there are no promising covalent hydrides yet, which can use for hydrogen storage [45, 53].
- Metal hydrides: here, hydrogen reacts with a metal to create a metal hydride with a chemical bond between the metal and hydrogen. The physical properties of these hydrides are often changed in comparison to the ionic hydrides, except their electrical and thermal conductivity [45, 53]. The metal hydrides can be grouped into two different classifications. The primary indicator of each classification is their stability. Classification I includes metals that form stable hydrides. Classification II includes metals that form unstable hydrides. Additionally, it is possible to combine between these two classifications for creating complex metal hydrides. Thanks to this combination, it can modify some physical properties of the metal hydrides according to the required application [45].

The thermal management is necessary for such a metal hydride storage. The tank temperature has to be cooled during hydrogen charging and heated up during hydrogen discharging. Therefore, the optimal temperature is important for the storage tank, especially for automotive applications that utilize a polymer electrolyte membrane fuel cell (PEMFC) as a power source. This fuel cell is operated at temperature levels of about 100°C or less. Therefore, the use of the metal hydride storage tank within the fuel cell vehicle requires a specific heating device in order to provide the required temperatures for this kind of storage. However, this leads to a decrease in the overall storage efficiency.

Such metal hydride storage tanks offer some advantages in comparison with other options. One advantage is that the volumetric capacity of metal hydrides is relatively high. Besides, hydrogen released during desorption has a high purity. However, such a storage tank has also some challenges. The low gravimetric energy density is one of the major challenges for most metal hydrides. Besides, some metal hydrides require a high temperature for the reaction to proceed. In addition, the filling of such a single tank is too slow for a hydrogen-powered car.

Metal hydrides are already tested in some applications as media for hydrogen storage. The submarine is one of the popular examples for metal hydride hydrogen storage. It uses metal hydride storage tanks combined with the fuel cell to power the propulsion system of the submarine. Additionally, the high volumetric capacity of metal hydrides is advantageous in space applications [47]. A delivery scooter is another example of using metal hydrides as media for hydrogen storage. This scooter is based on a hydrogen tank with fuel cell technology. The stored hydrogen amount within this hydride is 0.9wt.% [60].

Such applications show that the metal hydride has the ability to be a successful candidate for hydrogen storage and competitor in the market in the years to come. Additionally, another advantage is that the fuel cell combined with metal hydride tank may be refueled at the high-pressure hydrogen stations. Moreover, a further effort is still required for providing a reliable storage tank in terms of cost and efficiency as well as stability.

1.2 Magnesium hydride MgH_2

Magnesium hydride is one of the promising candidates to be used in hydrogen storage applications, especially for hydrogen vehicles. Currently, magnesium is used widely to fabricate lightweight structural alloys, which have importance in different industries. This element has attracted the community interested to the storage of hydrogen for half a century with the advantages of high hydrogen capacity (7.6wt.%) and high energy density (9MJ kg^{-1}).

1.2.1 Background to magnesium hydride

The name magnesium refers to a city in Greece called Magnesia where quantities of magnesium carbonate were largely discovered in olden times. Magnesium is relatively abundant by about 2.7% of the Earth's crust with three isotopes: ^{24}Mg(79%), ^{25}Mg(10%) and ^{26}Mg(11%). Magnesium is not existed as a metal in the nature but as ores or compounds. The synthesis of magnesium hydride goes back around 100 years by using the pyrolysis of ethylmagnesium halides to synthesize a mix of magnesium hydride, magnesium halide and ethylene. In 1951, the pure magnesium hydride was created for the first time by using the pyrolysis of diethylmagnesium at a temperature level of 400 K in vacuum. More recently, the reaction of magnesium with hydrogen at 850K under 200bar with the help of a catalyst that allows creating magnesium hydride:

$$Mg + H_2 \rightarrow MgH_2 \qquad (1.2)$$

Magnesium is a shiny gray metal with an atomic weight of 24.305u and an ignition temperature of around 918°C in dry air. It has a hexagonal crystal structure with space group $P6_3/mmc$ and lattice parameters of a = 0.321nm and c = 0.521nm at ambient conditions [61].

Magnesium hydride is a white solid and is liable to ignite spontaneously on exposure to air. Its desorption temperature is about 573K which is lower than many other hydrides shown in Figure 1.7. This temperature is considered too high to be practically applicable in different devices [62].

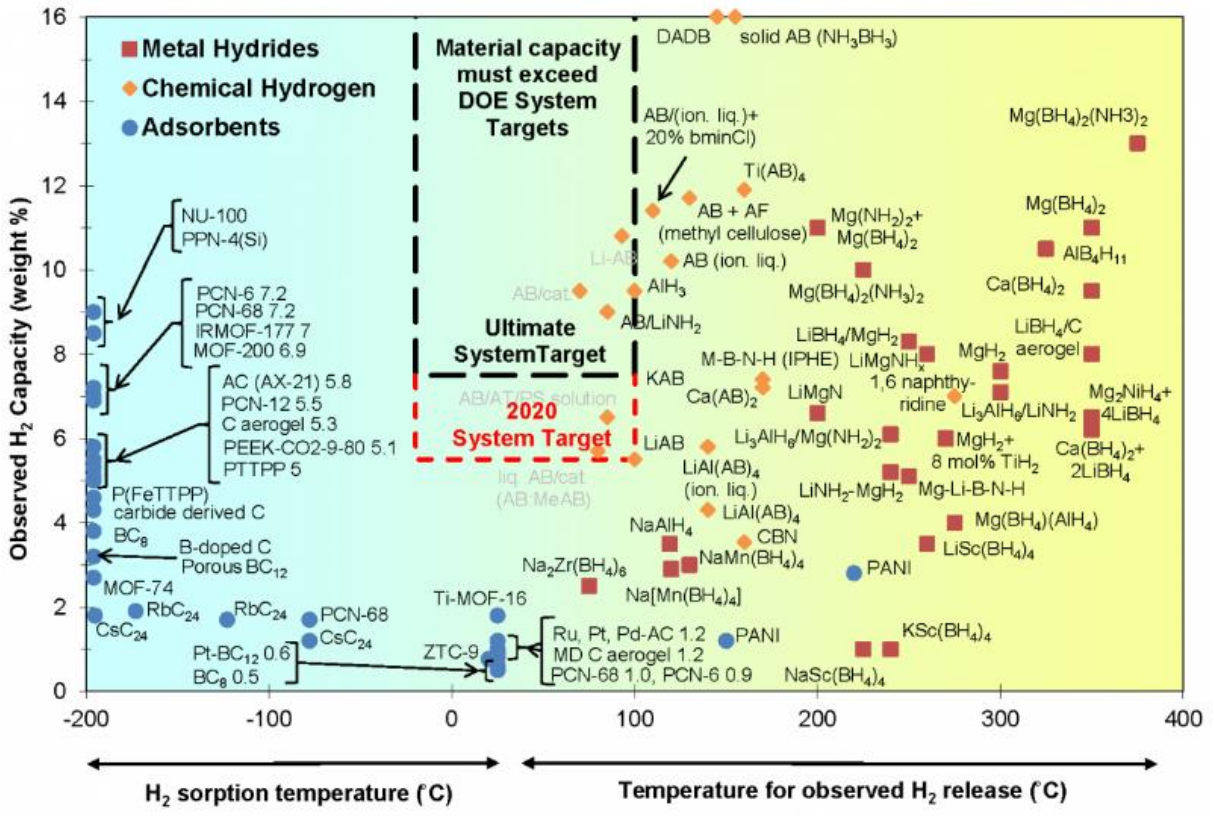

Figure 1.7: Gravimetric hydrogen capacity and desorption temperature of various hydrogen storage materials [63].

The interaction between metal and hydrogen is clarified by using the phase diagrams. The Pressure-Concentration-Temperature (PCT) diagrams are the most used diagrams for the hydride formation as shown in Figure 1.8. In order to plot the PCT diagram, the Van't Hoff equation allows relating the universal gas constant (R), the equilibrium pressure (P), the entropy change (ΔS) and the enthalpy changes (ΔH) of the hydride formation in one expression:

$$ln\, P = \frac{\Delta H}{R * T} - \frac{\Delta S}{R} \qquad (1.3)$$

Based on Figure 1.8, hydrogen gas starts to dissolve into the metal structure at low concentrations with increasing in the gaseous hydrogen pressure. At point 1, the hydride is locally formed by occupying the particular interstitial lattice sites. In the α-hydride phase, the atoms of hydrogen gas are randomly spread into the metal. Under idealized equilibrium conditions, the pressure of hydrogen gas becomes constant with absorbing hydrogen inside the metal, resulting in a transformation from the α phase into β phase. In the β phase, an organized structure is formed between the atoms of hydrogen gas and the metal. The transformation from the α phase into β phase is completely realized at point 2. Both length and slope of the equilibrium plateau provide a major importance for various hydrogen storage applications such as hydrogen vehicles. By increasing or decreasing the hydrogen pressure above or below the plateau pressure, hydrogen can be absorbed for forming the β phase or desorbed from a metal for transforming the hydride into the α phase.

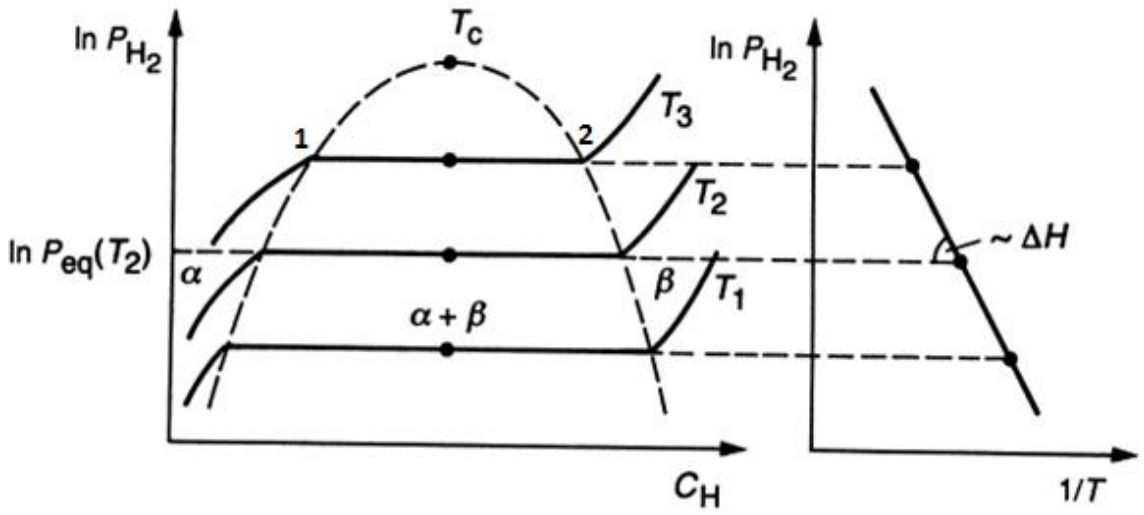

Figure 1.8: Pressure-composition-temperature diagram for the formation of hydrides [64].

In the case of magnesium hydride, the hydrogen gas molecules reach the metal surface. Then, the molecules are dissociated into atoms of hydrogen. Subsequently, the atoms of hydrogen are dissolved into the crystal structure of the metal. Finally, the atoms of hydrogen react with the metal to form the magnesium hydride.

In other words, hydrogen gas enters to the hexagonally close-packed (HCP) Mg metal lattice, the hydrogen atoms initially localize in the tetrahedral interstitial sites, forming the so-called α-phase of magnesium hydride (α-MgH_2 phase). Upon further addition of hydrogen, the so-called β-phase of magnesium hydride (β-MgH_2 phase) is formed. It has a body center tetragonal lattice of rutile type with space group $P4_2/mnm$ and lattice parameters a = 0.452nm

and c = 0.302nm [65]. With a high compressive stress (7–8GPa), β-MgH_2 phase is converted into the metastable γ-phase of magnesium hydride (γ-MgH_2 phase) [66]. This phase has an orthorhombic crystal structure analogous to α-PbO_2 phase with lattice parameters a = 0.453nm, b = 0.544nm, and c = 0.493nm and space group Pbcn [67, 68].

1.2.2 Improving the thermodynamic properties of MgH2

The reaction between hydrogen and magnesium (equation 1.2) is an exothermic reaction with a heat of formation of −75kJ/mol.H_2 and an entropy variation of −0.135kJ/mol.H_2 for the formation of magnesium hydride. However, the corresponding formation energy is still too high (−75kJ/mol.H_2) in comparison with the ideal formation energy –40 kJ/mol.H_2. Consequently, the decomposition temperature of MgH_2 is also too high because it still needs to improve in order to reach the optimum range for automotive applications.

The high formation energy and decomposition temperature represent a major obstacle and challenge to utilize this hydride for hydrogen storage. Furthermore, the slow hydrogen absorption/desorption kinetics are also another drawback in MgH_2. In addition, heat management is required for storing and maintaining the magnesium hydride during hydrogenation and dehydrogenation reaction. A range of improvements have been made to reduce the formation energy and speed up the kinetics into MgH_2 (e.g., transition metals).

1.2.2.1 Transition metals

The doping by transition metals (Ti, Fe, Co, Ni, Mn, Nb, V, Zr, etc.) has been regarded as one of the most successful methods to improve the thermodynamic properties of MgH_2. In the last few years, several transition metals have been treated and researched by different laboratories and institutions worldwide, including:

- **Nickel (Ni)**

According to recent studies, the transition metals doped in MgH_2 showed a great effect on developing the material and improving its hydrogen storage properties including the energy of formation and the temperature of desorption. Among all the transition metals (Fe, V, Co, Mn, Ti, Zr, Ni, Nb, etc) researched in recent years, nickel is considered as the mostly adopted for MgH_2. In 2005, Hanada and his co-authors [69] mixed powder of MgH_2 with Ni metal by using ball milling method to form the MgH_2+nano-Ni composite. The results were excellent, so that the hydrogen desorption peak of the MgH_2+nano-Ni composite reduced to a temperature of around 260°C compared to that of pure MgH_2 (370°C). In addition, other factors were also

confirmed for the features of Ni nanoparticles like the kinetic properties. Xie and his co-authors [70] showed that the MgH_2 doped with 10% of concentration of Ni nanoparticles can desorb about 6.1 wt.% within ten minutes at 250°C.

- **Titanium (Ti)**

Compared to nickel, titanium is also a good candidate to be used as a catalyst for improving the thermodynamic properties of magnesium hydride. Liang and his co-authors [71] investigated the mechanism of titanium through X-ray Powder Diffraction. They found using mechanical milling that the TiH_2 phase, which was formed by reacting MgH_2 with Ti, was very stable. The results also showed that hydrogen could be desorbed completely within 1000 s at a temperature of about 250°C for the MgH_2−5at%Ti composite while the pure MgH_2. In another work, the kinetic properties of magnesium hydride were investigated by Shao and his co-authors [72] for hydrogen storage applications.

1.2.2.2 Defects

The point defect is a new approach to enhance the dehydrogenation performance of MgH_2 by creating vacancies inside the material, and this method is investigated for the first time in our previous studies in addressing the problems and challenges of hydrogen storage. The point defects take a major place in different applications such as insulator semiconductor and metal physics [73, 74, 75]. Defects have a major influence on materials properties and can be used to control their properties. Small amounts of defects are sufficient to change the properties of materials. Ab-initio calculations have already an important area to understand the fundamental mechanisms of defects in different solids, and discover the fundamental processes that control and vary doping and defects [73].

A defect refers to any imperfection and deviation in the arrangement of atoms in a crystalline solid. Defects can be mainly categorized into four classifications according to their dimension:

- **Point defects:** placed imperfectly in crystals that occur only around or at a single lattice point with lattice defects of zero dimensionality.
- **Line defects:** are rows of atoms that are misaligned with lattice defects of one dimensionality.
- **Planar defects:** localized imperfections in crystals that occur a discontinuity of the perfect atomic arrangement across a surface with two dimensionality.

- **Extended defects:** formed from different defects that are combined together in a small crystal region of a solid with three dimensionality.

Point defects are primarily divided into six types including:

- **Vacancies** are lattice sites being vacant due to missing atoms in the crystal. In other terms, a vacancy defect is a missing atom from its normal place that it would occupied in the crystal (see Figure 1.9).
- **Interstitials:** when an extra atom is localizing in an unoccupied site in the crystal structure so that there is not an atom in this site, this kind of defect is called interstitial defect.
- **Frenkel defects:** when an atom is displacing from its lattice site to a nearby interstitial site in the crystal structure, this kind of defect is named Frenkel defect.
- **Substitutionals:** when a host atom is replaced by an extra atom, this defect is named substitutional defects.

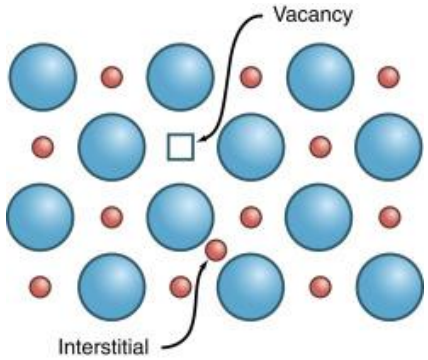

Figure 1.9: Vacancy defect in a crystalline structure [76].

Sputtering or ion irradiation are typically used to create vacancy defects in solids with controlling the desired concentrations. Sputtering uses energetic particles of a plasma or gas to bombard the structure of the solid material. Ion irradiation uses energetic ions that are shot on the material.

1.3 Conclusion

The thesis is based on the vacancy defects as a new method for improving the dehydrogenation of magnesium hydride and its capacity of storage. Therefore, the mechanism of this method will be explained practically and analytically in the chapter 3. The knowledge showed in this chapter will be used to evaluate the thermodynamic and electronic properties of

defects into the MgH_2 hydride using the Korringa-Kohn-Rostoker (KKR) method combined with the coherent potential approximation.

2 Density Functional Theory

Contents

2.1 Introduction

The study of structures of materials and their properties can be realized using the computation methods, which are valuable and useful to develop materials and their applications. They also offer an alternative way to interpret and explain the experimental results. This chapter aims to highlight one of the theoretical frameworks, which are widely used for the electronic structure calculations of materials in the field of condensed matter. The density functional theory (DFT) represents the basis of this thesis in calculating the electronic structure of defects and doping in the magnesium hydride and the lithium hydride. Therefore, the approach of the density functional theory is explained and discussed in the following sections.

2.2 The time-independent Schrödinger equation

The Schrödinger equation allows describing the atomic nuclei and the surrounding electrons of a crystal using a partial differential equation independent of multi-body time:

$$\hat{H}\psi(r_1, r_2, \dots, R_1, R_2, \dots) = E\psi(r_1, r_2, \dots, R_1, R_2, \dots) \quad (2.1)$$

where ψ is the many-body wave function of electrons, E is the electronic energy of the system, R_i and r_i are the positions of the ions and electrons respectively, and H is the Hamiltonian of the system, which is given upon the following terms:

$$\hat{H} = -\sum_i \frac{\hbar^2 \nabla_i^2}{2m_e} - \sum_I \frac{\hbar^2 \nabla_I^2}{2M_I} + \frac{1}{2}\sum_{i \neq j} \frac{e^2}{|r_i - r_j|} + \frac{1}{2}\sum_{I \neq J} \frac{Z_I Z_J e^2}{|R_I - R_J|} - \sum_{i,I} \frac{Z_I e^2}{|r_i - R_I|} \quad (2.2)$$

where ħ is Planck's constant devised by 2π, M_I and Z_I denote, respectively, the atomic mass and charge of the nucleus, and e and m_e indicate the charge and the mass of the electron respectively.

In the expression above, the first term refers to the kinetic energy of the electrons (T_e) and the second one to that of the nuclei (T_n). The reminder terms correspond to the Coulomb interactions of nucleus-nucleus (V_{nn}), electron-electron (internal potential V_{int}), and nucleus-electron (external potential V_{ext}). So, the fundamental Hamiltonian simply reads as:

$$\hat{H} = T_e + T_N + V_{int} + V_{nn} + V_{ext} \quad (2.3)$$

A number of approximations are mainly used to solve this kind of quantum many-body problem. Some of them are briefly discussed and explained in the next sections.

2.3 Born-Oppenheimer approximation

The Born-Oppenheimer approximation is the first approach to simplify the Schrödinger equation of the coupled nuclei-electrons system. This approach was proposed by Both Julius Robert Oppenheimer and Max Born in 1927 [77]. It is mainly based on the fact that the mass of the electrons is much less than that of the nuclei, and the velocity of the electrons is much larger than that of the nuclei, thus, the kinetic energy of the nuclei (T_n) is ignored in the expression above. Consequently, the nuclei are fixed (or frozen) at positions R_I with a time-independent potential (V_{nn}), and the total electronic Hamiltonian can be written as:

$$\widehat{H} \simeq T_e + V_{int} + V_{nn} + V_{ext} \tag{2.4}$$

In this approach, the many electron wave function depends parametrically (not variably) upon the coordinates of the nuclei, so the electronic Hamiltonian can be given as follows:

$$H = T_e + V_{int} + V_{ext} \tag{2.5}$$

The Schrödinger equation is rewritten as follows:

$$H\psi(r_1, r_2, \dots) = E_{elec}\psi(r_1, r_2, \dots) \tag{2.6}$$

The parametric dependence of ψ_{elec} on R_I is omitted explicitly in the Schrödinger equation. Then, the total energy E_{tot} is the sum between the Coulomb interaction of nucleus-nucleus and E_{elec}:

$$E_{tot} =< H > + E_{nuc} = E_{elec} + E_{nuc} \tag{2.7}$$

We note here that the Coulomb interactions term of nucleus-nucleus (V_{nn}) becomes just a classical constant E_{nuc}.

2.4 Hartree approximation

The Hartree approximation can be considered as the simplest solution for the Schrödinger equation [78, 79, 80]. Such an approximation, the many-body equation is formulated as a one-particle equation and the many-body wave function is then given as follows:

$$\psi(r_1, r_2, \dots, r_N) = \prod_{i=1}^{N} \psi(r_i) \tag{2.8}$$

$$\psi(r_1, r_2, \dots, r_N) = \psi_1(r_1) * \psi_2(r_2) \dots \psi_n(r_N) \tag{2.9}$$

In quantum theory, the variational method allows calculating the minimal approximate energy for any trail wave function ϕ

$$E[\phi] = \frac{\langle \phi | H | \phi \rangle}{\langle \phi | \phi \rangle} \geq E_0 \tag{2.10}$$

Now equation 2.6 can be used with the variational method to express the Hartree equation:

$$\left[-\sum_i \frac{\nabla_i^2}{2} - \sum_I \frac{Z_I}{|r_i - R_I|} + \sum_{j \neq i} \int dr_j \psi_j^*(r_j) \frac{1}{|r_i - r_j|} \psi_j(r_j) \right] \psi_i(r_i) = \epsilon_i \psi_i^*(r_i) \tag{2.11}$$

Due to this approximation, each independent electron i feels an effective potential of all electrons by the integration over the density of these electrons. Thus, the complicated many-body problem is replaced by n simpler one-electron equations and since the effective potential for each wave function depends on all other wave functions, this problem can be solved iteratively in a mean field potential.

2.5 The Hartree-Fock approximation

The previous approximation excludes the electron spins and their fermionic nature, consequently, the Pauli principle is not satisfied too. Besides this, the Hartree approximation neglects the fact that the wave function, for electrons as Fermi particles, has to be antisymmetric by the exchange of particles.

$$\psi(r_1, \dots r_k, \dots r_m, \dots r_N) = -\psi(r_1, \dots r_m, \dots r_k, \dots r_N) \tag{2.12}$$

This can be corrected using the Fock assumption, which incorporates the fermionic nature of electrons and guarantees its antisymmetry. It states that the many electron wave function should be written as a single Slater determinant [81, 82] instead of the product in Hartree approach, as follows:

$$\psi(r_1, r_2, \dots r_N) = \frac{1}{\sqrt{N!}} \begin{vmatrix} \phi_1(r_1) & \phi_1(r_2) & \cdots & \phi_1(r_n) \\ \phi_2(r_1) & \phi_2(r_2) & \cdots & \phi_2(r_n) \\ \vdots & \vdots & \cdots & \vdots \\ \phi_n(r_1) & \phi_n(r_2) & \dots & \phi_n(r_n) \end{vmatrix} \tag{2.13}$$

where N represents an N-electron system. Each column and line represent a certain position in space and a certain one-electron state, respectively. In this determinant, the sign of the wave function is changed when two lines or columns interchange. In addition, such a wave function guarantees that the Pauli principle is not violated in order to have a physically possible situation.

According to the variational principle and the single Slater determinant with equation 2.6, the Hartree-Fock equation can be defined as follows:

$$\left[-\sum_i \frac{\nabla_i^2}{2} - \sum_I \frac{Z_I}{|r_i - R_I|} + \sum_j \int dr_j \phi_j^*(r_j) \frac{1}{|r_i - r_j|} \phi_j(r_j)\right] \phi_i(r_i)$$
$$- \sum_j \left[\int dr_j \phi_j^*(r_j) \frac{1}{|r_i - r_j|} \phi_i(r_j)\right] \phi_j(r_i) = \epsilon_i \phi_i^*(r_i) \quad (2.14)$$

This equation is composed of an extra term in comparison with the Hartree equation. This extra term is called the exchange potential that describes the effects of exchange between electrons in Hartree-Fock wave function.

2.6 Basics of density functional theory

To solve the many-electron Schrödinger equation, a range of tools was developed to obtain the optimal physical quantities containing the more information. These tools are including: the coupled cluster method [83], the configuration interaction approach [84] or the Møller-Plesset perturbation theory [85]. In this point, Density functional theory (DFT) is considered as one of the optimal solutions of the Schrödinger equation for n electrons. The basis of DFT is explained and discussed in the following sections.

2.7 The Hohenberg-Kohn theorems

DFT is based on two fundamental and basic theorems introduced by Hohenberg-Kohn [86] and extended by Kohn-Sham [87]:

- **Theorem I:** For any system of interacting particles in an external potential $V_{ext}(r)$, the potential $V_{ext}(r)$ is determined uniquely, except for a constant, by the ground state density $n_0(r)$.
- **Theorem II:** A universal functional for the energy E[n] in terms of the density n(r) can be defined, valid for any external potential $V_{ext}(r)$. The exact ground state energy of the system is the global minimum of this functional and the density that minimizes the functional is the exact ground state density $n_0(r)$.

The first theorem indicates that the ground state energy of the many electron system is a unique functional of the electron number density n(r) which determines uniquely the external potential, the Hamiltonian and all the characteristic of the system:

$$E_{HK}[n] = T_e[n] + E_{int}[n] + E_{ext}[n] = F_{HK}[n] + \int n(r) V_{ext}(r) dr \quad (2.15)$$

$$F_{HK}[n] = T_e[n] + E_{int}[n] \quad (2.16)$$

where $F_{HK}[n]$ is the Hohenberg-Kohn universal functional which is separated into two terms: the functional of the Coulomb interaction of electron-electron and the functional of the kinetic energy.

The second theorem indicates that the exact groundstate energy of the system is the global minimum of FHK. This theorem can be obtained variationally:

$$E_0 \leq E_{HK}[n] = F_{HK}[n] + \int n(r)V_{ext}(r)dr \qquad (2.17)$$

2.8 Kohn-Sham equations

The formalism of the HK theorems was better developed by Kohn and Sham in 1965 [87]. Their approach states that the original system of interacting electrons with a particular external potential V_{ext} may be similar to a system of non-interacting electrons moving in an effective potential V_{KS} from all other electrons. Therefore, the Kohn-Sham method is considered an exact approach of the HK theorems because the same ground state density is used, and an explicit algorithm is provided by this approach for calculating the density and the ground state energy.

As mentioned above, the Hohenberg-Kohn ground state energy can be given as:

$$E_0 = min_{\psi \to n}\left(F_{KS}[n] + \int n(r)V_{ext}(r)dr\right) \qquad (2.18)$$

where the functionals for the Coulomb interaction and the kinetic energy are expressed in the Hohenberg-Kohn universal functional F_{HK}, and the minimizations over wave functions are performed, which leads to a certain density. All densities derived from wave functions can be defined from this functional. These densities are known as "N-representable" that are formulated by Lieb and Levy [88, 89]. The number of electrons is equal and constant to the summation of all densities in the solid.

$$N = \int_V n(r)dr \qquad (2.19)$$

Now the Kohn-Sham method recommends to perform the calculations using the exact kinetic energy T_{KS} of a non-interacting system with an identical density of the interacting one

$$T_{KS} = -\frac{1}{2}\sum_{i}^{N}\langle\phi_i|\nabla^2|\phi_i\rangle \qquad (2.20)$$

$$n_{KS}(r) = \sum_{i}^{N} |\phi_i(r)|^2 = n(r) \tag{2.21}$$

Thus, according to Kohn and Sham theory, we can separate the functional $F_{KS}[n]$ as follows:

$$F_{KS}[n] = T_{KS}[n] + E_H[n] + E_{XC}[n] \tag{2.22}$$

where $F_{KS}[n]$ is composed of three essential terms: the classical Coulomb interaction, the Kohn-Sham kinetic energy and the exchange-correlation energy. The comparison between this Kohn-Sham functional with the Hohenberg-Kohn functional, the exchange-correlation energy can be written as follows:

$$E_{XC}[n] = (T_e[n] - T_{KS}[n]) + (E_{int}[n] - E_H[n]) \tag{2.23}$$

Therefore, the exchange-correlation energy contains all the many-body effects that are unknown about the system and are not present in the kinetic energy and Coulomb interaction terms. So the Schrodinger-like equations called the Kohn-Sham equations are determined by the N lowest energy solutions of:

$$\left[-\frac{\nabla^2}{2} + V_{KS}(r)\right]\phi_i(r) = \epsilon_i \phi_i(r) \tag{2.24}$$

where V_{KS} is the effective Kohn-Sham potential in which the electrons move, and is expressed as follows:

$$V_{KS}(r) = V_{ext} + V_H + V_{XC} = -\sum_{I} \frac{Z_I}{|r_i - R_I|} + \int \frac{n(r')dr'}{|r - r'|} + \frac{\delta E_{XC}[n(r)]}{\delta[n(r)]} \tag{2.25}$$

and

$$\left(-\frac{\nabla^2}{2} V_{ext} + V_H + \frac{\delta E_{XC}[n(r)]}{\delta[n(r)]}\right)\phi_i(r) = \epsilon_i \phi_i(r) \tag{2.26}$$

The Kohn-Sham equations can be solved self-consistently and the orbitals Φi(r) give the electron density using $n_{KS}(r) = \sum_i^N |\phi_i(r)|^2 = n(r)$ (2.21) for obtaining the next iteration for n(r).

2.9 The exchange-correlation energy

Although the Kohn-Sham method offers an exact total energy, the so-called exchange-correlation energy functional as a term is still not known and then the solution of the Kohn-Sham equations is not possible. This section will discuss and explain some approximative expressions for the exchange-correlation energy.

2.9.1 The local density approximation

The Local density approximation (LDA) [90, 91] is considered as the first approximation and the simplest expression for the exchange-correlation energy as compared to other approximative expressions. The LDA approximation is mainly related to the uniform electron gas in its principle. The XC energy per particle of a homogeneous electron gas $\epsilon_{XC}(\mathrm{n(r)})$ equals to the local XC energy per particle with the same local density. Therefore, the expression of XC energy is given in the following form:

$$E_{XC}^{LDA}(n) = \int n(r)\epsilon_{XC}(n(r))\, dr \qquad (2.27)$$

Thus, the E_{XC} only depends upon the value of the electronic density at each point on the space. The expression $\epsilon_{XC}(\mathrm{n(r)})$ can be separated into two contributions: exchange and correlation.

$$\epsilon_{XC}\big(n(r)\big) = \epsilon_X\big(n(r)\big) + \epsilon_C\big(n(r)\big) \qquad (2.28)$$

where ϵ_X represents the exchange part of an electron in a homogeneous electron gas of a particular density, and this contribution is given by [92, 93]

$$\epsilon_X = -\frac{3}{4}\left(\frac{3n(r)}{\pi}\right)^{1/3} \qquad (2.29)$$

The correlation part ϵ_C does not have an explicit expression, so a number of approaches have been proposed. As an example, Ceperly and Alder in 1980 presented a numerical solution for ϵ_C by using an accurate numerical quantum Monte-Carlo simulations of the homogeneous electron gas [94] or Perdew and Wang who proposed another approximative expression for ϵ_C in 1992 [95].

The local density approximation depends on the local nature of the XC potential and on the assumption that the densities have a slow variation in order to have an accurate LDA for systems [87]. The accuracy of LDA is surprisingly good and acceptable in terms of several properties of crystal including structural parameters, binding trends, bond lengths, phonon spectra, vibrational energies and others. However, this approximation usually overestimates the binding energy, and underestimates both the band gap and the bond lengths [96]. For this reason, this moderate accuracy of LDA approximation is not sufficient for various applications.

2.9.2 The generalized gradient approximation

The generalized gradient approximation (GGA) for the XC energy functional generally includes extra information and improves the local density description (LDA) of crystals. The GGA approximation goes beyond the LDA approximation by utilizing not only the information about the density at a specific point (n(r)), but also by utilizing the density in the local vicinity through the dependence on the gradient (∇n(r)). Consequently, the GGA takes into consideration the non-homogeneity of the true electron density, so, the XC energy can be written in the following form:

$$E_{XC}^{GGA}(n) = \int n(r)\epsilon_{XC}(n(r), \nabla n(r))\, dr \qquad (2.30)$$

The accuracy of GGA approximation leads to a correct picture of bond lengths, binding energies and other properties than LDA. The GGA method has a range of forms that are used in different computations. In this thesis, we used two essential forms for our computations: the Perdew-Burke-Ernzerhof form (PBE) [97] and the Perdew and Wang form (PW91) [95].

2.10 Korringa-Kohn-Rostoker Green's function method

Initially, the first developer of the Korringa-Kohn-Rostoker (KKR) method was Korringa in 1947 [98] who used the multiple-scattering theory to find a solution for the Schrödinger equation. After seven years, Kohn and Rostoker [99] introduced another method that is equivalent to the Korringa one but this time by using Green's functions; this method is called in our days the Korringa-Kohn-Rostoker method.

To meet the physical properties of randomly disordered systems in the KKR method, the coherent potential approximation [100] is one of the most common methods in the calculation of the electronic and thermodynamic properties of such systems. In comparison with to the supercell method, the coherent potential approximation approach is more efficient for systematic systems design due to its ability to choose any arbitrary concentrations and computational speed.

2.11 Conclusion

In this chapter, the different mechanisms of ab-initio calculations in this thesis have been highlighted in order to inspect and evaluate the thermodynamic and electronic properties for the magnesium hydride (MgH_2) and the lithium hydride (LiH). The total energy of the studied hydrides is calculated by using DFT calculations for different concentrations of

magnesium/lithium vacancy defects with or without hydrogen dopant atoms, then the thermodynamic and electronic properties are deduced and explained using the analysis of the density of states (DOS).

3 Study of the thermodynamics of magnesium hydride by first principles calculations

Contents

3.1 Introduction

Up to day, the magnesium hydride (MgH_2) is considered as one of the most promising materials for hydrogen storage applications with the advantages of high gravimetric capacity (7.6wt.%) and high volumetric capacity (110gH_2/l) as well as high energy density (9MJ/kg Mg) [8, 9, 10, 11, 12, 13, 14, 15, 16, 17]. However, MgH_2 has some challenges including a high formation energy (ΔH = -75KJ/mol) and a high desorption temperature (above 573K) as well as the slow kinetics of absorption and desorption of hydrogen [13, 14, 15, 16, 17, 18].

There are a variety of attempts and improvements to overcome and address these challenges. Experimentally, it was found by using the ball-milling method that the doping with the transition metals or their oxides into the MgH_2 hydride improve its thermodynamic characteristics by decreasing the desorption temperature into MgH_2 [16, 17, 101, 102]. Theoretically, a number of theoretical calculations showed the alloying effects on the thermodynamic properties into MgH_2 [103, 104, 105].

Using the first principles calculations, this chapter aims to study the formation energy and the desorption temperature of MgH_2 for clarifying and understanding the mechanisms which make the material very stable thermodynamically. The calculated findings are supported by using an analysis of the density of states (DOS) to give a plausible explanation.

Then, the effect of magnesium vacancy defects into MgH_2 with or without hydrogen dopant atoms are investigated to address the problems of the thermodynamic properties of magnesium hydride for decreasing both the stability and the desorption temperature and increasing both the formation energy and the gravimetric capacity.

3.2 Thermodynamic properties of the pure MgH_2 from DFT method

3.2.1 Computational method

To calculate the total energy of the studied hydrides, the first principles calculations based on the Korringa-Kohn-Rostoker-Green's function method [106] is used to solve the Kohn-Sham equations. The exchange-correlation energy functional was parameterized by applying the generalized gradient approximation (GGA) with two essential forms for our computations: the Perdew-Burke-Ernzerhof form (PBE) [97] and the Perdew and Wang form (PW91) [95]. To guarantee an acceptable accuracy and precision in our computations, we used a precision of 10^{-6} for the self-consistent field (SCF) iterations. In addition, a mesh of (10×10×10) k-points

in the Brillouin zone is chosen to ensure more precision in our computation. The scalar-relativistic scheme is used to calculate the total energy for all studied systems.

At ambient conditions, the magnesium hydride MgH_2 (Figure 3.1) has a rutile-type structure with space group $P4_2/mnm$ (N°136) [107, 108]. The atomic positions of Mg atoms are located at (0, 0, 0) and (0.5a, 0.5b, 0.5c) and that of H atoms are (0.304a, 0.304 b, 0), (0.696a, 0.696 b, 0), (0.804a, 0.196 b, 0.5c) and (0.196a, 0.804 b, 0.5c). The lattice parameters for the studied systems are the experimental values, a = b = 4.501 A and c = 3.01 A for MgH_2 [107], and a = b = 3.210 A and c = 5,210 A for Mg [61]. The electronic structure of hydrogen is $1s^1$ and that of magnesium is $1s^22s^22p^63s^2$.

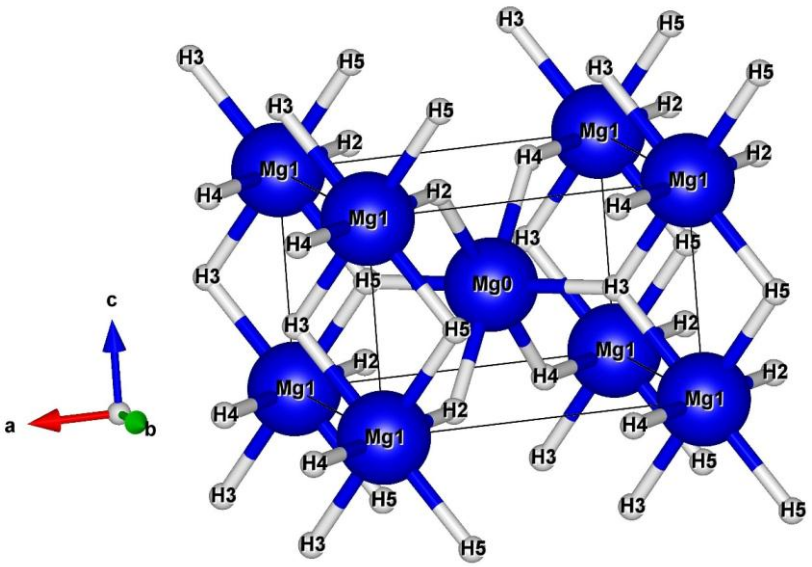

Figure 3.1: Crystal structure of magnesium hydride MgH_2.

3.2.2 Thermodynamic properties of MgH_2

3.2.2.1 Equilibrium lattice parameters

To study the thermodynamics of magnesium hydride, we first examine the structural properties using the relaxation method. The optimization of the MgH_2 and Mg structures is evaluated by calculating the total energy for each variation in the cell volume (a*b*c), Figure 3.2. Our findings are shown in

Table 3.**1**. It observes that the relaxed parameters for the pure magnesium hydride are a = b = 4.601A and c = 3.050A as well as the ratio c/a = 0.6629, and for the magnesium element are a = b = 3.210A, c = 5.200A and c/a = 1.620. These results are consistent with the experimental values obtained in other works [61, 107].

Table 3.1: Formation energy, desorption temperature and total energies of MgH_2 and Mg.

Elements	Relaxed parameters (Å)	Crystal structure	Total energy (Ry/f.u)	Formation energy (KJ/mol.H_2)	Desorption temperature (K)
MgH_2	a = b = 4.601 c = 3.050	Rutile	-403.05358	-88.571	677.67
Mg	a = b = 3.210 c = 5.200	HCP	-400.66611		

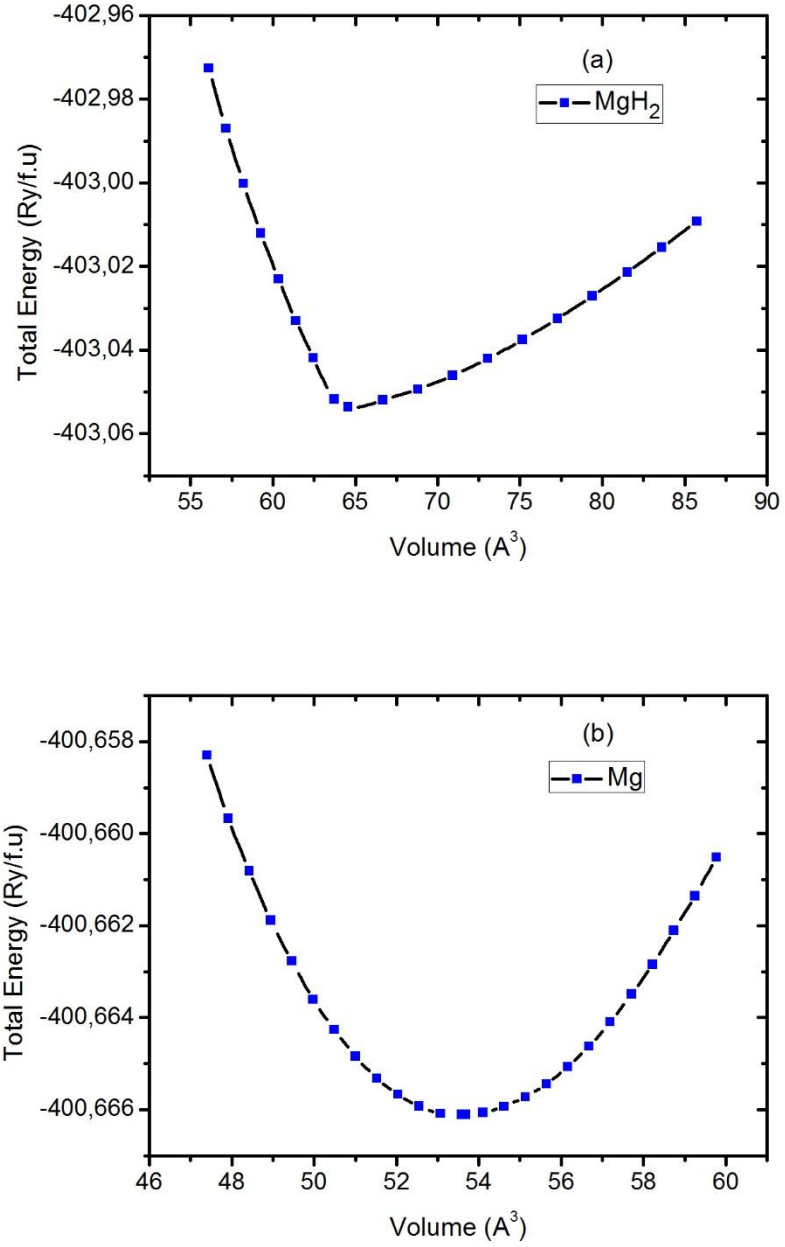

Figure 3.2: Total energy as a function of unit cell volume for (a) MgH_2 and (b) Mg.

3.2.2.2 Heat of formation and temperature of desorption

To study the thermodynamic properties of magnesium hydride, two fundamental parameters in the thermodynamics are needed: the heat of formation (ΔH) and the temperature of desorption (T_{des}). The MgH_2 hydride is formed according to the reaction between Mg and H_2:

$$Mg + H_2 \rightarrow MgH_2 \tag{3.1}$$

The formation energy of the MgH_2 hydride is calculated by subtracting the total energies of magnesium element and hydrogen molecule from that of magnesium hydride obtained by the relaxation method:

$$\Delta H = \sum E_{tot}(products) - \sum E_{tot}(reactants) \tag{3.2}$$

$$\Delta H(MgH_2) = E_{tot}(MgH_2)_{relax} - E_{tot}(Mg)_{relax} - E_{tot}(H_2) \tag{3.3}$$

The total energy of magnesium hydride and that of magnesium are calculated using the KKR-CPA method and shown in

Table 3.**1**. While the total energy of hydrogen, $E_{tot}(H_2) = -2.320 \text{Ry/f.u}$, is taken from [109]. Based on our calculation, the calculated formation energy of the pure MgH_2 is -88.57KJ/mol.H_2. This result is consistent with the previous theoretical and experimental values obtained using different methods: -85.709KJ/mol.H_2 [103] and -82KJ/mol.H_2 [110], respectively. It should be noted that the small difference observed between different values is primarily related to different approaches and methods used in DFT calculations.

The decomposition temperature for the studied systems can be determined using the standard Gibbs energy, where ΔH and ΔS are the enthalpy and entropy changes of the hydride formation, respectively:

$$\Delta G = \Delta H - T\Delta S \tag{3.4}$$

In equilibrium, the decomposition temperature of the hydride can be estimated by the following expression:

$$T_{des} = \frac{\Delta H}{\Delta S} \tag{3.5}$$

where the hydride entropy changes during dehydrogenation is related to the evolution of the hydrogen gas with a value of: ΔS = –130.7J/Kmol.H_2 [111]. Using the obtained formation

energy, the desorption temperature for the pure magnesium hydride is 677.67K. It is close to the previous works such as 673K [112].

The pure magnesium hydride has a gravimetric capacity of about 7.6wt.% and a volumetric capacity of about 110gH_2/l, which offer a successful candidate for the storage of hydrogen. However, the both high formation energy and desorption temperature of MgH_2 represent a major obstacle and challenge to utilize this hydride for mobile hydrogen storage.

3.2.3 Electronic structure

The electronic structure is evaluated using the density of states (DOS), which is the primary method to discover the chemical bonding properties of the studied hydrides and thus to clarify and explain the high stability in MgH_2. We plot, in Figure 3.3, the total and partial DOS of MgH_2 with using the same relaxed parameters and approximations in this calculation.

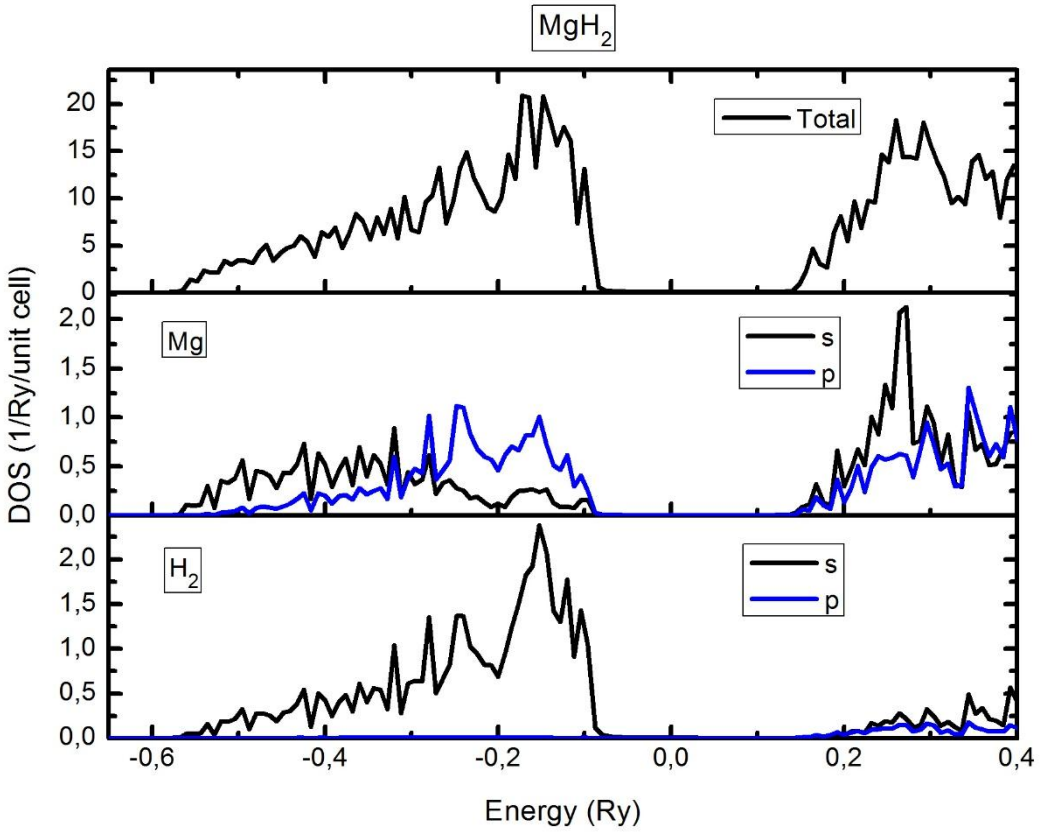

Figure 3.3: Total and partial DOS of MgH_2.

The energy gap (E_g) for the pure MgH_2 is equal to 3.048 eV, this value is agreed with the experimental and theoretical gaps such as 5.16 eV [113] and 3.9 eV [114], respectively. The different results between the experimental and theoretical gaps are well known in the ab initio calculations, because the GGA approximation underestimates the calculation of the gap.

For the pure MgH_2, the valance band (VB) is composed of two parts, the first one is mainly hybridized with the H-1s and Mg-3p states, and the second part is attributed to the Mg-3s and H-1s states. For the conduction band (CB), it is formed from Mg-2p, Mg-3s and a small account of H-1s states.

This demonstrates that a strong hybridization occurs mostly between hydrogen and magnesium atoms, which can be seen by the high formation energy and therefore the high stability and desorption temperature.

In this thesis, a new approach has been developed to improve the thermodynamic properties of MgH_2 by creating magnesium vacancy defects and introducing hydrogen atoms into the hydride, as we will see in the next sections.

3.3 Improving hydrogen storage properties in MgH_2 by magnesium vacancies

Using the first principles calculations based on the KKR-CPA method, the purpose of this part is to improve the thermodynamic properties, which involve the formation energy and the desorption temperature, by creating vacancy defects into the pure magnesium hydride. Our calculated findings are discussed and explained in detail below.

3.3.1 Thermodynamic properties of MgH_2 containing vacancy defects

The effect of the magnesium vacancy defects on the magnesium hydride was investigated by creating vacancy defects into magnesium hydride and varying their concentration until the value of the formation energy becomes zero.

The same equation in the last section (equation 3.2) is also used to calculate the heat of formation and determine the temperature of desorption for the magnesium hydride containing magnesium vacancy defects $Mg_{1-x}H_2$ with ($0.01 \leq x \leq 0.08$, where x is the concentration of magnesium vacancy defects):

$$Mg_{1-x} + H_2 \rightarrow Mg_{1-x}H_2. \quad (3.6)$$

$$\Delta H(Mg_{1-x}H_2) = E_{tot}(Mg_{1-x}H_2)_{relax} - E_{tot}(Mg_{1-x})_{relax} - E_{tot}(H_2) \quad (3.7)$$

The calculated total energies of the studied hydrides ($Mg_{1-x}H_2$ and Mg_{1-x}) are listed in Table 3.2.

Table 3.2: Formation energy, desorption temperature and total energies of $Mg_{1-x}H_2$ and Mg_{1-x}.

Concentration of magnesium vacancy defects (x)	$Mg_{1-x}H_2$			Mg_{1-x}			Formation energy (KJ/mol.H_2)	Desorption temperature (K)
	System	Total energy (Ry/f.u)	Crystal structure	System	Total energy (Ry/f.u)	Crystal structure		
0	MgH_2	-403.05358	Rutile	Mg	-400.66611	HCP	-88.571	677.67
0.01	$Mg_{0.99}H_2$	-399.03459		$Mg_{0.99}$	-396.65601		-76.901	588.38
0.02	$Mg_{0.98}H_2$	-395.01626		$Mg_{0.98}$	-392.64602		-65.953	504.61
0.03	$Mg_{0.97}H_2$	-390.99806		$Mg_{0.97}$	-388.63609		-55.096	421.55
0.04	$Mg_{0.96}H_2$	-386.97999		$Mg_{0.96}$	-384.62621		-44.345	339.29
0.05	$Mg_{0.95}H_2$	-382.96206		$Mg_{0.95}$	-380.61640		-33.685	257.73
0.06	$Mg_{0.94}H_2$	-378.94428		$Mg_{0.94}$	-376.60666		-23.131	176.98
0.07	$Mg_{0.93}H_2$	-374.92662		$Mg_{0.93}$	-372.59697		-12.668	96.92
0.08	$Mg_{0.92}H_2$	-370.90912		$Mg_{0.92}$	-368.58735		-2.324	17.78

The concentration of magnesium vacancy defects is varied from 1 to 8% (until the value of the formation energy becomes zero). According to equation 3.7, the different results of the calculated formation energy for the $Mg_{1-x}H_2$ hydrides are plotted in Figure 3.4. The calculated results demonstrate that when the concentration of Mg vacancies increases, the formation energy increases into the MgH_2 hydride. This leads to an improvement in the desorption temperature as we will see in the next paragraph.

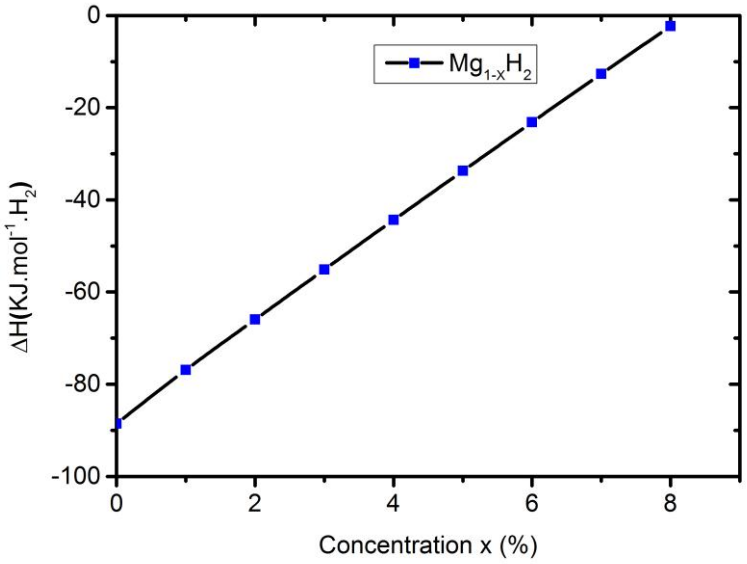

Figure 3.4: Formation energy as a function of concentration for MgH_2.

According to equation 3.5, the different results of the calculated desorption temperature for the $Mg_{1-x}H_2$ hydrides are plotted in

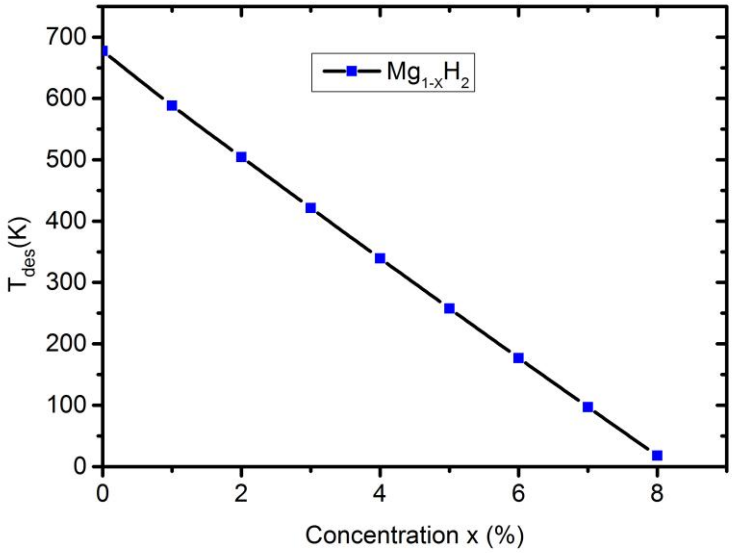

Figure 3.5. It demonstrates that when the concentration of Mg vacancies increases, the temperature of desorption decreases into the MgH_2 hydride. This decrease is not interesting beyond ~4.8%, because the obtained decomposition temperature deviates from the optimum range (289 – 393 K) for the practical use of a PEMFC in hydrogen storage applications [115]. Therefore, the optimal concentration for Mg vacancies is around 3.7%, where its temperature of desorption is close to the operating temperature of a PEMFC.

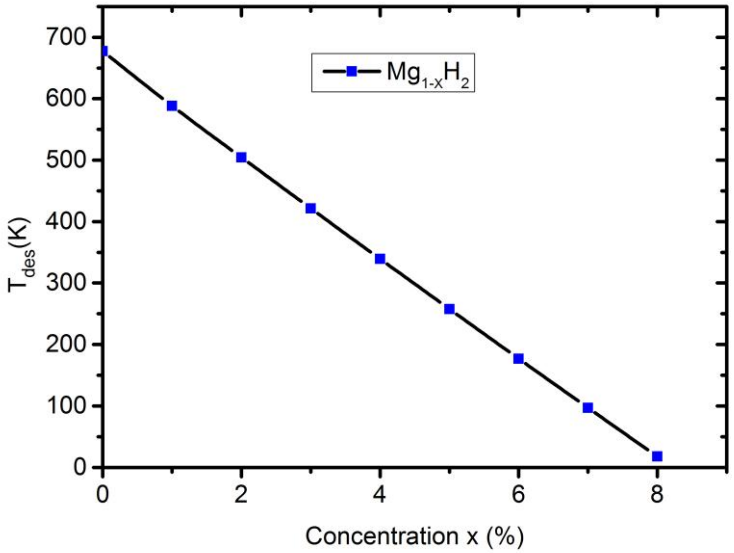

Figure 3.5 also shows that the small amounts of concentration allow getting superior modification impacts on the hydrogen storage properties of MgH_2

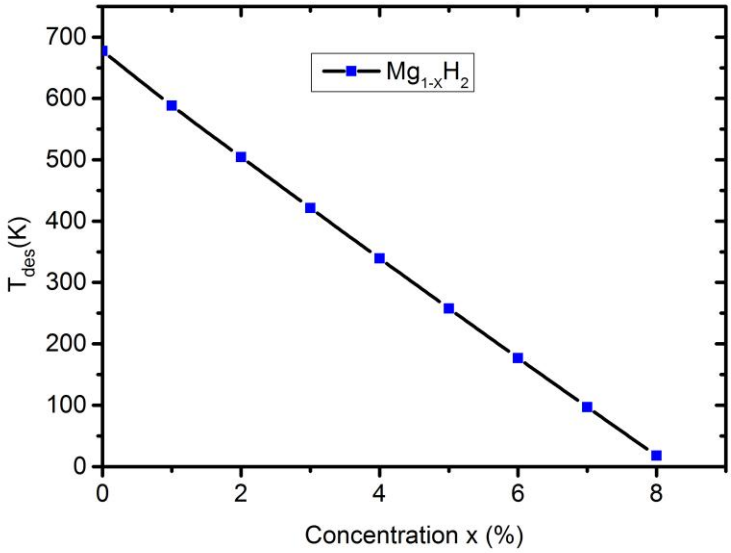

Figure 3.5: Desorption temperature as a function of concentration of vacancies for $Mg_{1-x}H_2$.

The high gravimetric capacity of MgH_2 has to be influenced by vacancy defects, so, in order to evaluate the effect of the concentration of Mg vacancy defects on the storage capacity of MgH_2, we use the following relation:

$$C_g = \frac{2*m(H)}{(1-x)*m(Mg)+2*m(H)} \qquad (3.8)$$

where m(H) = 1.00784u and m(Mg) = 24.305u are the atomic masses of hydrogen and magnesium, respectively. The observed behavior into the MgH_2 hydride is illustrated in Figure 3.6. We observe that the gravimetric hydrogen capacity of MgH_2 increases with increasing the concentration of magnesium vacancy defects from 7.658wt.% (x=0%) to 8.269wt.% for x=8%. This variation allows making the hydride more lightweight and useable in mobile applications.

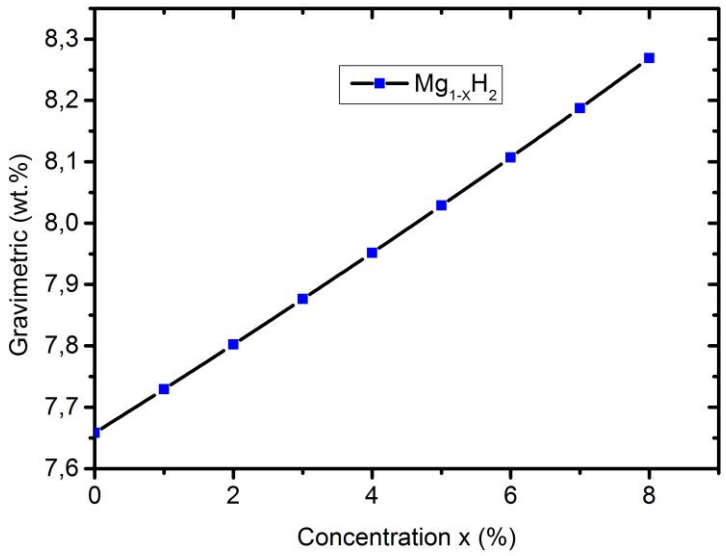

Figure 3.6: Gravimetric hydrogen capacity as a function of concentration for $Mg_{1-x}H_2$.

3.3.2 Electronic structure

The density of state (DOS) is investigated to clarify and explain the results of the effect of magnesium vacancies on MgH_2. We plot, in Figure 3.7, the total and partial DOS of the studied systems with using the relaxed parameters and the GGA approximation in this calculation.

Since the same behaviour of DOS is observed for different concentrations into MgH_2, we plot only the total and partial DOS of $Mg_{0.99}H_2$, $Mg_{0.952}H_2$ and $Mg_{0.92}H_2$. We can see that the Mg-2p, Mg-3s and H-1s states of MgH_2 shift from the valence band towards the conduction band and, consequently, the stability decreases into magnesium hydride. This leads to an improvement of the thermodynamic properties, which involve the heat of formation and the temperature of desorption, into the MgH_2 hydride.

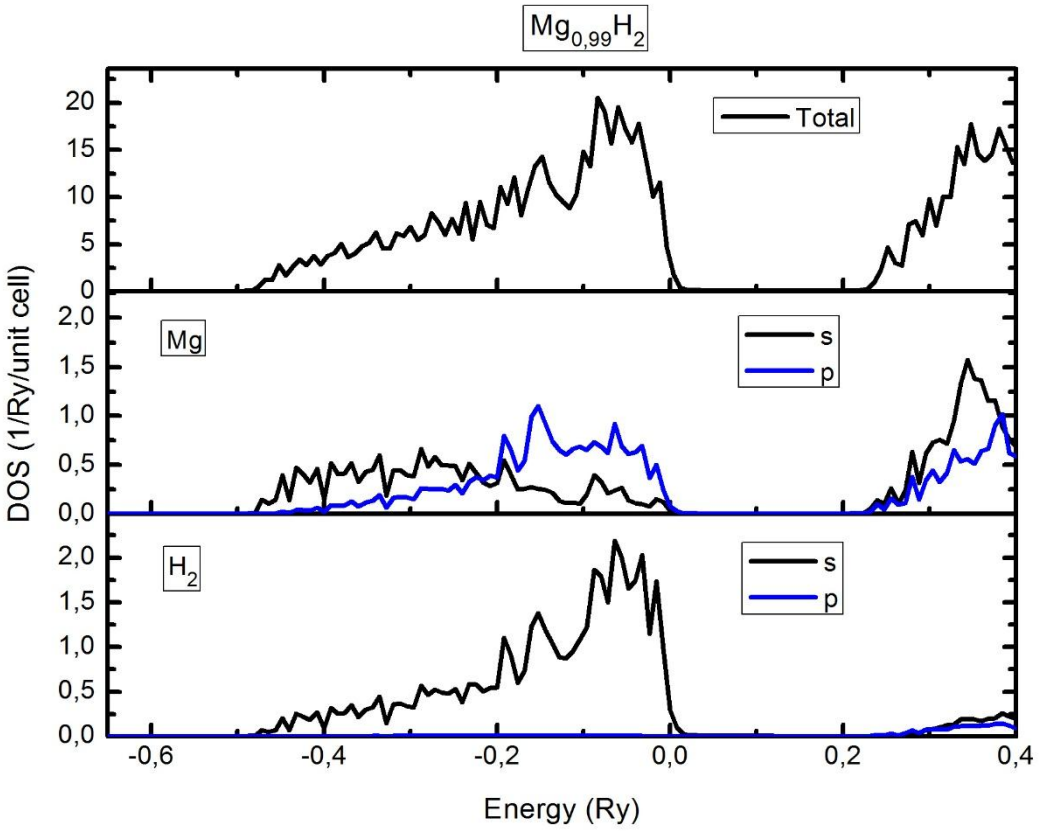
Mg0,99H2
Total
Mg
s
p
H2
s
p
DOS (1/Ry/unit cell)
Energy (Ry)

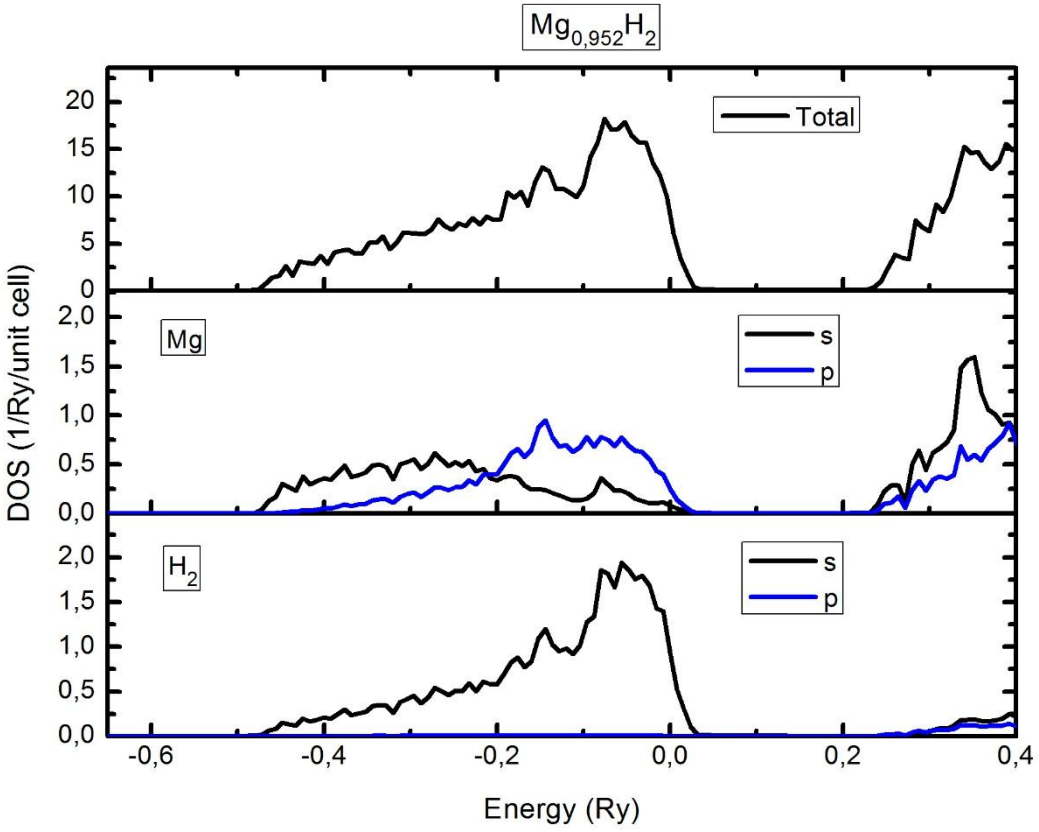
Mg0,952H2
Total
Mg
s
p
H2
s
p
DOS (1/Ry/unit cell)
Energy (Ry)

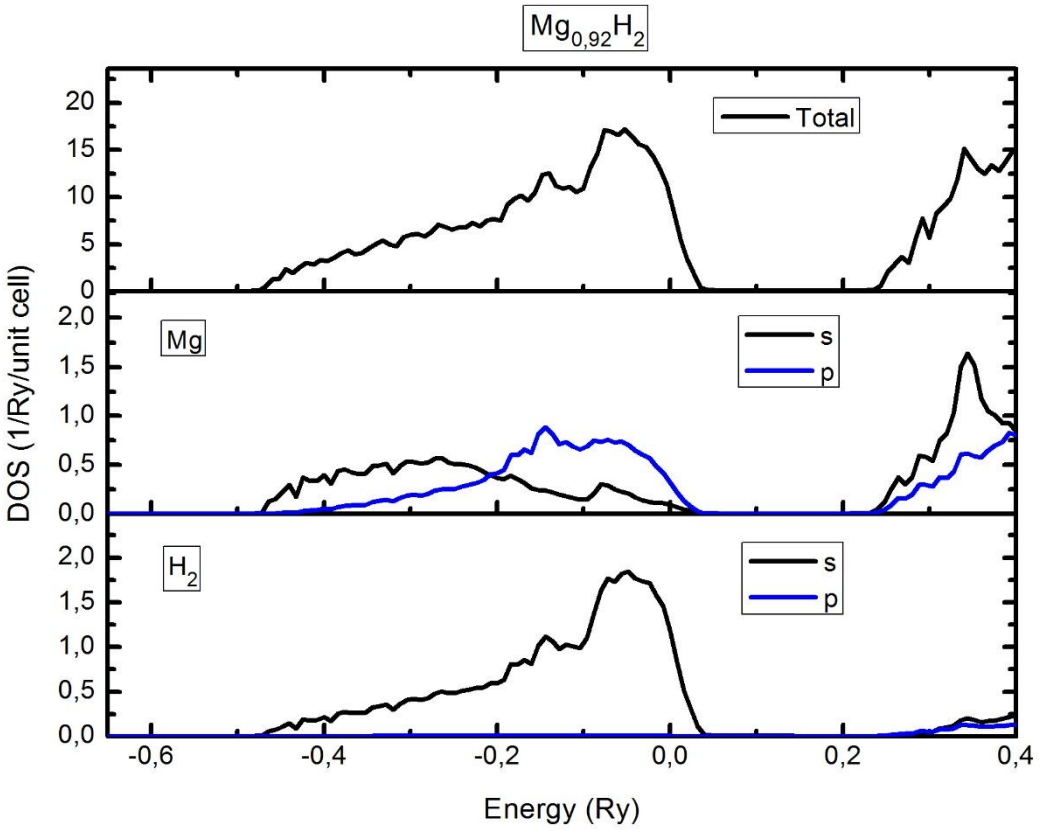

Figure 3.7: Total and partial DOS of $Mg_{0.99}H_2$, $Mg_{0.952}H_2$ and $Mg_{0.92}H_2$.

3.4 Improving hydrogen storage properties in MgH_2 by magnesium vacancies and hydrogen doping

The purpose of this section is to create Mg vacancy defects and introduce H atoms with the same concentration into the pure magnesium hydride for evaluating their effects on the hydrogen storage properties.

3.4.1 Thermodynamic properties of MgH_2 containing magnesium vacancies and hydrogen doping

The formation of the magnesium hydride containing magnesium vacancies and hydrogen atoms ($Mg_{1-x-y}H_{2+x}$, with x and y are the concentrations of hydrogen dopant atoms and magnesium vacancy defects, respectively) is done according to the following reaction:

$$Mg_{1-x-y}H_x + H_2 \rightarrow Mg_{1-x-y}H_{2+x} \quad (3.9)$$

$$\Delta H\left(Mg_{1-x-y}H_{2+x}\right) = E_{tot}\left(Mg_{1-x-y}H_{2+x}\right)_{relax} - E_{tot}\left(Mg_{1-x-y}H_x\right)_{relax} - E_{tot}(H_2) \quad (3.10)$$

The high thermodynamic stability of magnesium hydride prevents its application. So, as another attempt to reduce this stability, the effect of Mg vacancy defects and H dopant atoms can be a good approach to reach this goal. Therefore, the concentrations of magnesium vacancy defects and hydrogen dopant atoms will be varied from 1 to 10% (until the value of the formation energy becomes zero). According to $\Delta H(Mg_{1-x-y}H_{2+x}) = E_{tot}(Mg_{1-x-y}H_{2+x})_{relax} - E_{tot}(Mg_{1-x-y}H_x)_{relax} - E_{tot}(H_2)$ (3.10), the calculated values of the formation energy are listed in Table 3.3 and plotted in Figure 3.8. We note here that there is no change in the crystal structure of the studied hydrides.

Table 3.3: Formation energy, desorption temperature and total energies of $Mg_{1-x-y}H_{2+x}$.

Concentration		$Mg_{1-x-y}H_{2+x}$		Mg_{1-x-y}		Formation energy (KJ/mol.H_2)	Desorption temperature (K)
Magnesium vacancy defects (x)	Hydrogen dopant atoms (y)	System	Total energy (Ry/f.u)	System	Total energy (Ry/f.u)		
0	0	MgH_2	-403.0535	Mg	-400.6661	-88.571	677.67
0.005	0.005	$Mg_{0.99}H_{2.005}$	-399.0417	$Mg_{0.99}$	-396.6615	-79.030	604.66
0.01	0.01	$Mg_{0.98}H_{2.01}$	-395.0305	$Mg_{0.98}$	-392.6569	-70.341	538.18
0.015	0.015	$Mg_{0.97}H_{2.015}$	-391.0194	$Mg_{0.97}$	-388.6525	-61.543	470.87
0.02	0.02	$Mg_{0.96}H_{2.02}$	-387.0084	$Mg_{0.96}$	-384.6481	-52.876	404.56
0.025	0.025	$Mg_{0.95}H_{2.025}$	-382.9974	$Mg_{0.95}$	-380.6437	-44.255	338.60
0.03	0.03	$Mg_{0.94}H_{2.03}$	-378.9866	$Mg_{0.94}$	-376.6394	-35.696	273.11
0.035	0.035	$Mg_{0.93}H_{2.035}$	-374.9758	$Mg_{0.93}$	-372.6351	-27.184	207.98
0.04	0.04	$Mg_{0.92}H_{2.04}$	-370.9652	$Mg_{0.92}$	-368.6309	-18.717	143.20
0.045	0.045	$Mg_{0.91}H_{2.045}$	-366.9546	$Mg_{0.91}$	-364.6268	-10.307	78.85
0.05	0.045	$Mg_{0.90}H_{2.05}$	-362.9441	$Mg_{0.90}$	-360.6227	-1.946	14.88

We observe that the formation energy of MgH_2 increases with increasing the concentration of magnesium vacancy defects and hydrogen dopant atoms from -88.571 for x+y=0 to -1.946KJ/mol. H_2 for a value of 10%. This result allows us to make more improvement for the desorption temperature in MgH_2.

The second parameter in our thermodynamic properties is the temperature of desorption (T_{des}). Using equation 3.5, the findings are listed in Table 3.3 and illustrated in

Figure 3.**9**. It is shown in

Figure 3.**9** that when the concentration of magnesium vacancy defects and hydrogen dopant atoms increases, the decomposition temperature decreases from 677.67 (0%) to 14.88K (10%). It also shows that the value of the desorption temperature can be controlled and varied to any concentration needed. In order to reach the optimum range 289 – 393K for the practical use of a PEMFC, the concentrations (x + y) must be from 4.2 to 5.8%.

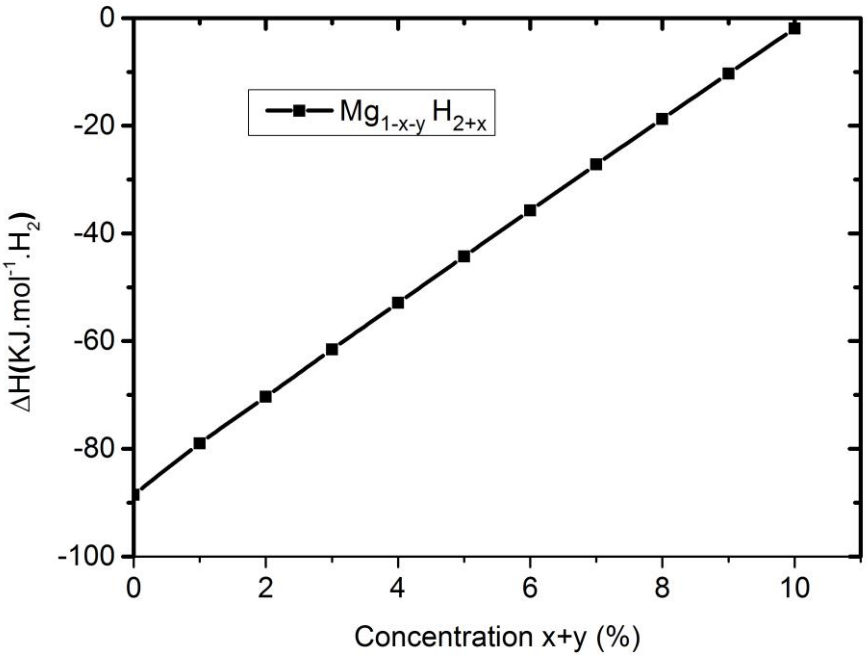

Figure 3.8: Formation energy as a function of concentrations for MgH_2.

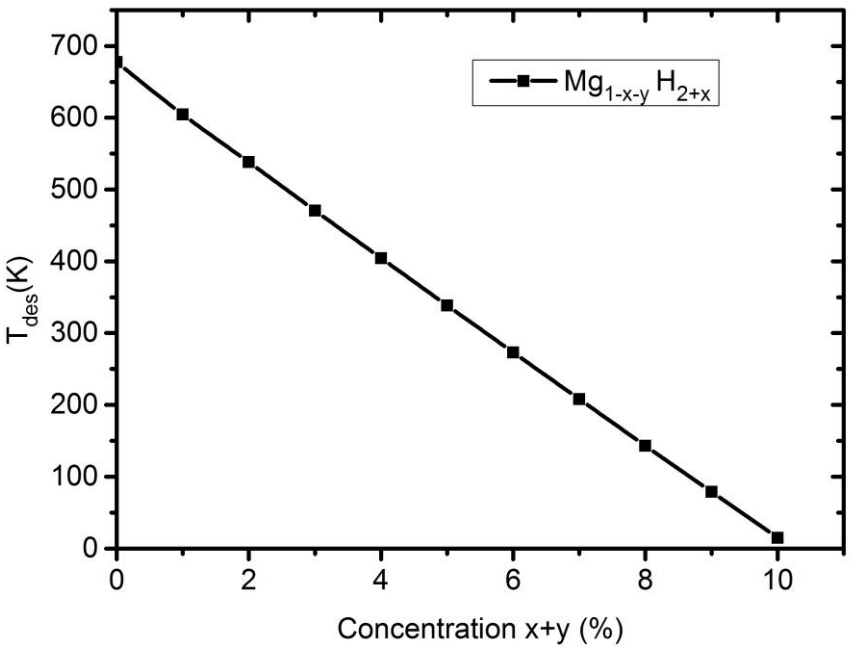

Figure 3.9: Desorption temperature as a function of concentrations for $Mg_{1-x-y}H_{2+x}$.

The high gravimetric capacity of $Mg_{1-x-y}H_{2+x}$ is also influenced by introducing hydrogen atoms and creating magnesium vacancies. Thus, in order to evaluate the effect of the concentrations of magnesium vacancy defects and hydrogen dopant atoms on the gravimetric capacity of MgH_2, we use the following equation:

$$C_g = \frac{(2+x)*m(H)}{(1-x-y)*m(Mg)+(2+x)*m(H)} \quad (3.11)$$

According to equation 3.11, the calculated gravimetric capacities of $Mg_{1-x-y}H_{2+x}$ are illustrated in Figure 3.10, where x and y are the concentrations of hydrogen dopant atoms and magnesium vacancy defects with $0 \leq x+y \leq 0.1$. We can see that when the concentrations of magnesium vacancy defects and hydrogen dopant atoms increase, the gravimetric density of magnesium hydride increases from 7.658 (x+y=0%) to 9.816 wt.% for x+y=10%. On the other hand, the use of the transition metals inside the hydride has also the ability to improve the thermodynamic properties. However, this improvement leads to a negative decrease in the gravimetric capacity as we will see in the next chapter.

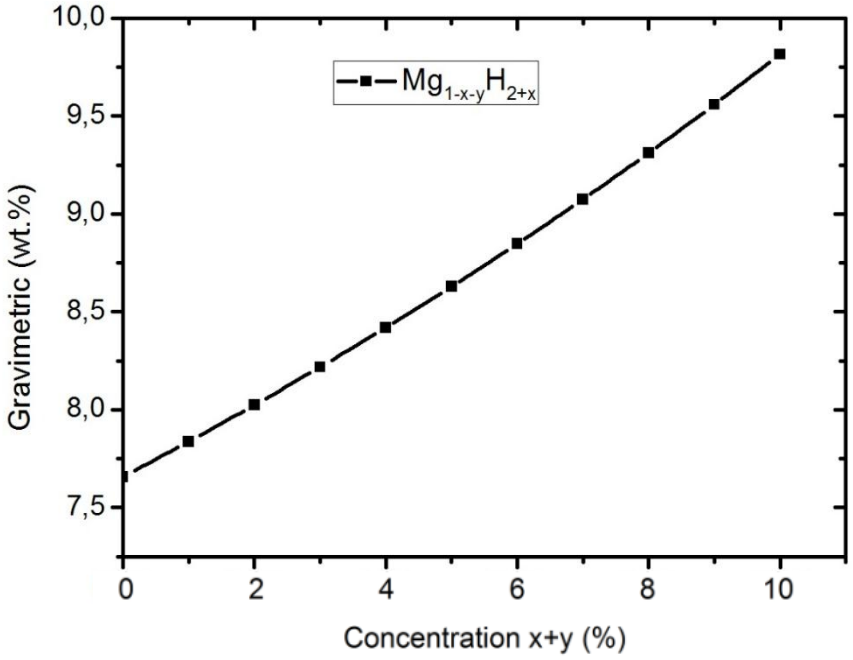

Figure 3.10: Gravimetric hydrogen capacity as a function of concentrations for $Mg_{1-x-y}H_{2+x}$.

3.4.2 Electronic structure

The electronic structure can be also used here to inspect the chemical bonding characteristics of the studied hydrides and give a plausible explanation to the observed decrease in the desorption temperature. By utilizing the GGA approximation and the relaxed parameters in this DOS calculation, we plot, in Figure 3.11, the total and partial density of states for the magnesium hydride containing vacancy defects and hydrogen doping atoms. The same behavior is observed for all the density of states of $Mg_{1-x-y}H_{2+x}$ with $0 \leq x \leq 0.1$, so, the only DOS of $Mg_{0.98}H_{2.01}$ and $Mg_{0.90}H_{2.05}$ are plotted. As shown in this figure, the DOSs of the magnesium hydride containing Mg vacancy defects and H dopant atoms show that there is a decease in the strong hybridization established between magnesium and hydrogen atoms. This decrease can be explained by the shift of the magnesium and hydrogen states from the valence band towards the highest energies in the DOS, which can explain the observed decrease in the stability and the desorption temperature, and consequently the increase in the formation energy into the MgH_2 hydride.

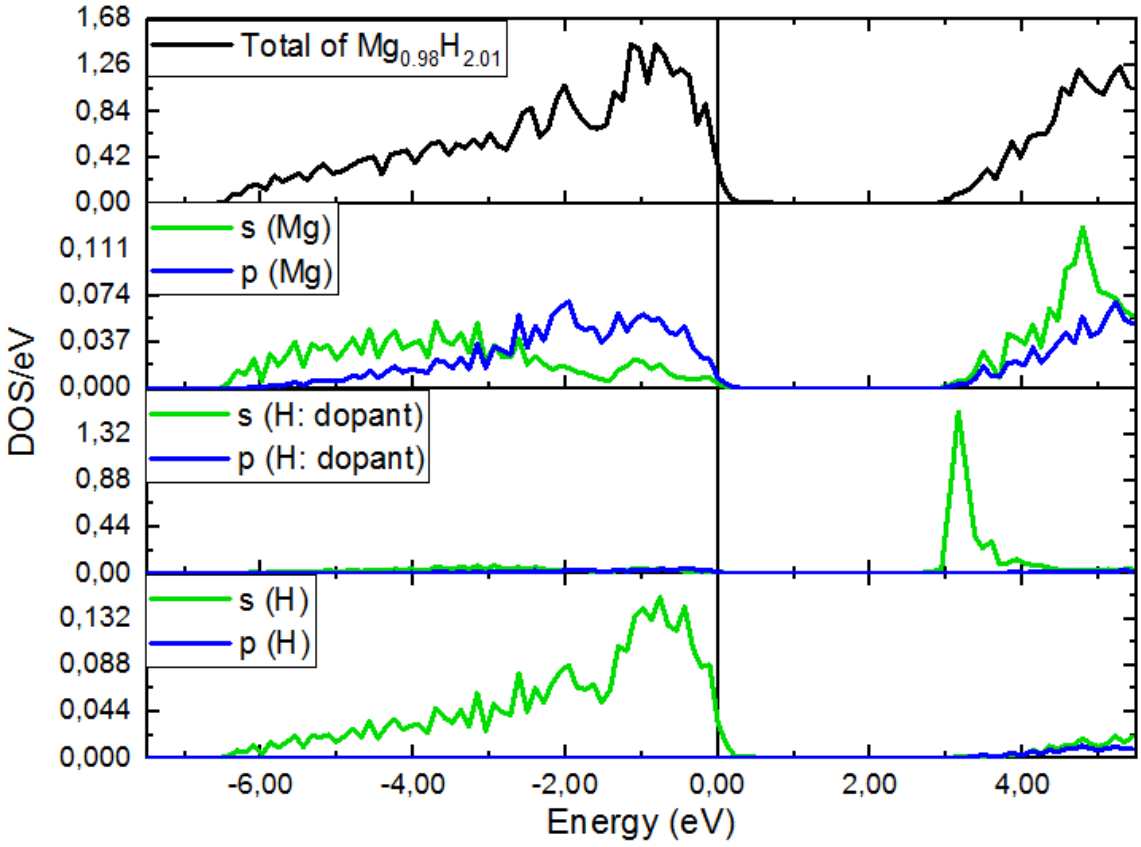

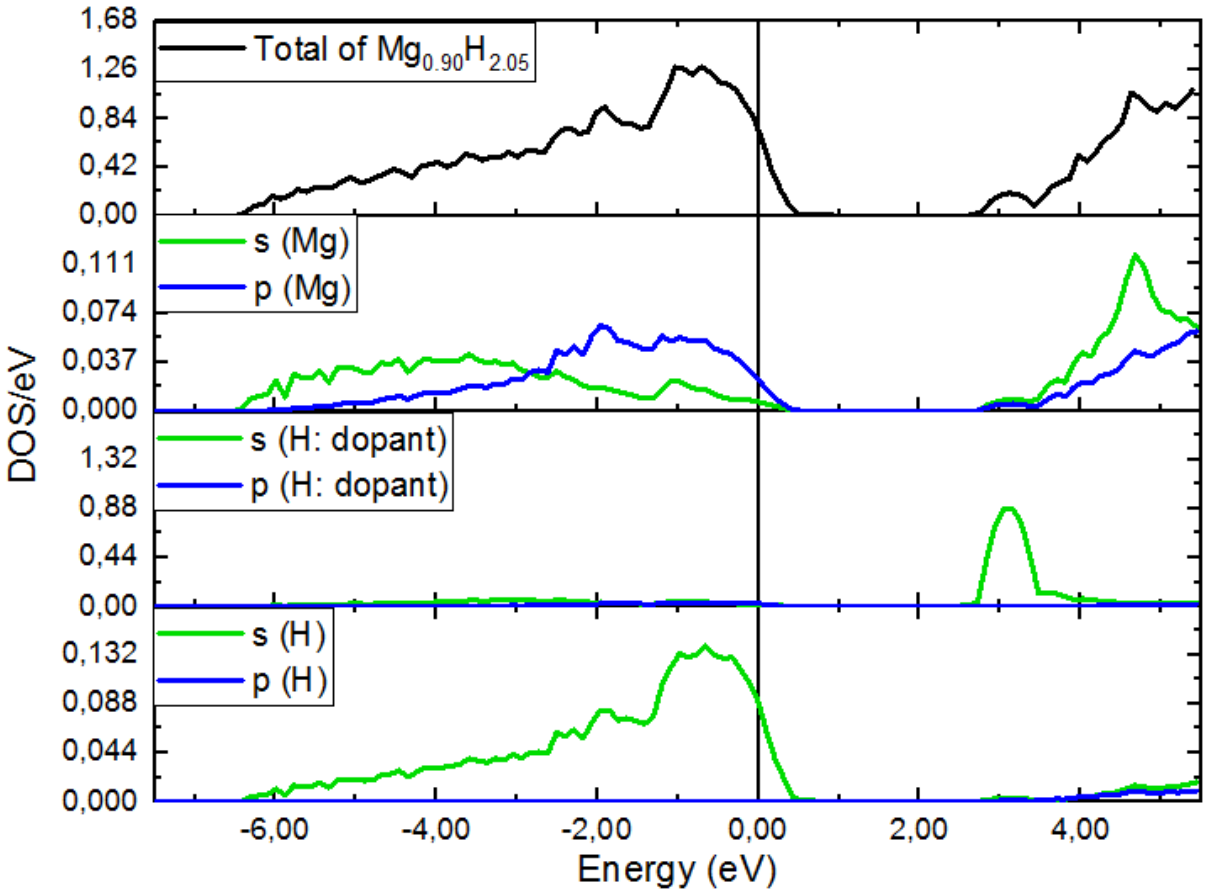

Figure 3.11: Total and partial DOS of $Mg_{0.98}H_{2.01}$ and $Mg_{0.90}H_{2.05}$.

3.5 Conclusion

The purpose of this chapter was to highlight the effect of magnesium vacancy defects into MgH_2 with or without hydrogen dopant atoms on the thermodynamic and electronic properties. For this reason, ab-initio calculations based on the KKR-CPA method were performed to predict the properties of the magnesium hydride before and after creating defects and introducing dopant atoms.

At the start, using the KKR-CPA method, the structural and thermodynamic properties of the pure MgH_2 are calculated, including the lattice parameters, the formation energy and the desorption temperature. The obtained resulted are consistent with other works in the literature.

Then, the effect of magnesium vacancy defects into MgH_2 with or without hydrogen dopant atoms has been performeed using the KKR-CPA method to evaluate their advantages on the thermodynamic properties. The calculations of the heat of formation and the temperature of desorption have confirmed that the magnesium vacancies and the hydrogen doping allow

destabilizing the system and, consequently, decreasing the desorption temperature with increasing the formation energy and the gravimetric hydrogen capacity of MgH_2.

Finally, in order to understand and analyse the previous findings, the total and partial densities of states have been plotted for each case; for the use of magnesium vacancy defects alone or mixed with hydrogen dopant atoms into MgH_2. We have found that the increase in the concentrations of magnesium vacancy defects and hydrogen dopant atoms allow shifting the valence band towards the highest energies which explain the decrease in the stability of the system.

4 Effects of transition metals and vacancy defects on the desorption temperature of MgH_2

Contents

4.1 Introduction

The main objective of this work is to compare between two different methods including the vacancy defects and the doping with metal transitions on the temperature of desorption of MgH_2. The comparison is based on the assessment of the efficiency of each method in term of the practical use of PEMFC (Proton Exchange Membrane Fuel Cells Or Polymer Electrolyte Membrane Fuel Cells), giving that the optimum range 289-393 K for the temperature of desorption of MgH_2 [115]. The used transition elements in this work are chromium (Cr) and manganese (Mn) with x and y are the concentrations of magnesium vacancy defects and transition elements, respectively.

4.2 Thermodynamic properties of MgH_2 containing magnesium vacancies and transition metals

In order to have an optimal material for hydrogen storage, the heat of formation is required to approach ΔH= - 40 kJ/mol (H_2) [105]. As we know that the more the heat of formation is negative, the more the system is thermodynamically stable. The studies reported that the use of the magnesium vacancy defects or the transition metals into MgH_2 allows improving its thermodynamic properties. To identify the best method in term of the heat of formation and desorption temperature, we use the following equations:

- For magnesium hydride doped with transition metals (Cr and Mn):

$$Mg_{1-y}M_y + H_2 \rightarrow Mg_{1-y}M_yH_2 \quad (4.1)$$

$$\Delta H\left(Mg_{1-y}M_yH_2\right) = E_{tot}\left(Mg_{1-y}M_yH_2\right) - E_{tot}\left(Mg_{1-y}M_y\right) - E_{tot}(H_2) \quad (4.2)$$

- For magnesium hydride containing vacancy defects:

$$Mg_{1-x} + H_2 \rightarrow Mg_{1-x}H_2 \quad (4.3)$$

$$\Delta H(Mg_{1-x}H_2) = E_{tot}(Mg_{1-x}H_2) - E_{tot}(Mg_{1-x}) - E_{tot}(H_2) \quad (4.4)$$

- For magnesium hydride mixed with transition metals (Cr and Mn) and magnesium vacancy defects:

$$Mg_{1-x-y}M_y + H_2 \rightarrow Mg_{1-x-y}M_yH_2 \quad (4.5)$$

$$\Delta H\left(Mg_{1-x-y}M_yH_2\right) = E_{tot}\left(Mg_{1-x-y}M_yH_2\right) - E_{tot}\left(Mg_{1-x-y}M_y\right) - E_{tot}(H_2) \quad (4.6)$$

For a practical use of a PEMFC in hydrogen storage applications, the desorption temperature must be around 289 – 393 K. Thus, the T_{des} is a key player in this comparison

between the magnesium vacancy defects and/or the transition metals to choose the best method for magnesium hydride. The obtained heats of formation are used to calculate the desorption temperature using equation 3.5:

The main challenge was always to improve the stability and the temperature of desorption in MgH_2, many experimental and theoretical methods was used in this stage such as the transition metals, which achieved remarkable results in term of the improvement of the thermodynamic properties of MgH_2 [103]. Therefore, the idea here is to compare between the transition metals and the vacancy defects which also exposed a positive effect on the heat of formation and the temperature of desorption of MgH_2. The mixture between the magnesium vacancy defects and the doped elements is also taken into consideration in this calculation. Using the KKR-CPA code, the total energy, heat of formation and temperature of desorption are calculated for each system using the relaxed parameters. The obtained results are plotted in Figure 4.1.

Indeed, our calculations confirm that the transition metals have the ability to decrease the high stability and desorption temperature of MgH_2. In particular, we can obtain any desorption temperature in MgH_2 by varying the concentrations of doped elements. Thus, in order to have an ideal temperature within the optimal range for the practical use of PEMFC, the concentration of transition metals must be from 4.4 to 5.7% for $Mg_{1-x}Cr_yH_2$, and 4.3 to 5.6% for $Mg_{1-x}Mn_yH_2$. The same idea is used for the mixture between the magnesium vacancy defects and transition metals into MgH_2, the optimum range of total concentrations (x+y) is 4.9 – 6.3% for $Mg_{1-x-y}Cr_yH_2$ and 4.7 – 6% for $Mg_{1-x-y}Mn_yH_2$. For magnesium hydride containing vacancy defects ($Mg_{1-x}H_2$), the concentration range is 3.3 – 4.5% as mentioned in the previous chapter. Thus, the use of magnesium vacancy defects into MgH_2 is greatly favorable compared to the use of transition metals alone or their mixture with the magnesium vacancy defects into MgH_2 (see Figure 4.1).

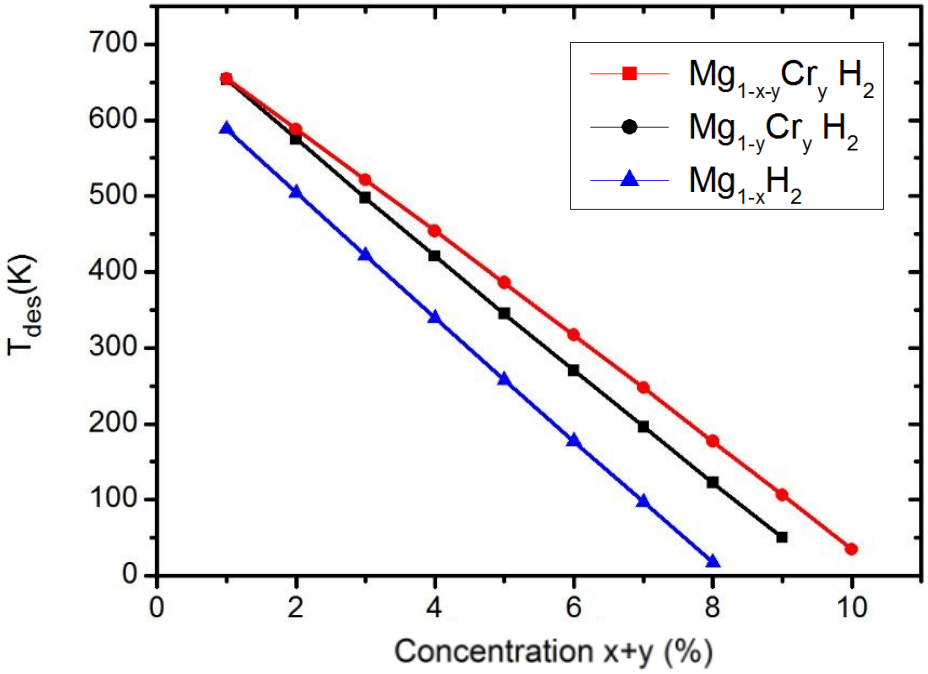

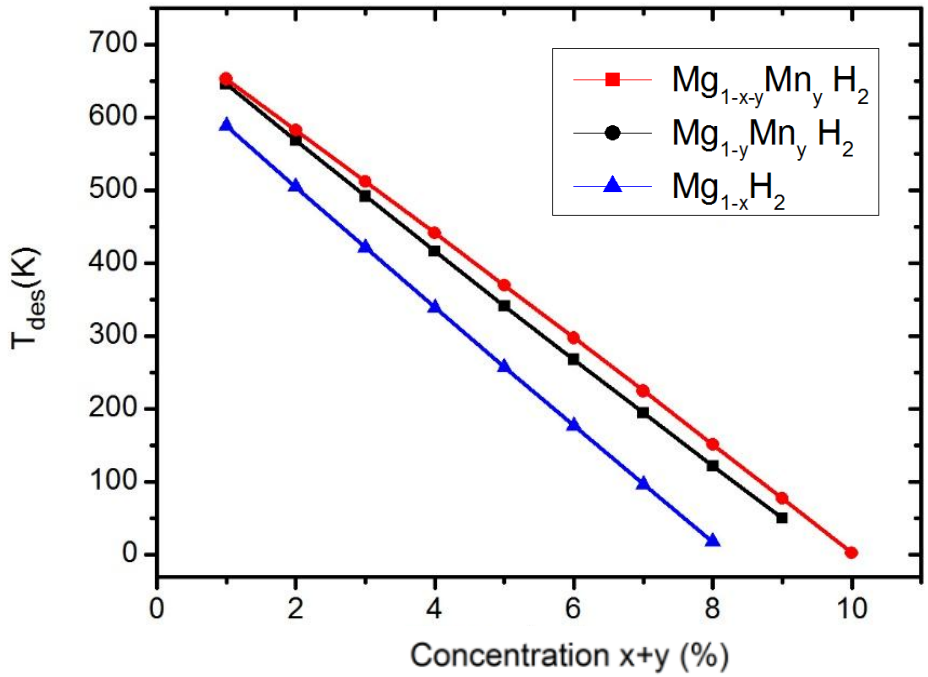

Figure 4.1: Desorption temperature as a function of concentrations of vacancies (x) and transition metals (y) for $Mg_{1-y}M_yH_2$, $Mg_{1-x-y}M_yH_2$ and $Mg_{1-x}H_2$with M = Cr and Mn.

4.3 Electronic structure

Following the dehydrogenation performances of MgH_2 containing the vacancies and doped elements, the total and partial density of states are investigated to clarify and explain the different results. We note that the same effect is observed for different concentrations.

The total and partial DOS of the magnesium hydride doped with transition metals ($Mg_{0.95}M_{0.05}H_2$) or mixed with magnesium vacancy defects ($Mg_{0.95}M_{0.025}H_2$) are plotted in Figure 4.2 and Figure 4.3, respectively. We observe that there is a new peak in the gap band between Mg and M, which is a hybridization between the orbitals of Mg and M. The apparition of this pick is due to the bond created between the Mg and H atoms that becomes weaker, and may explain the observed decrease in the stability. On the other hand, the shift of the Mg, Cr, Mn and H orbitals to the valence band is also a key factor in decreasing the stability.

In contrast, in Figure 3.7, the magnesium hydride containing vacancy defects has an increasing in the stability, which is due to the shift of Mg and H orbitals to the conduction band as explained in the previous chapter. Additionally, the increase in the stability as a function of the concentration can be explained by the diminution of the number of Mg atoms which establish a strong bond with H atoms, and that can be seen by the decrease of the intensity of states in the total and partial DOS.

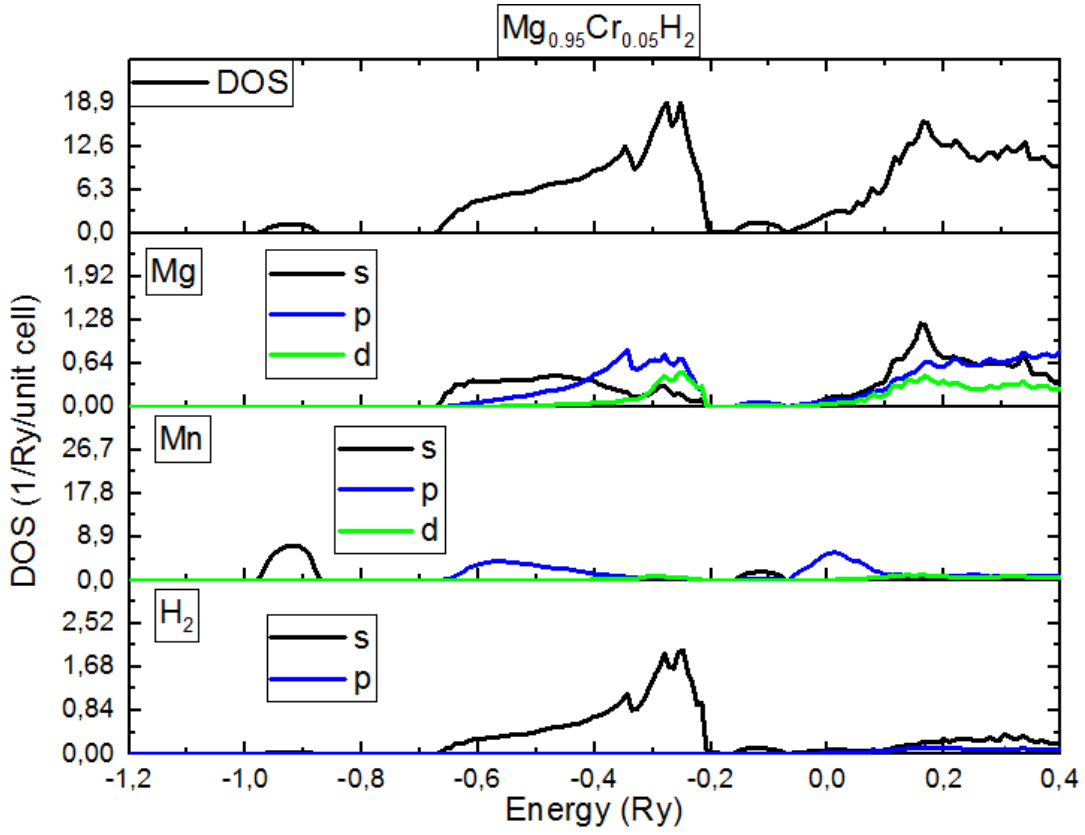

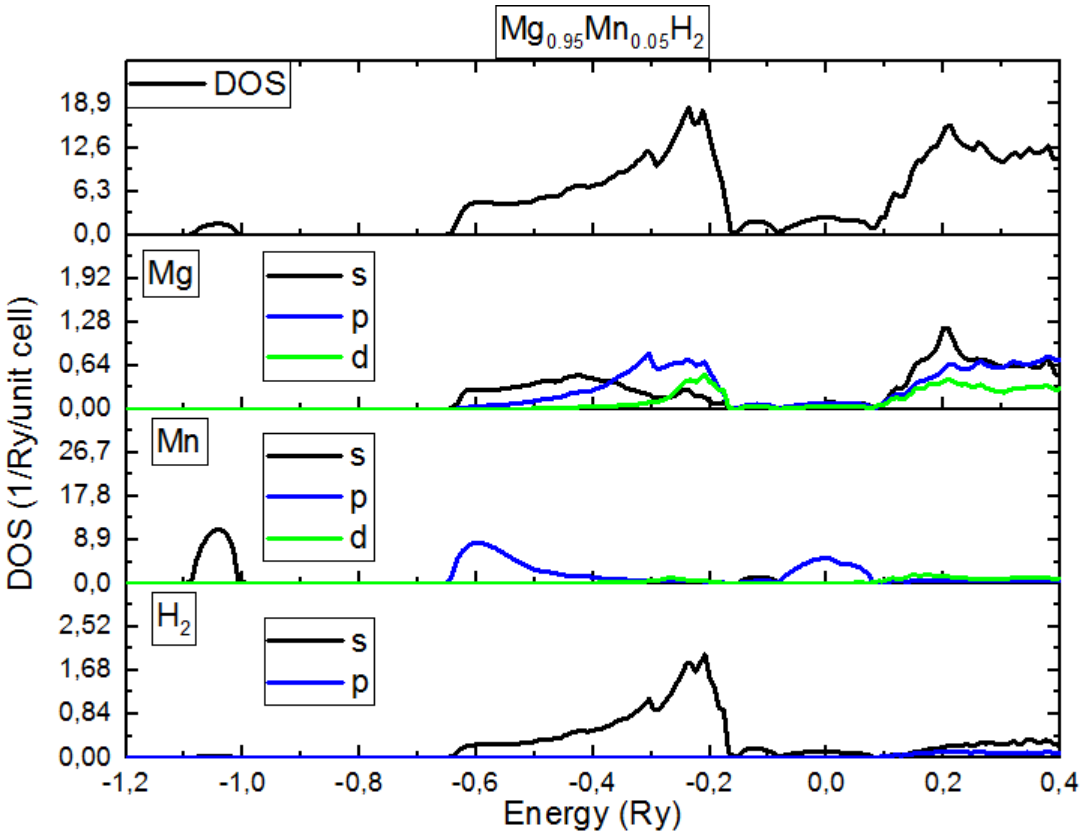

Figure 4.2: Total and partial DOS of $Mg_{0.95}M_{0.05}H_2$ with M = Cr and Mn.

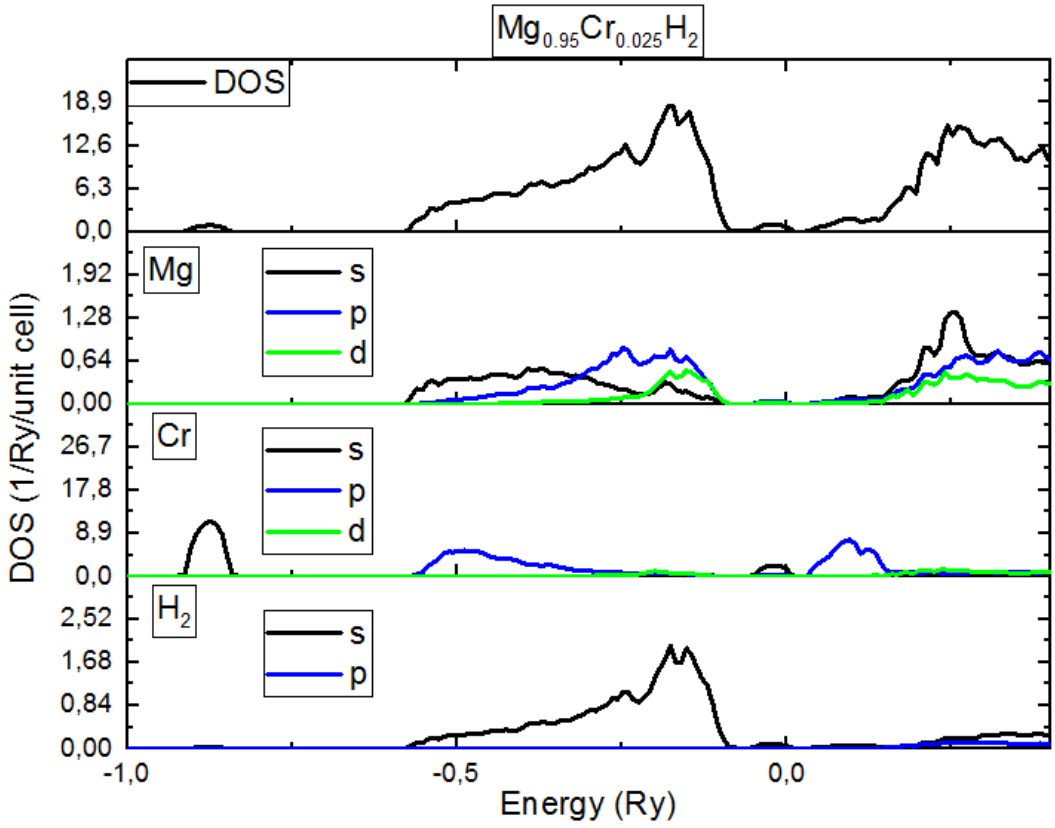

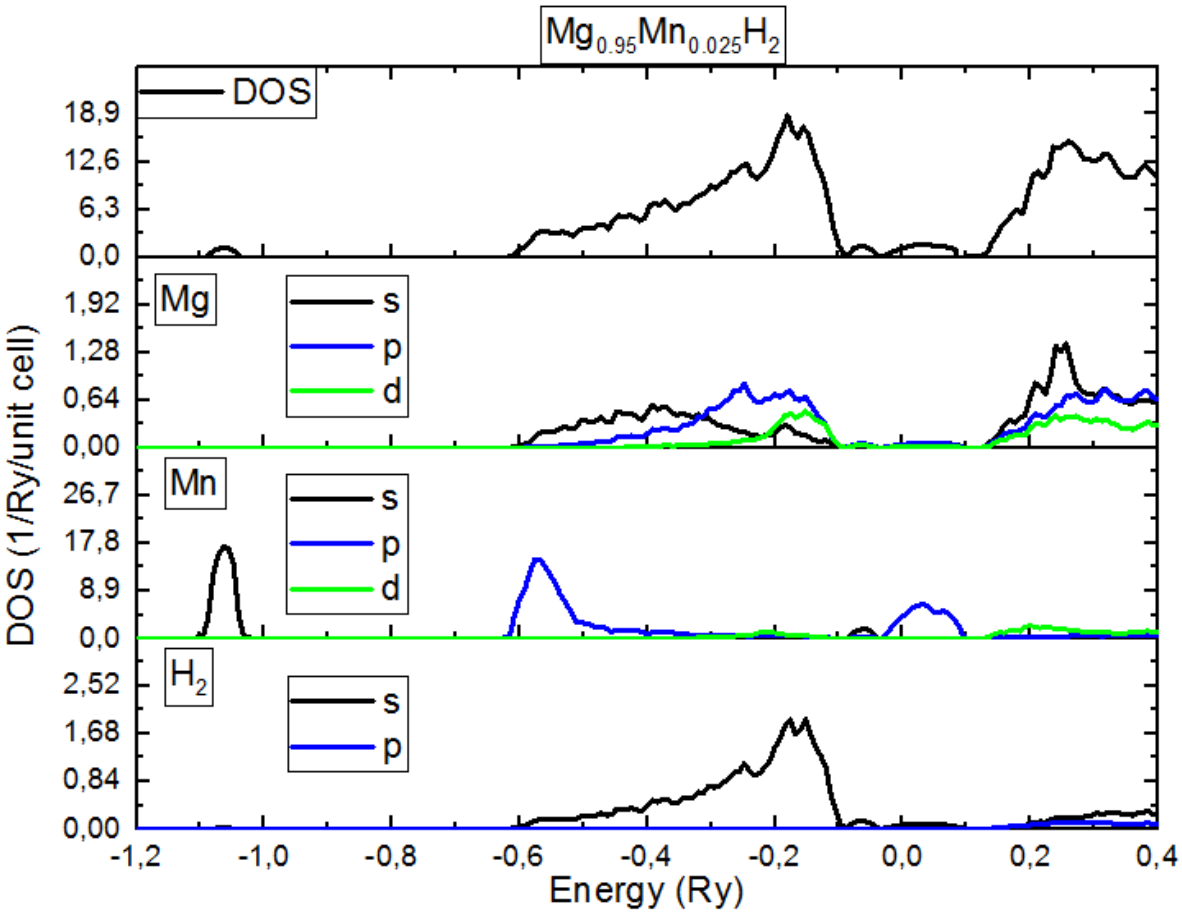

Figure 4.3: Total and partial DOS of $Mg_{0.95}M_{0.025}H_2$ with M = Cr and Mn.

4.4 Conclusion

The assessment of the effect of magnesium vacancy defects and/or transition metals (Cr and Mn) on the temperature of desorption into MgH_2 is the purpose of this chapter. The KKR – Green's function method integrated with the coherent potential approximation has chosen to perform our calculation for each Mg based hydride (MgH_2, Mg $Mg_{1-y}M_yH_2$, $Mg_{1-y}M_y$, $Mg_{1-x}H_2$, Mg_{1-x}, $Mg_{1-x-y}M_yH_2$ and $Mg_{1-x-y}M_y$ (M = Cr and Mn)). The obtained results have revealed that the optimum range of concentration for the practical use of PEMFC has to be between:

- 4.9 – 6.3% and 4.7 – 6% for magnesium hydride mixed with magnesium vacancy defects and chromium or manganese, respectively;
- 4.4 – 5.7% and 4.3 – 5.6% for magnesium hydride doped with chromium or manganese, respectively;
- 3.3 – 4.5% for magnesium hydride containing vacancy defects.

Therefore, the magnesium vacancy defects appear to be the best method for the magnesium hydride in comparison with using the transition metals alone or their mixture with the magnesium vacancy defects, because its optimum range of concentration is the fastest and smallest to the required range of desorption temperature for the practical use. On the basis of the electronic structure of Mg based hydride, the process of vacancy defects can be explained by the diminution of the number of Mg atoms which establish a strong bond with H atoms, and that can be seen by the decrease of the intensity of states in the total and partial DOS.

5 Effects of vacancy defects on the desorption temperature of LiH

Contents

5.1 Introduction

In this work, the vacancy defects were investigated to reduce both the stability and the desorption temperature of the lithium hydride to meet different applications without sacrificing its high hydrogen storage capacity. The investigation aims to study the effect of Li vacancy defects on the hydrogen storage properties of the system and give a plausible explanation to the observed decrease using the density of states.

5.2 Computational method

In this chapter, the Korringa – Kohn – Rostoker (KKR) package is chosen to perform our calculations, because it allows us controlling different concentrations of lithium vacancy defects into the material by using the coherent potential approximation (CPA) method combined in the package. The generalized gradient approximation GGA91 [97] is used to calculate both the total energy and the DOS for $Li_{1-x}H$ and PBE approximation [95] for the total energy of Li_{1-x} with $0 \leq x \leq 0.25$. A 10×10×10 k-point mesh is used for the Brillouin zone integration to achieve more accurate results. The convergence of the self-consistent field (SCF) iterations is used with a precision of 10^{-6} Ry. The angular momentum quantum number is fixed at $l = 2$ for both lithium hydride and lithium element with or without vacancy defects. The lithium hydride (LiH) (Figure 5.1) has a space group N° 225 (Fm-3m) with unit cell parameters a = b = c = 4.083 Å. The atomic position for lithium atoms is (0, 0, 0) and for hydrogen atoms is (0.5, 0.5, 0.5) [116]. The electronic structure of hydrogen is $1s^1$ and that of lithium is $1s^2 2s^1$.

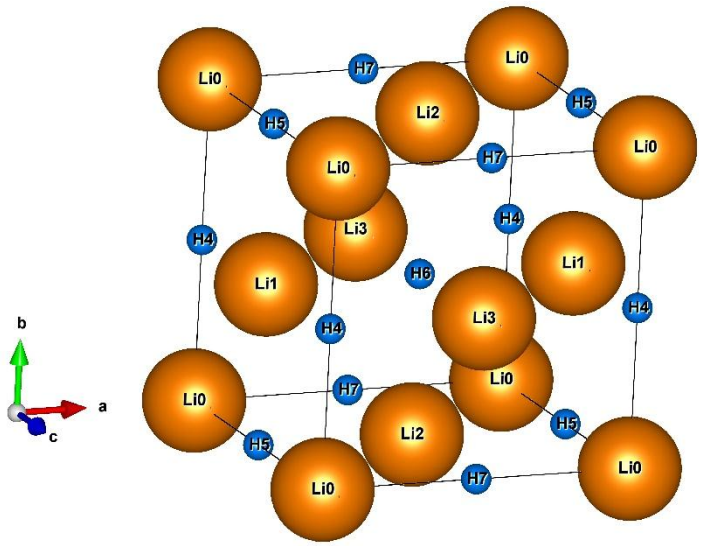

Figure 5.1: Primitive cell of LiH.

5.3 Thermodynamic properties of LiH containing vacancy defects

The total energy will be used to calculate the formation energy and deduce the desorption temperature of $Li_{1-x}H$ with $0 \leq x \leq 0.25$. Thus, in order to have accurate values in the total energy, the lattice parameters for both the lithium hydride (LiH) and the pure element Li are optimized using the relaxation method as it was done in the previous calculations for MgH_2.

The experimental parameters (a = 4.083 Å) [116] and (a = 3.510 Å) [117] of LiH and Li, respectively, are taken as the initial lattice parameters for the relaxation method, then, the parameters 'a' for both systems are varied to different values until they reach the equilibrium parameters which correspond to the minimal total energies as shown in Figure 5.2. The same process is used in order to optimize the lattice parameters and calculate the minimal total energies for both LiH and Li with different concentrations of vacancy defects.

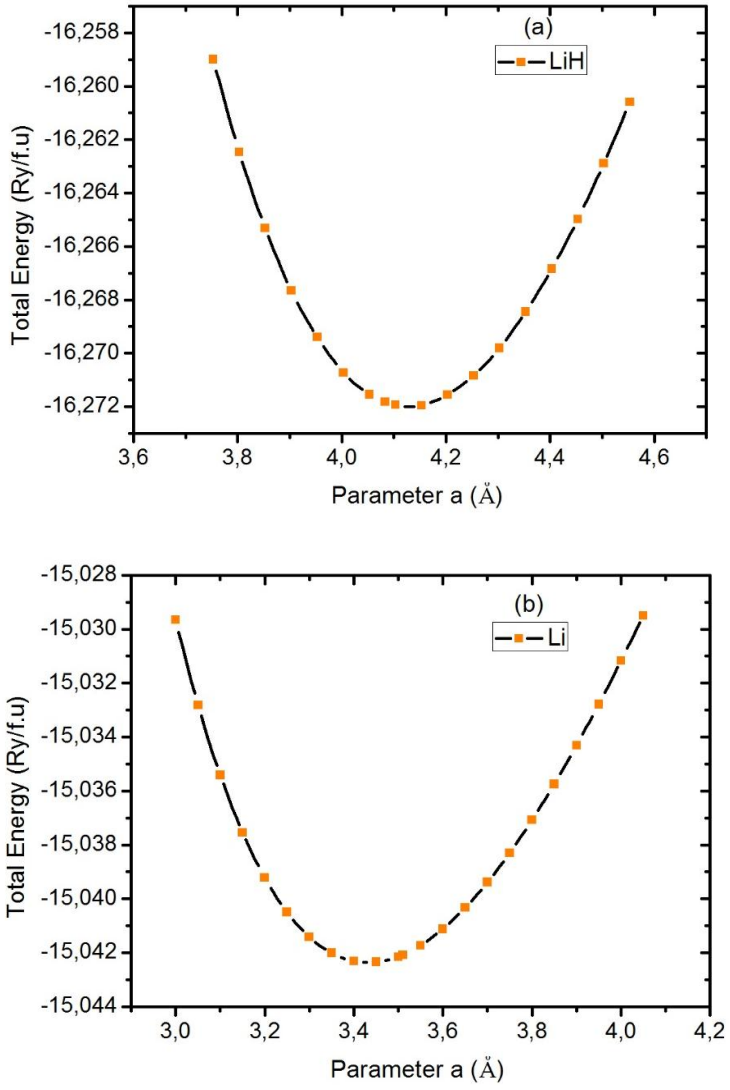

Figure 5.2: Total energy as a function of parameter a for LiH (a) and Li (b).

The optimized parameters 'a' for both LiH and Li are 4.129 Å and 3.439 Å, respectively. These results are in good agreement with the obtained values of other works, a = 4.083 Å for LiH [116] and a = 3.510 Å for Li [117]. This concordance with the previous results allows us to validate our calculation methods including the KKR-CPA method and the use of GGA91 approximation for LiH and PBE approximation for Li. The formation of the pure LiH is done according to the following reaction:

$$Li + H \rightarrow LiH \tag{5.1}$$

Using the difference between the total energy of products and reactants, the formation energy of our studied hydrides can be calculated by using equation 3.2:

By projecting the relation (2) on the reaction (1), the formation energy of LiH is written as follows:

$$\Delta H(LiH) = E_{tot}(LiH)_{relax} - E_{tot}(Li)_{relax} - \frac{1}{2}E_{tot}(H_2) \tag{5.2}$$

The same approach is used for calculating the formation energy of the lithium hydride containing vacancy defects $Li_{1-x}H$ ($0 \leq x \leq 0.25$):

$$Li_{1-x} + H \rightarrow Li_{1-x}H \tag{5.3}$$

$$\Delta H(Li_{1-x}H) = E_{tot}(Li_{1-x}H)_{relax} - E_{tot}(Li_{1-x})_{relax} - \frac{1}{2}E_{tot}(H_2) \tag{5.4}$$

The needed total energies of Li, Li_{1-x}, LiH and $Li_{1-x}H$ are calculated using the KKR-CPA method, except the total energy of the hydrogen (H_2) is taken from Ref. [118]. Some calculated values of the total energy and the formation energy are listed in Table 5.1.

Based on our calculations, LiH has a high stability and that is due to its formation energy which is equal to -91.371 KJ/mol. H_2. This value is in perfect agreement with that measured experimentally -90.5 KJ/mol. H_2 [119] or obtained theoretically -87 KJ/mol. H_2 [119].

The high thermodynamic stability of lithium hydride prevents its application for mobile hydrogen storage. So, as an attempt to reduce this stability, the effect of Li vacancy defects ($Li_{1-x}H$) can be a good approach to reach this goal. Thus, in this work, the concentration of lithium vacancy defects will be varied from 1 to 25% (until the value of the formation energy becomes positive). The different results are plotted in Figure 5.3.

Table 5.1: Formation energy, desorption temperature and total energies of $Li_{1-x}H$ and Li_{1-x}.

Concentration of lithium vacancy defects (x)	$Li_{1-x}H$			Li_{1-x}			Formation energy (KJ/mol. H_2)	Desorption temperature (K)
	System	Total energy (Ry/f.u)	Crystal structure	System	Total energy (Ry/f.u)	Crystal structure		
0	LiH	-16.27196	FCC	Li	-15.04235	BCC	-91.371	699.09
0.01	$Li_{0.99}H$	-16.11630		$Li_{0.99}$	-14.89021		-86.757	663.79
0.03	$Li_{0.97}H$	-15.80694		$Li_{0.97}$	-14.58601		-79.982	611.95
0.05	$Li_{0.95}H$	-15.49772		$Li_{0.95}$	-14.28193		-73.245	560.41
0.07	$Li_{0.93}H$	-15.18859		$Li_{0.93}$	-13.97797		-66.374	507.83
0.09	$Li_{0.91}H$	-14.87957		$Li_{0.91}$	-13.67417		-59.457	454.91
0.11	$Li_{0.89}H$	-14.57064		$Li_{0.89}$	-13.37049		-52.714	403.32
0.13	$Li_{0.87}H$	-14.26177		$Li_{0.87}$	-13.06693		-45.726	349.85
0.15	$Li_{0.85}H$	-13.95300		$Li_{0.85}$	-12.76351		-38.727	296.31
0.17	$Li_{0.83}H$	-13.64437		$Li_{0.83}$	-12.46023		-31.683	242.41
0.19	$Li_{0.81}H$	-13.33581		$Li_{0.81}$	-12.15707		-24.598	188.20
0.21	$Li_{0.79}H$	-13.02733		$Li_{0.79}$	-11.85406		-17.420	133.28
0.23	$Li_{0.77}H$	-12.71898		$Li_{0.77}$	-11.55118		-10.229	78.27
0.25	$Li_{0.75}H$	-12.41073		$Li_{0.75}$	-11.24843		-3.021	23.12

We observe that the formation energy of LiH increases with increasing the concentration of lithium vacancy defects from -91.371 for x=0 to -3.021 KJ/mol. H_2 for a value of 25% as defect concentration. This result also allows us to improve the desorption temperature in LiH as we will see in the next section. The explanation of this trend will be discussed using the density of states in the next section.

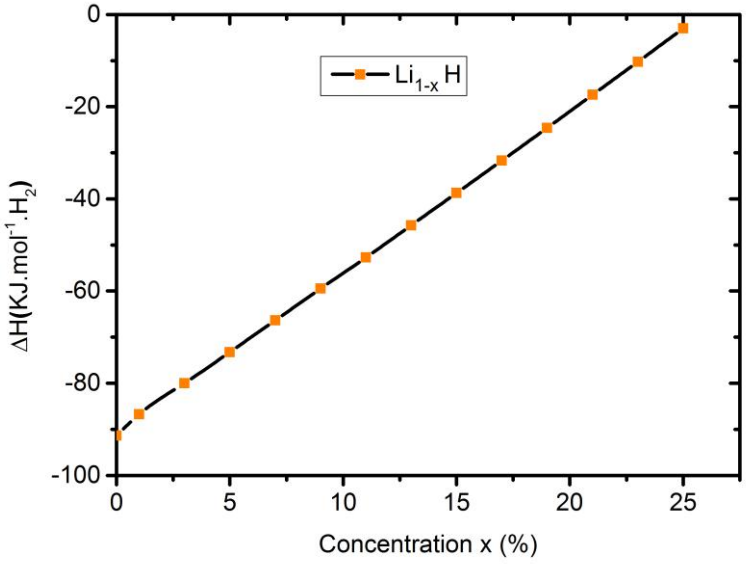

Figure 5.3: Formation energy as a function of the defect concentration x in $Li_{1-x}H$.

The second parameter in our thermodynamic properties is the temperature of desorption (T_{des}). Based on our calculations, the T_{des} of LiH is ~700 K. This value is very high and in agreement with that announced in Ref. [120]. It is also shown in Figure 5.4 that when the concentration increases, the decomposition temperature decreases linearly from 699.09 (x = 0%) to 23.12 K (x = 25%). It follows that the value of the heat of formation and the desorption temperature can be controlled by varying the concentration of lithium vacancy defects to reach the optimum range 289 – 393 K for the practical use of a PEMFC. This decrease is not interesting beyond 16%, because the obtained decomposition temperature deviates from the optimum.

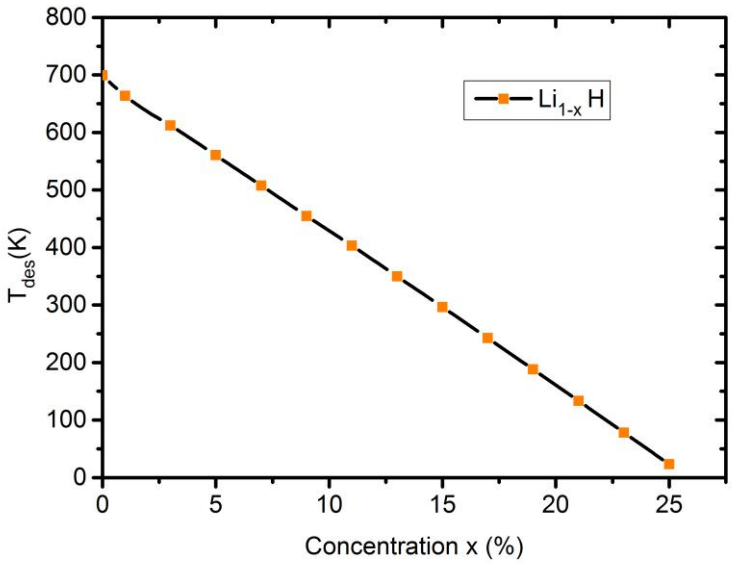

Figure 5.4: Desorption temperature as a function of the defect concentration x in $Li_{1-x}H$.

In order to evaluate the effect of the concentration of lithium vacancy defects on the storage capacity of LiH, we use the following relation:

$$C_g = \frac{m(H)}{(1-x) * m(Li) + m(H)} \qquad (5.5)$$

where m(H) = 1.00784u and m(Li) = 6.941u are the atomic masses of hydrogen and lithium, respectively. The observed behavior is shown in Figure 5.5.

We observe that the gravimetric hydrogen capacity of LiH increases with increasing the concentration of lithium vacancy defects from 12.679wt.% (x=0%) to 14.738wt.% for x=16%.

In summary, the performed study shows that the Li vacancy defects have a beneficial effect on the hydrogen storage properties of the hydride by increasing both its formation energy and gravimetric capacity and decreasing its desorption temperature.

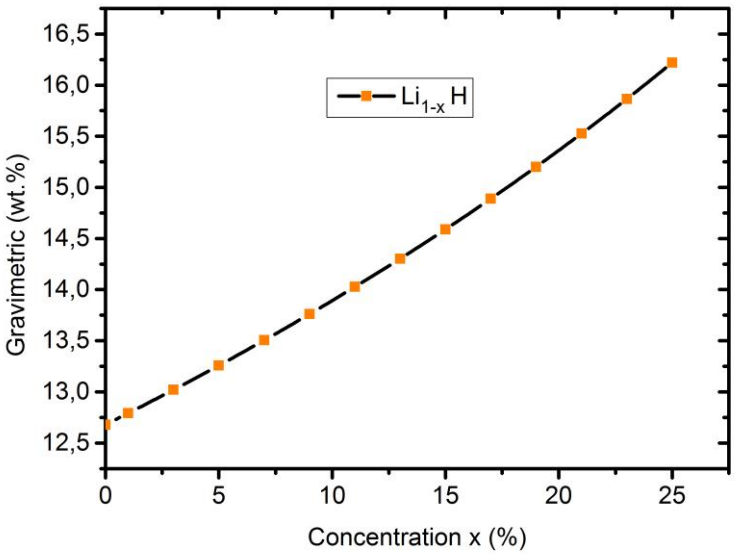

Figure 5.5: Gravimetric hydrogen capacity as a function of the defect concentration x in $Li_{1-x}H$.

5.4 Electronic structure

Using the GGA91 approximation and the optimized parameters in this calculation, the total and partial densities of states for LiH with and without vacancy defects are illustrated in Figure 5.6. Due to the same trend observed in all calculations of $Li_{1-x}H$ with $0 \leq x \leq 0.25$, only the DOS of $Li_{0.99}H$, $Li_{0.90}H$ and $Li_{0.75}H$ are plotted.

Based on this figure, we can see that there is two parts in the valance band (VB), the first one is formed from a strong hybridization between s(H) and p(Li) states and the second part is also composed of a high hybridization, but this time between Li-2s and H-1s states. The conduction band (CB) is mainly attributed to Li-2p state.

Firstly, for the pure LiH, the high stability and consequently the high decomposition temperature is related to the strong interaction between H and Li atoms. Secondly, the observed decrease in the stability as a function of the concentration can be explained on the one hand by the diminution of the number of Li atoms which establish a strong bond with H atoms, and that can be seen by the decrease of the intensity of states in the total and partial DOS, and on the other hand by the shift of the Li and H states on the right of the Fermi level.

As we know that when the electronic states shift towards the positive energies, the system is thermodynamically less stable [121]. Therefore, from the DOS, we notice that when the concentration of vacancies increases from 0 to 16%, the shift of the states towards the positive energies is more observed. Consequently, the stability decreases in LiH with improving in its thermodynamic properties.

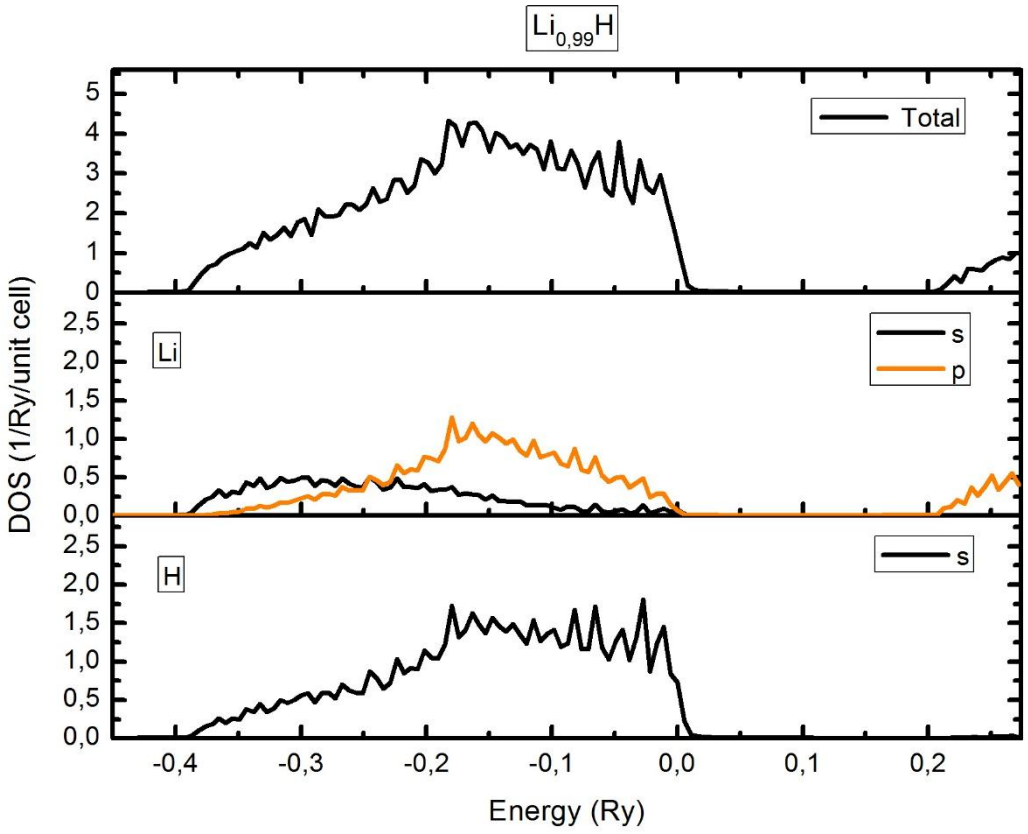
Li0,99H
Total
Li
s
p
H
s
DOS (1/Ry/unit cell)
Energy (Ry)

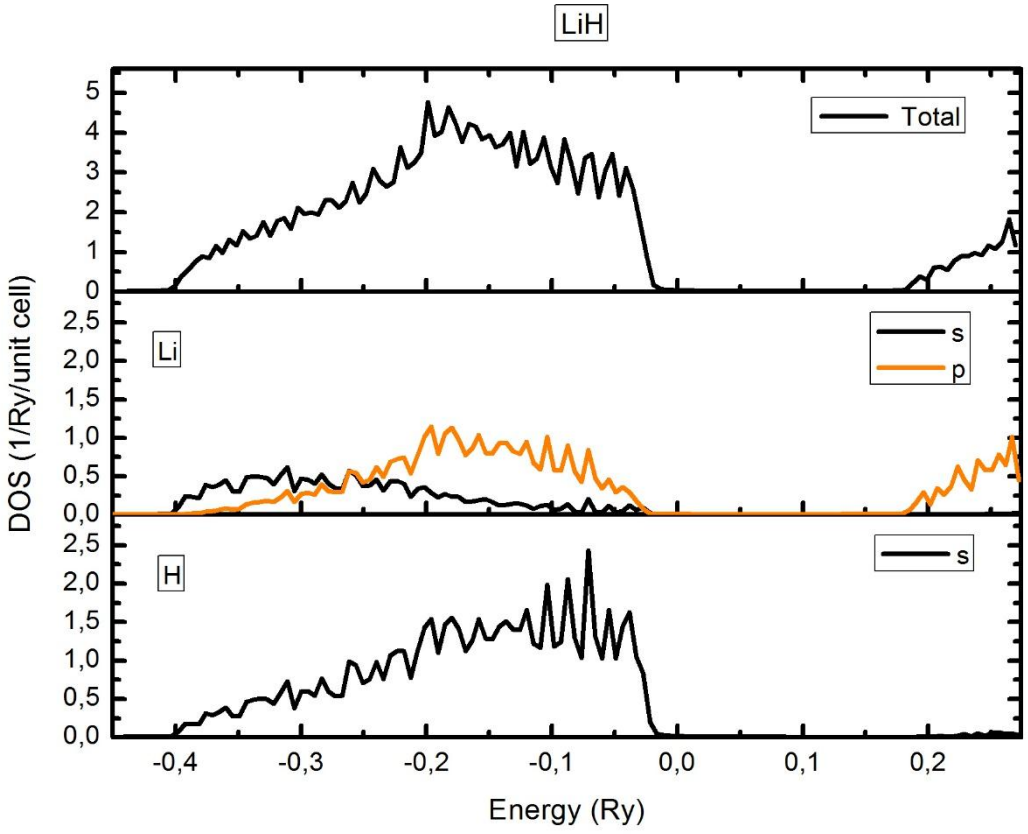
LiH
Total
Li
s
p
H
s
DOS (1/Ry/unit cell)
Energy (Ry)

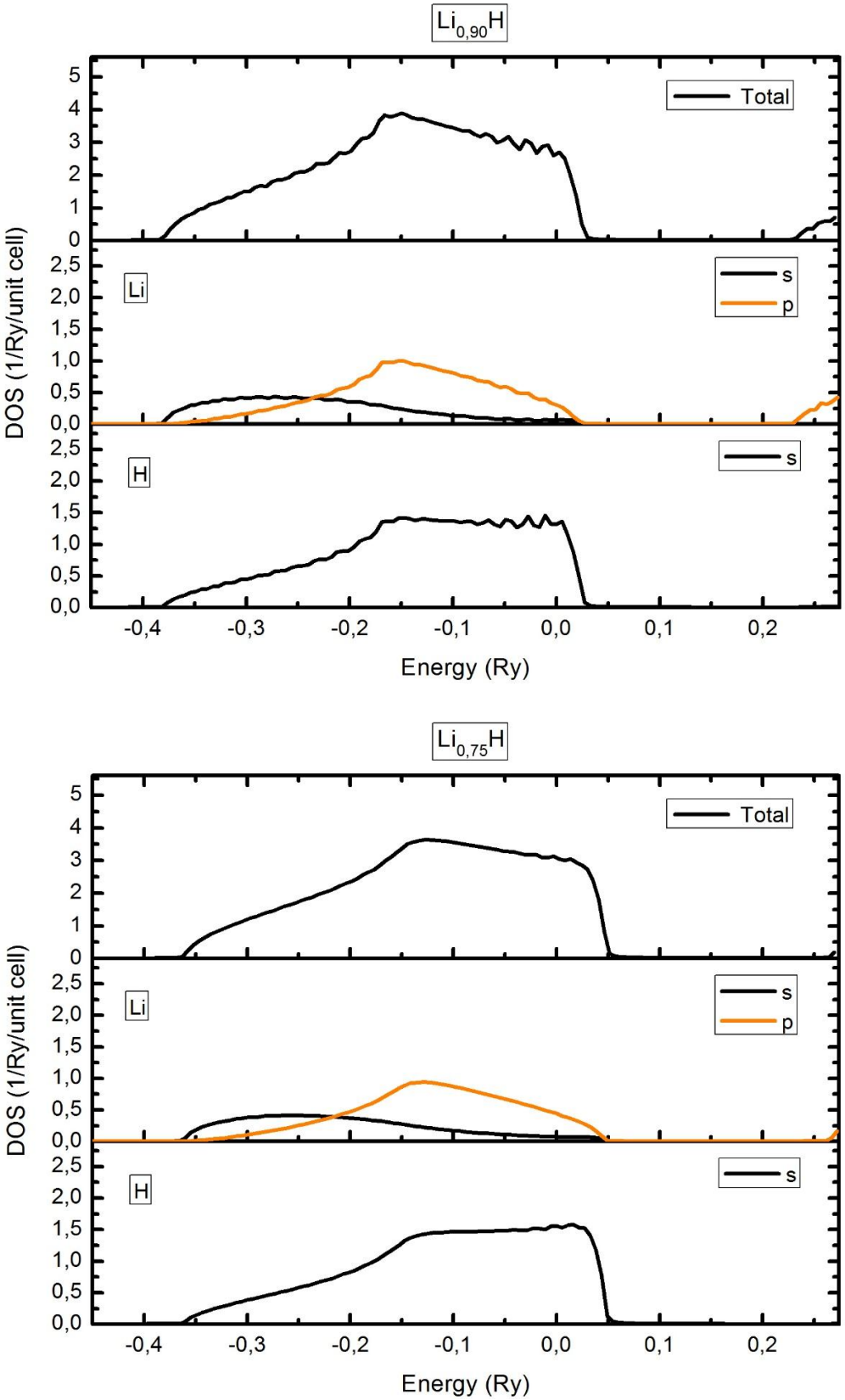

Figure 5.6: Total and partial DOS of LiH, $Li_{0.99}H$, $Li_{0.90}H$ and $Li_{0.75}H$.

5.5 Conclusion

The improvement of the thermodynamic properties of LiH is one of the challenges that faces this hydride for using it in several hydrogen storage applications. In this context, we have investigated the vacancy defects to improve both the heat of formation and the temperature of desorption in LiH. In particular, we have varied the concentration of lithium vacancy defects from 1 to 25% into the hydride, and we have observed that the thermodynamic properties have been improved by increasing the heat of formation and decreasing both the desorption temperature and the stability in LiH. Additionally, we have also found that the gravimetric capacity of LiH increases from 12,679 to 14.738 wt.% when the concentration of lithium vacancy defects increases from 0 to 16%. This improvement in LiH is explained using the density of states (DOS), which indicates that when the concentration of lithium vacancy defects increases in the hydride, the Li and H states shift to the conduction band.

General Conclusion

The assessment of the effect of magnesium vacancy defects into MgH_2 and LiH with or without hydrogen dopant atoms on the gravimetric hydrogen capacity, formation energy, desorption temperature and stability into MgH_2 and LiH is the purpose of this work. The Korringa – Kohn – Rostoker – Green's function method integrated with the coherent potential approximation has chosen to perform our calculation.

The effect of magnesium vacancy defects into MgH_2 with or without hydrogen dopant atoms on the MgH_2 hydride has revealed that:

- The pure MgH_2 presents a high formation energy of -88.571kJ/mol.H_2 and a high desorption temperature of 677.67K.
- The obtained results are consistent with the theoretical and experimental values obtained in other studies.
- The strong hybridization between magnesium and hydrogen atoms is the main raison to have a high stability in the MgH_2.
- The stability and the temperature of desorption decrease considerably with the increase of the concentration of magnesium vacancies and hydrogen dopant atoms and, vice versa, for the formation energy and the gravimetric hydrogen capacity.

In the case of the use of magnesium vacancies in MgH_2 without introducing the hydrogen dopant atoms, the obtained results have shown that when the concentration of magnesium vacancies increase from 0 to 8%:

- The formation energy increases from -88.571 to -2.324KJ/mol.H_2.
- The desorption temperature decreases from 677.67 to 17.78K.
- The gravimetric hydrogen capacity increases from 7.658 to 8,269wt.%.

In the case of the use of magnesium vacancies in MgH_2 with introducing the hydrogen dopant atoms, the obtained results have revealed that when the concentration of magnesium vacancies and hydrogen dopant atoms increase from 0 to 10%:

- The formation energy increases from -88.571 to -1.946KJ/mol.H_2.
- The desorption temperature decreases from 677.67 to 14.88K.
- The gravimetric hydrogen capacity increases from 7.658 to 9.816wt.%.

The comparison between the vacancy defects and the doping with metal transitions on the temperature of desorption of MgH_2 has revealed that the magnesium vacancy defects appear to be the best method for the magnesium hydride in comparison with using the transition metals alone or their mixture with the magnesium vacancy defects.

On the other hand, the pure LiH has shown a high formation energy of -91.371kJ/mol.H2 and a high desorption temperature of 699.09K, and the effect of lithium vacancy defects had a significant effect on these thermodynamic properties. The results have revealed that when the concentration of lithium vacancies increase from 0 to 25%:

- The formation energy increases from -91.371 to -3.021KJ/mol.H2.
- The desorption temperature decreases from 699.09 to 23.12K.
- The gravimetric hydrogen capacity increases from 12.679 to 16,2wt.%.191919

Bibliography

[1] Lahnaoui A, Wulf C, Heinrichs H, Dalmazzone D. *Optimizing hydrogen transportation system for mobility by minimizing the cost of transportation via compressed gas truck in North Rhine-Westphalia*. Appl Energy 2018;223:317-328. https://doi.org/10.1016/j.apenergy.2018.03.099.

[2] Feng P, Zhu L, Zhang Y, Yang F, Wu Z, Zhang Z. *Optimum output temperature setting and an improved bed structure of metal hydride hydrogen storage reactor for thermal energy storage*. Int J Hydrogen Energy 2019;44(35):19313-19325. https://doi.org/10.1016/j.ijhydene.2018.04.220.

[3] Manaia MS, Leturia M, Pohlmann C, Oubraham J, Mottelet S, Levy M, et al. *Comparative study of different storage bed designs of a solid-state hydrogen tank*. J Energy Storage 2019;26:101024-101034. https://doi.org/10.1016/j.est.2019.101024.

[4] Abe JO, Popoola API, Ajenifuja E, Popoola OM. *Hydrogen energy, economy and storage: review and recommendation*. Int J Hydrogen Energy 2019;44(29):15072-15086. https://doi.org/10.1016/j.ijhydene.2019.04.068.

[5] Benzidi H, Lakhal M, Abdellaoui M, Garara M, Benyoussef A, El kenz A, et al. *Improved thermodynamic properties of doped $LiBH_4$ for hydrogen storage: first-principal calculation*. Int J Hydrogen Energy 2019;44:16793-16802. https://doi.org/10.1016/j.ijhydene.2019.04.241.

[6] Potapov SN, Gvozdkov IA, Belyaev VA, Verbetsky VN, Mitrokhin SV. *Magnesium hydride based hydrogen chemical source: development and application perspectives*. Int J Hydrogen Energy 2019;44(54):28578-28585. https://doi.org/10.1016/j.ijhydene.2019.09.094.

[7] Lutz M, Bhouri M, Linder M, Bu¨ rger I. *Adiabatic magnesium hydride system for hydrogen storage based on thermochemical heat storage: numerical analysis of the dehydrogenation*. Appl Energy 2019;236:1034-1048. https://doi.org/10.1016/j.apenergy.2018.12.038.

[8] Pranevicius L, Milcius D, Templier C. *The effects of dynamic structural transformations on hydrogenation properties of Mg and MgNi thin films*. Int J Hydrogen Energy 2009;34(12):5131-5137. https://doi.org/10.1016/j.ijhydene.2009.04.034.

[9] Bassetti A, Bonetti E, Pasquini L, Montone A, Grbovic J, Vittori Antisari M. *Hydrogen desorption from ball milled MgH_2 catalyzed with Fe*. Eur Phys J B 2005;43(1):19-27. https:// doi.org/10.1140/epjb/e2005-00023-9.

[10] Novakovic N, Novakovic JG, Matovic L, Manasijevic M, Radisavljevic I, Paskas Mamula B, et al. *Ab initio calculations of MgH_2, MgH_2:Ti and MgH_2:Co compounds*. Int J Hydrogen Energy 2010;35(2):598-608. https://doi.org/10.1016/j.ijhydene.2009.11.003.

[11] Pozzo M, Alfe D. *Hydrogen dissociation and diffusion on transition metal (¼ Ti, Zr, V, Fe, Ru, Co, Rh, Ni, Pd, Cu, Ag)-doped Mg(0001) surfaces*. Int J Hydrogen Energy 2009;34(4):1922-1930. https://doi.org/10.1016/j.ijhydene.2008.11.109.

[12] Yang WN, Shang CX, Guo ZX. *Site density effect of Ni particles on hydrogen desorption of MgH_2*. Int J Hydrogen Energy 2010;35(10):4534-4542. https://doi.org/10.1016/j.ijhydene.2010.02.047.

[13] Huot J, Liang G, Boily S, Van Neste A, Schulz R. *Structural study and hydrogen sorption kinetics of ball-milled magnesium hydride*. J Alloys Compd 1999;293-295:495-500. https://doi.org/10.1016/S0925-8388(99)00474-0.

[14] Tanniru M, Slattery DK, Ebrahimi F. *A study of stability of MgH2 in Mge8at%Al alloy powder*. Int J Hydrogen Energy 2010;35(8):3555-3564. https://doi.org/10.1016/j.ijhydene.2010.01.109.

[15] Sakintuna B, Lamari FD, Hirscher M. *Metal hydride materials for solid hydrogen storage: a review*. Int J Hydrogen Energy 2007;32(9):1121-1140. https://doi.org/10.1016/j.ijhydene.2006.11.022.

[16] Song MY, Kwon SN, Park HR, Hong S-H. *Improvement in the hydrogen storage properties of Mg by mechanical grinding with Ni, Fe and V under H_2 atmosphere*. Int J Hydrogen Energy 2011;36(21):13587-13594. https://doi.org/10.1016/j.ijhydene.2011.07.107.

[17] Cabo M, Garroni S, Pellicer E, Milanese C, Girella A, Marini A, et al. *Hydrogen sorption performance of MgH_2 doped with mesoporous nickel- and cobalt-based oxides*. Int J Hydrogen Energy 2011;36(9):5400-5410. https://doi.org/10.1016/j.ijhydene.2011.02.038.

[18] Shang CX, Bououdina M, Song Y, Guo ZX. *Mechanical alloying and electronic simulations of (MgH_2+M) systems (M=Al, Ti, Fe, Ni, Cu and Nb) for hydrogen storage*. Int J Hydrogen Energy 2004;29(1):73-80. https://doi.org/10.1016/S0360-3199(03)00045-4.

[19] Dagdougui H, Sacile R, Bersani C, Ouammi A, Dagdougui H, Sacile R, et al. *Hydrogen storage and distribution: implementation scenarios*. Hydrog Infrastruct Energy Appl 2018:37-52. https://doi.org/10.1016/B978-0-12-812036-1.00004-4.

[20] Nabi G, Kamran MA, Alharbi T, Rafique M, Tahir MB, Hussain S, et al. *Gallium vacancies role in hydrogen storage of single-crystalline GaN hexagonal micro-sheets*. Int J Hydrogen Energy 2020;45(7):4731-4742. https://doi.org/10.1016/j.ijhydene.2019.12.042.

[21] Xueping Z, Yuan X, Xinyue L, Runnan J, Yongsheng Z, Zhihao Z, et al. *Hydrogen storage performance of HPSB hydrogen storage materials*. Chem Phys Lett 2019;734:136697-136703. https://doi.org/10.1016/j.cplett.2019.136697.

[22] Ball M, Wietschel M. *The future of hydrogen - opportunities and challenges*. Int J Hydrogen Energy 2009;34(2):615-627. https://doi.org/10.1016/j.ijhydene.2008.11.014.

[23] Singh R, Altaee A, Gautam S. *Nanomaterials in the advancement of hydrogen energy storage*. Heliyon 2020;6(7):e04487. https://doi.org/10.1016/j.heliyon.2020.e04487.

[24] Schüth F, Bogdanović B, Felderhoff M. *Light metal hydrides and complex hydrides for hydrogen storage*. Chem Commun 2004:2249–58. https://doi.org/10.1039/B406522K.

[25] Bramwell PL, Ngene P, de Jongh PE. *Carbon supported lithium hydride nanoparticles: Impact of preparation conditions on particle size and hydrogen sorption*. Int J Hydrogen Energy 2017;42(8):5188–98. https://doi.org/10.1016/j.ijhydene.2016.10.062.

[26] Hwang HT, Varma A. *Hydrogen storage for fuel cell vehicles*. Curr Opin Chem Eng 2014;5:42–8. https://doi.org/10.1016/j.coche.2014.04.004.

[27] Demirci UB, Miele P. *Chemical hydrogenstorage: 'material' gravimetric capacity versus 'system' gravimetric capacity*. Energy Environ Sci 2011;4(9):3334–41. https://doi.org/10.1039/C1EE01612A.

[28] Chamoun R, Demirci UB, Miele P. *Cyclic Dehydrogenation–(Re)Hydrogenation with Hydrogen-Storage Materials: An Overview*. Energy Technol 2015;3(2):100–17. https://doi.org/10.1002/ente.201402136.

[29] Puszkiel J, Garroni S, Milanese C, Gennari F, Klassen T, Dornheim M, et al. *Tetrahydroborates: Development and Potential as Hydrogen Storage Medium*. Inorganics 2017;5(4):74–97. https://doi.org/10.3390/inorganics5040074.

[30] Wang L, Quadir MZ, Aguey-Zinsou K-F. *Ni coated LiH nanoparticles for reversible hydrogen storage*. Int J Hydrogen Energy 2016:41(15):6376–86. https://doi.org/10.1016/j.ijhydene.2016.01.173.

[31] Wang L, Quadir MZ, Aguey-Zinsou K-F. *Direct and reversible hydrogen storage of lithium hydride (LiH) nanoconfined in high surface area graphite*. Int J Hydrogen Energy 2016;41(40):18088–94. https://doi.org/10.1016/j.ijhydene.2016.07.073.

[32] Wolverton C, Ozoliņš V, Asta M. *Hydrogen in aluminum: First-principles calculations of structure and thermodynamics*. Phys Rev B 2004;69(14):144109–24. https://doi.org/10.1103/PhysRevB.69.144109.

[33] Howie RT, Narygina O, Guillaume CL, Evans S, Gregoryanz E. *High-pressure synthesis of lithium hydride*. Phys Rev B 2012;86(6):064108–11. https://doi.org/10.1103/PhysRevB.86.064108.

[34] Milanese C, Jensen TR, Hauback BC, Pistidda C, Dornheim M, Yang H, et al. *Complex hydrides for energy storage*. Int J Hydrogen Energy 2019:44(15):7860–74. https://doi.org/10.1016/j.ijhydene.2018.11.208.

[35] Kong VCY, Kirk DW, Foulkes FR, Hinatsu JT. *Development of hydrogen storage for fuel cell generators II: utilization of calcium hydride and lithium hydride*. Int J Hydrogen Energy 2003;28(2):205–14. https://doi.org/10.1016/S0360-3199(02)00039-3.

[36] Gislon P, Prosini PP. *Devices for producing hydrogen via NaBH4 and LiH hydrolysis*. Int J Hydrogen Energy 2011;36(1):240–46. https://doi.org/10.1016/j.ijhydene.2010.09.052.

[37] Strawser D, Thangavelautham J, Dubowsky S. *A passive lithium hydride based hydrogen generator for low power fuel cells for long-duration sensor networks*. Int J Hydrogen Energy 2014;39(19):10216–29. https://doi.org/10.1016/j.ijhydene.2014.04.110.

[38] Miyaoka H, Ishida W, Ichikawa T, Kojima Y. *Synthesis and characterization of lithium–carbon compounds for hydrogen storage*. J Alloy Comp 2011;509(3):719–23. https://doi.org/10.1016/j.jallcom.2010.08.002.

[39] Mori D, Hirose K. *Recent challenges of hydrogen storage technologies for fuel cell vehicles*. Int J Hydrog Energy 2009 34;(10):4569–4574.

[40] Von Helmolt R, Eberle U. *Fuel cell vehicles: status 2007*. J Power Sources 2007;165(2):833–43.

[41] Ahluwalia RK, Hua TQ, Peng JK, Kumar R. *System Level Analysis of Hydrogen Storage Options*. DOE Hydrogen Program Review. 2010.

[42] Kendall M. Fuel cell development for New Energy Vehicles (NEVs) and clean air in China. Prog Nat Sci: Mat Int 2018;28(2):113-20.

[43] Fesmire JE. Aerogel insulation systems for space launch applications. Cryogenics 2006;46(2-3):111-117.

[44] Schlapbach L, Zuttel A. *Hydrogen-storage materials for mobile applications*. Nature 2001;414(6861):353–358.

[45] Hirscher M. *Handbook of Hydrogen Storage: New Materials for Future Energy Storage*. Wiley-VCH, Weinheim, 2010.

[46] Paggiaro R, Benard P, Polifke W. *Cryo-adsorptive hydrogen storage on activated carbon. I. Thermodynamic analysis of adsorption vessels and comparison with liquid and compressed gas hydrogen storage*. Int J Hydrog Energy 2010a;35(2):638–647.

[47] Emonts B, Stolten D. *Hydrogen Science and Engineering: Materials, Processes, Systems and Technology*. Wiley-VCH, Weinheim, 2016a.

[48] Stolten PD, Samsun DRC, Garland DN, Stolten D, Garland N, Samsun RC. *Fuel Cells: Data, Facts, and Figures*. Wiley-VCH, Weinheim, 2016.

[49] Aceves SM, Espinosa-Loza F, Ledesma-Orozco E, Ross TO, Weisberg AH, Brunner TC, Kircher O. *High-density automotive hydrogen storage with cryogenic capable pressure vessels*. Int J Hydrog Energy 2010;35(3):1219–1226.

[50] Müller K, Aslam R, Fischer A, Stark K, Wasserscheid P, Arlt W. *Experimental assessment of the degree of hydrogen loading for the dibenzyl toluene based Lohc system*. Int J Hydrog Energy 2016;41(47):22097–22103.

[51] Teichmann D, Arlt W, Wasserscheid P, Freymann R. *A future energy supply based on liquid organic hydrogen carriers (LOHC)*. Energy Environ Sci 2011;4(8):2767- -2773.

[52] Bimbo N, Xu W, Sharpe JE, Ting VP, Mays TJ. *High-pressure adsorptive storage of hydrogen in mil-101 (Cr) and Ax-21 for mobile applications*. Cryocharging and cryokinetics Mater Des 2016;89:1086–1094.

[53] Klebanoff L. *Hydrogen Storage Technology: Materials and Applications*. CRC Press, Boca Raton FL, 2013.

[54] Burchell TD, Contescu CI, Gallego NC. *Activated carbon fibers for gas storage*. Activated Carbon Fiber and Textiles. 2017:305–335.

[55] Javaid A. *Activated carbon fiber for energy storage*. Activated Carbon Fiber and Textiles. 2017:281–303.

[56] Paggiaro R, Michl F, Benard P, Polifke W. *Cryo-adsorptive hydrogen storage on activated carbon. II. Investigation of the thermal effects during filling at cryogenic temperatures*. Int J Hydrog Energy 2010b;35(2):648–659.

[57] Ahluwalia RK, Peng JK. *Automotive hydrogen storage system using cryo-adsorption on activated carbon*. Int J Hydrog Energy 2009;34(13):5476–5487.

[58] Wenger D. *Metallhydridspeicher zur Wasserstoffversorgung und Kühlung von Brennstoffzellenfahrzeugen*. Düsseldorf: VDI Verlag, 2009.

[59] Thiangviriya S, Utke R. *Improvement of dehydrogenation kinetics of 2libh4–Mgh2 composite by doping with activated carbon nanofibers*. Int J Hydrog Energy 2016;41(4):2797–2806.

[60] Mahytec, hydrogen storage solutions. Website: http://www.mahytec.com/ (accessed 12.25.2020).

[61] Selvam P, Viswanathan B, Swamy CS, Srinivasan V. Studies on the thermal characteristics of hydrides of Mg, Mg_2Ni, Mg_2Cu and $Mg_2Ni_{1-x}M_x$ (M ¼ Fe, Co, Cu or Zn; $0 < x < 1$) alloys. Int J Hydrogen Energy 1988;13(2):87-94.

[62] Bérubé B, Radtke G, Dresselhaus M, Chen G. *Size effects on the hydrogen storage properties of nanostructured metal hydrides: a review*, International Journal of Energy Research 2007;31:637–663.

[63] Reports of US DOE - The Fuel Cell Technologies Office (FCTO) - http://energy.gov/eere/fuelcells/materials-based-hydrogen-storage.

[64] Kohlmann H. *Metal Hydrides*. Encyclopedia of Physical Science and Technology (Third Edition). 2003:441-458.

[65] Noritake T, Aoki M, Towata S, Seno Y, Hirose Y, Nishibori E, et al. *Chemical bonding of hydrogen in MgH_2*. Applied Physics Letters 2002;81:2008–2010.

[66] San-Martin A, Manchester FD. *The H–Mg (hydrogen–magnesium) system*. Bulletin of Alloy Phase Diagrams 1987;8:431–437.

[67] Semenenko KN, Verbestkii VN, Kalashnikov YA, Temofeeva NV, Ioffe MI. *Phase transitions of metal hydrides under condition of superhigh pressure*. Vest Mosk Univ Ser 2, Khim 1978;19:718–722.

[68] Bastide J P, Bonnetot B, Letoffe JM, Claudy P. *Polymorphism of magnesium hydride under high pressure*. Materials Research Bulletin, 1980;15:1215–1224.

[69] N. Hanada, T. Ichikawa, H. Fujii, Catalytic effect of Ni nano-particle and Nb oxide on H-desorption properties in MgH2 prepared by ball milling, J. Alloys Compd. 404 (2005) 716-719.

[70] L. Xie, Y. Liu, X.Z. Zhang, J.L. Qu, Y.T. Wang, X.G. Li, Catalytic effect of Ni nanoparticles on the desorption kinetics of MgH2 nanoparticles, J. Alloys Compd. 482 (2009) 388-392.

[71] Liang G, Huot J, Boily S, Van Neste A, Schulz R. Catalytic effect of transition metals on hydrogen sorption in nanocrystalline ball milled MgH2-Tm (Tm¼Ti, V, Mn, Fe and Ni) systems. J Alloys Compd 1999;292:247-52.

[72] H Shao, M Felderhoff, F Schüth, C Weidenthaler. Nanostructured Ti-catalyzed MgH2 for hydrogen storage. 2011 Nanotechnology 22 235401.

[73] Van de Walle CG, Neugebauer J. *First-principles calculations for defects and impurities: Applications to III-nitrides*. Journal of Applied Physics 2004;95(8):3851–3879.

[74] Drabold DA, Estreicher SK. *Theory of defects in semiconductors*. 2007.

[75] Alkauskas A, Deák P, Neugebauer J, Pasquarello A, Van de Walle CG. *Advanced Calculations for Defects in Materials: Electronic Structure Methods*. John Wiley & Sons 2011.

[76] Broberg D, Medasani B, Zimmermann NE, Yu G, Canning A, Haranczyk M, at al. *PyCDT: A Python toolkit for modeling point defects in semiconductors and insulators*. Comput Phys Commun 2018;226:165-179.

[77] Born M, Oppenheimer JR. *Zur quantentheorie der molekeln*. Ann der Physik 1927; 389:457-484.

[78] Hartree DR. The Wave Mechanics of an Atom with a Non-Coulomb Central Field. Part I. Theory and Methods. Proc Cam Phil Soc 1928;24(1):89-110.

[79] Hartree DR. The wave mechanics of an atom with a non-coulomb central field. Part II. results and discussion. Proc Cam Phil Soc 1928;24(1):111–132.

[80] Hartree DR. The wave mechanics of an atom with a non-coulomb central field. Part III. term values and intensities in series in optical spectra. Proc Cam Phil Soc 1928;24(1):426–437.

[81] Fock V. *Näherungsmethode zur Lösung des quantenmechanischen Mehrkörperproblems*. Z. Physik 1930;61:126-148.

[82] Slater JC. *The Theory of Complex Spectra*. Phys Rev 1929;34:1293.

[83] Kümmel H. Origins of the Coupled Cluster Method. Theoretica chimica acta 1991;80(2-3):81–89.

[84] Sherrill CD,Schaefer HF III. *The Configuration Interaction Method: Advances in Highly Correlated Approaches*. Advances in quantum chemistry 1999;34:143-269.

[85] Møller C, Plesset MS. *Note on an approximation treatment for many-electron systems*. Phys Rev 1934;46:618–622.

[86] Hohenberg P, Kohn W. *Inhomogeneous electron gas*. Physical Review 1964;136:B864–B871.

[87] Kohn W, Sham LJ. *Self-consistent equations including exchange and correlation effects*. Physical Review 1965;140:A1133–A1138.

[88] Lieb, EH. *Density functionals for Coulomb systems*. Inequalities 2002:269-303.

[89] Levy M. *Universal variational functionals of electron densities, firstorder density matrices, and natural spin-orbitals and solutions of the v-representability problem*. Proc Natl Acad Sci 1979;76(12):6062-6065.

[90] Perdew JP. *Density functional theory and the band gap problem*. Int J Quantum Chem 1985;28:497.

[91] Perdew JP, Burke K. *Comparison shopping for a gradient-corrected density functional.* Int J Quant Chem 1996;57:309.

[92] Dirac PAM. *Note on Exchange Phenomena in the Thomas Atom*. Proceedings of the Cambridge Philosophical Society 1930;26:376-385.

[93] Slater JC. *A simplification of the hartree-fock method*. Physical Review 1951;81:385–390.

[94] Ceperley DM, Alder BJ. *Ground state of the electron gas by a stochastic method*. Phys Rev Lett. 1980;45:566–569.

[95] Perdew JP, Chevary JA, Vosko SH, Jackson KA, Pederson MR, Singh DJ, et al. Atoms, molecules, solids, and surfaces: applications of the generalized gradient approximation for exchange and correlation. Phys Rev B 1992;46(11):6671-87.

[96] Perdew JP. *Density functional theory and the band gap problem*. Int J Quantum Chem, 1986;30(3):451–451.

[97] Perdew JP, Burke K, Ernzerhof M. *Generalized gradient approximation made simple*. Phys Rev Lett 1996;77(18):3865-8.

[98] Korringa J. *On the calculation of the energy of a Bloch wave in a metal*. Physica 1947;13(6-7):392-400.

[99] Kohn W, Rostoker N. *Solution of the Schrödinger equation in Periodic Lattices with an Application to Metallic Lithium*. Phys Rev 1954;94;1111.

[100] Gonis A, Butler WG. *Multiple scattering in solids.* Springer Science & Business Media 2012.

[101] Gasan H, Celik ON, Aydinbeyli N, Yaman YM. *Effect of V, Nb, Ti and graphite additions on the hydrogen desorption temperature of magnesium hydride*. Int J Hydrogen Energy 2012;37(2):1912-8.

[102] Barkhordarian G, Klassen T, Bormann R. *Catalytic mechanism of transition-metal compounds on Mg hydrogen sorption reaction*. J Phys Chem B 2006;110(22):11020-4.

[103] Bhihi M, Lakhal M, Labrim H, Benyoussef A, El Kenz A, Mounkachi O, et al. *Hydrogen storage of Mg1-xMxH_2 (M ¼ Ti, V, Fe) studied using first-principles calculations*. Chin Phys B 2012;21(9):097501-7.

[104] Bahou S, Labrim H, Lakhal M, Bhihi M, Hartiti B, EzZahraouy H. Improving desorption temperature and kinetic properties in MgH_2 by vacancy defects: DFT study. Int J Hydrogen Energy 2020;45(18):10806e13.

[105] Bahou S, Labrim H, Lakhal M, Bhihi M, Hartiti B, EzZahraouy H. Magnesium vacancies and hydrogen doping in MgH2 for improving gravimetric capacity and desorption temperature. Int J Hydrogen Energy 2021;46(2):2322-9.

[106] KKR-CPA Package. http://kkr.issp.u-tokyo.ac.jp/ (accessed 12.27.2020).

[107] Vajeeston P, Ravindran P, Kjekshus A, Fjellva°g H. *Pressure- Induced structural transitions in MgH2*. Phys Rev Lett 2002;89(17):175506-9.

[108] Bortz M, Bertheville B, Bottger G, Yvon K. *Structure of the high pressure phase g-MgH_2 by neutron powder diffraction*. J Alloys Compd 1999;287(1e2):L4-6.

[109] Nakamura H, Nguyen-Manh D, Pettifor DG. *Electronic structure and energetics of LaNi5, a-La2Ni10H and b-La2Ni10H14*. J Alloys Compd 1998;281(2):81-91.

[110] Pozzo M, Alfe D. *Structural properties and enthalpy of formation of magnesium hydride from quantum Monte Carlo calculations*. Phys Rev B 2008;77(10):104103-10.

[111] Zeng Q, Su K, Zhang L, Xu Y, Cheng L, Yan X. *Evaluation of the thermodynamic data of CH_3SiCl_3 based on quantum chemistry calculations*. J Phys Chem Ref Data 2006;35(3):1385-90.

[112] Kurko S, Matovic L, Novakovic N, Matovic B, Jovanovic Z, Paskas Mamula B, et al. *Changes of hydrogen storage properties of MgH_2 induced by boron ion irradiation*. Int J Hydrogen Energy 2011;36(1):1184-9.

[113] Yu R, Lam PK. *Electronic and structural properties of MgH2*. Phys Rev B 1988;37(15):8730-7.

[114] Kelkar T, Pal S, Kanhere DG. Density functional investigations of electronic structure and dehydrogenation reactions of Al and Sisubstituted magnesium hydride. Chem Phys Chem 2008;9(6):928-34.

[115] Klebanoff LE, Keller JO. *5 Years of hydrogen storage research in the U.S. DOE metal hydride center of excellence (MHCoE)*. Int J Hydrogen Energy 2013;38(11):4533-76.

[116] Napán R, y Blancá ELP. *First-principles studies of lithium hydride series for hydrogen storage*. Int J Hydrogen Energy 2012;37(7)5784–9. https://doi.org/10.1016/j.ijhydene.2011.12.117.

[117] Nadler MR, Kempier CP. *Crystallographic Data 186. Lithium*. Anal Chem 1959;31(12):2109. https://doi.org/10.1021/ac60156a007.

[118] Nakamura H, Nguyen-Manh D, Pettifor DG. *Electronic structure and energetics of LaNi_5, α-La_2 Ni_10H and β-La_2 Ni_10 H_14*. J Alloy Comp 1998;281(2):81–91. https://doi.org/10.1016/S0925-8388(98)00794-4.

[119] Wolverton C, Ozoliņš V, Asta M. *Hydrogen in aluminum: First-principles calculations of structure and thermodynamics*. Phys Rev B 2004;69(14):144109–24. https://doi.org/10.1103/PhysRevB.69.144109.

[120] Howie RT, Narygina O, Guillaume CL, Evans S, Gregoryanz E. *High-pressure synthesis of lithium hydride*. Phys Rev B 2012;86(6):064108–11. https://doi.org/10.1103/PhysRevB.86.064108.

[121] Abdellaoui M, Lakhal M, Benzidi H, Garara M, Benyoussef A, El Kenz A, et al. *Enhancing of hydrogen storage properties of perovskite-type MgNiH_3 by introducing cobalt dopant (MgCo_x Ni_(1-x) H_3) using first-principle calculations*. Appl Phys A 2019;125:760–7. https://doi.org/10.1007/s00339-019-3052-4.